Universitetet
i Stavanger

FACULTY OF SCIENCE AND TECHNOLOGY

MASTER'S THESIS

Study programme/specialization: Petroleum Engineering/ Reservoir Engineering	Spring / Autumn semester, 2019 Open
Author: Agnes Kahlbom Wathne	Agnes Kahlbom Wathne (signature of author)

Supervisor(s): Skule Strand, Tina Puntervold, Iván Darío Piñerez Torrijos

Co-supervisor: Pål Østebø Andersen

Title of master's thesis:

Effect of Wettability on Waterflooding and Relative Permeability at Slightly Water-Wet Conditions

Credits (ECTS): 30

Keywords: Wettability Relative permeability Smart Water Spontaneous imbibition Forced imbibition Carbonate SENDRA simulations	Number of pages: 108 + supplemental material/other: 13 Stavanger, 14th of June 2019

Effect of Wettability on Waterflooding and Relative Permeability at Slightly Water-Wet Conditions

By

Agnes Kahlbom Wathne

Master Thesis

Presented to the Faculty of Energy Resources

University of Stavanger

Spring 2019

Acknowledgements

First, I would like to express my gratitude to my supervisors Associate Professors Skule Strand and Tina Puntervold for their exceptional guidance and support through this thesis. I appreciate them for always keeping the doors open and for sharing their knowledge and discuss results.
I would also like to express my gratitude to Dr. Iván Darío Piñerez Torrijos for his supervision, and for always being available for guidance and help during the laboratory work.

I would also like to express my sincere gratitude towards my co-supervisor Dr. Pål Østebø Andersen for his professional knowledge and for always being available for guidance and support.

I also acknowledge The National IOR Centre for the funding and collaboration.

Finally, I would like to express my thankfulness towards my fellow laboratory partners Amalie Harestad and Katarina Radenkovic for the great collaboration and work on this study. I could never have done this without you, and thanks to Erlend Andreassen and Markus Lindanger for always providing good environment in the laboratory.

Agnes Kahlbom Wathne

Abstract

The wettability of a porous system is of high importance when waterflood behavior and relative permeability are investigated, because both will be strongly affected. Adsorption of polar organic components (POC) are responsible for wettability alteration towards an oil-wet state. In carbonate reservoir, the acidic POC plays a major role for the initial wettability. This study aims to improve the understanding of initial wettability on oil recovery and if the experimental data can be further used to evaluate relative permeability curves for wettability alteration processes by Smart Water.

In this experimental work, chalk material from Stevns Klint was used to evaluate the effect of initial wettability on unsteady state relative permeability estimations. Two chalk cores were prepared to be strongly water-wet and used as reference cores, while two other cores were prepared to be mixed-wet by flooding the restored cores with crude oil with POC at *Swi*=20%. The acid number of the crude oil was, AN=0.67 mgKOH/g. A mineral oil without POC was introduced to both systems, to ensure that the experiments were performed under the same conditions. Oil recovery tests by forced- and spontaneous imbibition were conducted on the cores at 23°C. The effect of adsorption of polar organic components on initial wettability were investigated by spontaneous imbibition (SI), while the fraction of water-wet surface area was measured by a chromatographic wettability test. It was further investigated if reliable relative permeability curves could be modelled by the software SENDRA based on the experimental data.

The oil production by forced imbibition (FI) for both systems showed favorable mobility conditions for high displacement efficiency, and over 70 %OOIP were produced for both systems. Active capillary forces were observed in all cores during both oil recovery tests. The reference cores were confirmed to be strongly water-wet as the FW imbibed rapidly and a recovery plateau was reached after only hours. The cores exposed to crude oil were confirmed to be less water-wet, i.e., fractional-wet. Reliable relative permeability curves were modelled only for the strongly-water wet system. In conclusion, only one set of reliable relative permeability curves for the wettability alteration process by Smart Water were modelled based on experimental data.

Table of contents

Acknowledgements III
Abstract IV
List of figures IX
List of tables XIII
Nomenclature XIV

1 Introduction 1
1.1 Objectives 3
2 Fundamentals of oil recovery 4
2.1 Oil recovery mechanisms 4
2.1.1 Primary recovery 4
2.1.2 Secondary recovery 4
2.1.3 Tertiary recovery 5
2.1.4 Smart Water 7
2.2 Displacement forces 7
2.2.1 Gravity forces 8
2.2.2 Viscous forces 9
2.2.3 Capillary forces 9
2.2.3.1 Capillary entry pressure 12
2.2.4 Interfacial tension 12
2.3 Important parameters during waterflooding 13
2.3.1 Sweep efficiency 13
2.3.2 Porosity 13
2.3.3 Permeability 14
2.3.4 Mobility ratio 15
2.3.5 Flow regimes 16
3 Wettability 17
3.1 Wettability classification 17
3.2 Wettability measurements methods 19
3.2.1 Contact angle 19
3.2.2 Amott method 20
3.2.3 United states bureau of mines (USBM) method 22
3.2.4 Spontaneous imbibition 23

3.2.5 Chromatographic wettability test 24
3.3 Effect of wettability on core analyses 25
3.3.1 Effect of wettability on relative permeability 26
3.3.2 Effect of wettability on capillary pressure 28
3.3.3 Effect of wettability on waterflooding 29
4 Carbonate reservoirs 31
4.1 Carbonate rocks 31
4.1.1 Smart Water EOR processes in carbonates 33
4.1.2 Initial wetting in carbonates 34
5 Modelling of relative permeability curves during waterflooding 40
5.1 Laboratory measurements of relative permeability 40
5.2 Relative permeability curves with Corey correlations 41
5.3 Two-phase capillary pressure curves with Skjæveland correlations 42
5.4 Prediction of waterflood performance 44
6 Experimental work 46
6.1 Materials 46
6.1.1 Core materials 46
6.1.2 Oils 48
6.1.3 Brines 49
6.1.4 Chemicals 50
6.2 Analyses 51
6.2.1 pH measurements 51
6.2.2 Density measurements 51
6.2.3 Viscosity measurements 51
6.2.4 Interfacial tension measurements 52
6.2.5 Determination of AN and BN 52
6.2.6 Ion chromatography 53
6.2.7 Scanning Electron Microscopy (SEM), EDAX 53
6.2.8 Simulating with SENDRA 53
6.3 Methods 54
6.3.1 Core preparation 54
6.3.1.1 Permeability measurements 55
6.3.2 Core restoration 55
6.3.2.1 Establishing initial water saturation 55

6.3.2.2 Oil saturation 56
6.3.2.3 Aging 57
6.3.3 Oil recovery tests 58
6.3.3.1 Oil recovery by forced imbibition 59
6.3.3.2 Oil recovery by spontaneous imbibition 59
6.3.3.3 Mild core cleaning 60
6.3.4 Chromatographic wettability test 60
7 Results and discussion 62
7.1 Core characterization 62
7.1.1 Energy dispersive x-ray spectroscopy (EDAX) 63
7.1.2 Pore size distribution 64
7.1.3 pH analyses 64
7.1.4 Permeability measurements 65
7.2 Oil characterization 66
7.2.1 Mineral oil: Marcol 85 mixture 66
7.2.2 Effect of crude oil acids on interfacial tension 67
7.3 Oil recovery tests on water-wet cores 68
7.3.1 Oil recovery by FI 68
7.3.2 Oil recovery by SI 70
7.3.3 Oil recovery by SI+FI 71
7.3.4 Chromatographic wettability test for water-wet core 71
7.3.5 Summary oil recovery tests for water-wet systems 72
7.4 Oil recovery tests on fractional-wet cores 73
7.4.1 Oil recovery by FI 73
7.4.2 Oil recovery by SI 75
7.4.3 Oil recovery by SI+FI 75
7.4.4 Chromatographic wettability tests for fractional wet cores 79
7.4.5 Summary oil recovery tests for fractional-wet system 80
7.5 Comparison water-wet and fractional-wet core 81
7.6 Comparison and summary of all oil recovery tests 82
7.7 Numerical core analyses 87
7.7.1 History matching procedure 87
7.7.2 History matching 89
7.7.3 Relative permeability curves for strongly water-wet cores 93

7.7.4 Relative permeability curves for fractional-wet core 95
7.7.5 Capillary pressure curves 96
7.7.6 Fractional flow curves 98
7.7.7 Summary and comparison of the numerical core analyses 99
8 Conclusion and future work 102
8.1 Conclusion 102
8.2 Future work 103
9 References 105
Appendix A: Chemicals 110
Acid number solutions 110
Base number solutions 110
Appendix B: Experimental data 111
Spontaneous and forced imbibition data 111
Chromatographic data 119
Appendix C: Input parameters for SENDRA 121

List of figures

Figure 2.1 Illustration of wettability alteration by smart water (Smart Water EOR group spring 2019) 7
Figure 2.2 Radii R1 and R2 of the curvature of a meniscal surface (Zolotukhin & Ursin, 2000) 10
Figure 2.3 Capillary pressure resulting from interfacial forces in a capillary tube. Redrawn after Green and Willhite (1998) 11
Figure 2.4 (left) a favorable mobility ratio, displacement of oil by water in a water-wet system. A mobile oil bank will develop ahead of the advancing water. (right) an unfavorable mobility ratio, water is capable to travel faster than oil, which will result in discontinuities in the water saturation. Redrawn after Apostolos et al. (2016) 16
Figure 3.1 Displacement of oil by water for a (a) water-wet rock, and (b) oil-wet rock. Modification of Raza et al. (1968) 18
Figure 3.2 Wettability of the oil/water/rock system. Redrawn after Anderson (1986b) 20
Figure 3.3 Capillary pressure curves for different wettability tests; Amott and USBM. Redrawn after Morrow (1990) 21
Figure 3.4 Illustration of the chromatographic separation of SO_4^{2-} and SCN^- for a preferential water-wet, mixed-wet and oil-wet core (Strand et al., 2006b) 24
Figure 3.5 Characteristics of typical relative permeability curves for a two-phase flow, where S_w is the wetting phase. (Left) a strongly water-wet formation and (right) a strongly oil-wet formation. Redrawn after Craig (1971) 27
Figure 3.6 Oil/water capillary pressure curves measured in a (left) strongly water-wet system and (right) strongly oil-wet system. Redrawn after Anderson (1987b) 28
Figure 3.7 Idealized production from three different conditions of wettability. Redrawn after Donaldson and Alam (2013) 30
Figure 4.1 (a) Scanning Electron Microscopy (SEM) picture of Stevns Klint outcrop material (Smart Water EOR group spring 2019). (b) Pore size distribution in SK chalk, redrawn from (Milter, 1996) 32
Figure 4.2 Oil recovery from a chalk core by spontaneous imbibition of FW, viscous flooding using FW and finally viscous flooding using SW (Strand et al., 2008) 33
Figure 4.3 Schematic model of the mechanism for the wettability alteration induced by seawater. (A) Ca^{2+} and SO_4^{2-} are active at lower temperature. (B) Mg^{2+}, Ca^{2+} and SO_4^{2-} are active at higher temperatures (Zhang et al., 2007) 34
Figure 4.4 Zeta potential of the chalk core with potential determining ions present in the seawater (Strand et al., 2006a) 35
Figure 4.5 AN and BN measurements of effluent crude oil samples during 15 PV of Res 40-0.4 flooding of SK chalk core at Swi=0%. The core is flooded in one direction at rate of 4 PV/day (Mjøs et al., 2018) 35
Figure 4.6 Spontaneous imbibition of brine into chalk cores saturated with crude oils with different AN number at 40°C (Standnes & Austad, 2000) 36
Figure 4.7 Spontaneous imbibition experiments with the effect of bases in crude oil. Increasing oil recovery versus time with increasing BN (Puntervold, 2008) 37
Figure 4.8 Oil recovery by SI from SK chalk cores with Swi = 10% with formation brines with different types of cations. The formation brine was also the imbibing brine, oil with AN=0.17 mgKOH/g was used. (Shariatpanahi et al., 2016) 37

Figure 4.9 Chemical model describing initial wetting in carbonates. Figures based the experimental work done from (Shariatpanahi et al., 2016) 38
Figure 5.1 Illustration of measuring relative permeability for water and oil at (a) Unsteady-state method and (b) Steady-state method. Redrawn after Lucia (2007)..... 41
Figure 5.2 Schematic of bounding curve, capillary pressure P_c as function of water saturation S_w, secondary imbibition, redrawn after Skjæveland et al. (1998). 43
Figure 5.3 Fractional flow curves. (left) Strongly water-wet rock, (right) strongly oil-wet rock. Redrawn after Craig (1971) 44
Figure 5.4 Determination of front saturation S_{wf} and average water saturation S_{wbt} at water breakthrough from S_{wi}. Redrawn after Craig (1971)..... 45
Figure 6.1 Example of viscosity measurements by Anton Paar rotational rheometer..... 51
Figure 6.2 Illustration of IFT measurement between oil and DI-water with the Du Noüy ring method. A lamella is produced between the two immiscible fluids. 52
Figure 6.3 Illustration of the Hassler cell used in the experimental work. 54
Figure 6.4 Illustration of saturation of the chalk cores with FW in a desiccator under vacuum to establish initial water saturation. 56
Figure 6.5 Effluent oil samples after each PV injected to compare with the 100% mineral oil to the right. 57
Figure 6.6 Illustration of the experimental set-up for oil saturation 57
Figure 6.7 Procedure of the experimental work in this study 58
Figure 6.8 Illustration of the Amott imbibition cell..... 59
Figure 6.9 Illustration of the experimental set-up for sampling effluent to the chromatographic wettability test at 23°C..... 61
Figure 7.1 Scanning electron microscopy (SEM) photo of the chalk outcrop material, magnification 1000 times..... 63
Figure 7.2 Scanning electron microscopy (SEM) photo of the chalk outcrop material, magnification 10 000 times..... 63
Figure 7.3 (Left) Pore size distribution for Stevns Klint Chalk material, redrawn after (Milter, 1996). (Right) pore size distribution in Valhall reservoir chalk. Redrawn after (Webb et al., 2005). 64
Figure 7.4 (Left) pH measurements of effluent samples from the produced formation water of the reference cores (SKR1 and SKR2) and the fractional-wet cores (SKC1 and SKC4). (Right) oil production and pH versus time for core reference core SKR1. 65
Figure 7.5 (left) injection rate proportional to pressure-drop, (right) linear regression of dP used for calculation of absolute permeability. The experimental data is for core SKC1 66
Figure 7.6 Viscosity measurements for preparation of the mineral oil..... 67
Figure 7.7 Measured IFT at 23°C between oil and DI-water versus measured acid number of the oils..... 67
Figure 7.8 Oil production profile and pressure drop for two water-wet reference cores. (a) reference core (SKR1) and (b) reference core (SKR2) during forced imbibition with FW. The cores with S_{wi}=20% were flooded at a rate of 1 PV/day at 23°C. At the end, the injection rate was increased to 4 PV/day. Figure (c) compare oil production and (d) compare ΔP for the two cores. 69
Figure 7.9 Oil production profiles for two strongly water-wet reference cores (SKR1 and SKR2) during spontaneous imbibition with FW at 23°C. 70

Figure 7.10 Oil production profile for a water-wet reference core (SKR2) during a spontaneous imbibition test followed by a forced imbibition test with FW at 23°C. 71
Figure 7.11 Chromatographic separation between tracer and sulfate for initially strongly water-wet cores. (Left) reference core (SKR1) and (right) reference core (SKR2) 72
Figure 7.12 Oil production profile and differential pressure for a core exposed to POC (SKC1, AN=0.67mgKOH/g) during forced imbibition with FW at S_{wi}=20%. 73
Figure 7.13 Less water-wet core SKC1 (AN=0.67 mgKOH/g) compared to reference core SKR2. The oil production profiles are identical, while the pressure-drop is lower and stabilize more quickly for the fractional-wet core. 74
Figure 7.14 Oil production profile for a core exposed to crude oil (SKC1, AN=0.67 mgKOH/g) and a water-wet reference core (SKR2) during spontaneous imbibition with FW. The less water-wet core has a reduced imbibing rate and the production is lower compared to the water-wet core. 75
Figure 7.15 Spontaneous imbibition tests of one core exposed to crude oil (SKC4, AN=0.67 mgKOH/g compared to one reference core (SKR2) and one core exposed to the same crude oil (SKC1, AN=0.67 mgKOH/g) at 23°C. The less water-wet core, SKC4 produced lower volumes of oil and the imbibition rate was low compared to the other two cores. SKC1 has been through a mild cleaning process before SI, and there is less contamination of POC in the core. 76
Figure 7.16 Oil production profiles for a core at S_{wi}=20% exposed to crude oil (SKC4, AN=0.67 mgKOH/g) during (left) spontaneous imbibition test followed by a forced imbibition test with FW at 23°C, and (right) forced imbibition test with FW at 23°C, oil production and pressure drop is plotted versus time. 77
Figure 7.17 (left) Oil recovery compared for all cores and (right) pressure drop compared for all cores 77
Figure 7.18 Chromatographic separation between tracer and sulfate for core exposed to crude oil, (AN=0.67 mgKOH/g), i.e. initially fractional-wet. (Left) fractional-wet core (SKC1) and (right) fractional-wet core (SKC4) 79
Figure 7.19 Oil recovery tests at 23°C with FW for a water-wet reference core (SKR2) at S_{wi}=20%, compared with a fractional-wet core exposed to crude oil at S_{wi}=20% with AN=0.67 mgKOH/g (SKC4). 81
Figure 7.20 Forced imbibition at 23°C with FW for three cores exposed to crude oils with different AN. SKC1, AN=0.67mgKOH/g. SKC2, AN=0.34mgKOH/g. SKC3, AN=0.15mgKOH/g 83
Figure 7.21 Spontaneous imbibition at 23°C with FW for three cores exposed to crude oils with different AN. SKC1, AN=0.67mgKOH/g. SKC2, AN=0.34mgKOH/g. SKC3, AN=0.15mgKOH/g. 84
Figure 7.22 Oil recovery by spontaneous imbibition followed by forced imbibition with FW at 23°C for cores exposed to crude oil with S_{wi}=20%. (a) SKC4, AN=0.67 mgKOH/g. (b) SKC5, AN=0.34mgKOH/g. (c) SKC6, AN=0.15mgKOH/g. 85
Figure 7.23 Automatic history match of differential pressure and oil production for the strongly water-wet systems. (left) reference core SKR1 and (right) reference core SKR2. 89
Figure 7.24 Manual history matching of experimental data for the strongly water-wet reference cores. (a) SKR1 without influence of Pc. (b) SKR1 with influence of Pc. (c) SKR2 without influence of Pc. (d) SKR2 with influence of Pc. 91

Figure 7.25 Automatic history match of differential pressure and oil production for a less water-wet system, SKC1 (AN = 0.67 mgKOH/g). 92
Figure 7.26 Manual history match of differential pressure and oil production for a less water-wet system, SKC1 (AN = 0.67 mgKOH/g). 93
Figure 7.27 Relative permeability curves for strongly water-wet reference cores. (a) core SKR1, (b) core SKR2 (c) comparison of the relative permeability curves for the two reference cores. 94
Figure 7.28 (left) Relative permeability curves for core SKC1 exposed to oil C (AN=0.67 mgKOH/g) compared to (right) the relative permeability curves for the strongly water-wet reference cores. 95
Figure 7.29 Capillary pressure curves for (left) fractional-wet system, core SKC1 and (right) compared with two water-wet reference cores 97
Figure 7.30 Fractional flow curves for two systems with different initial wettability. (a) Strongly water-wet reference core SKR1. (b) Strongly water-wet reference core SKR2. (c) Core SKC1 exposed to crude oil with AN=0.67 mgKOH/g, SKC1. (d) For both systems. 98
Figure 7.31 Comparison of: relative permeability curves based on the Corey correlation, capillary pressure curves based on Skjæveland correlation and fractional flow curves based on relative permeability for the strongly water-wet systems, with the three less water-wet systems exposed to different crude oils. (SKC1, oil C) (SKC2, oil B) (SKC3, oil A). 100

List of tables

Table 1 Classification of EOR methods (Taber et al., 1997; Thomas, 2008; Torrijos, 2017) .. 6
Table 2 EOR methods by water-based wettability alteration 6
Table 3 Core properties 47
Table 4 Properties of the oils utilized in this experimental work. 49
Table 5 Synthetic Seawater for Chromatographic tests 50
Table 6 Determined PV and injection rates of cores during forced imbibition. 59
Table 7 Element analysis of outcrop chalk material with EDAX 64
Table 8 Experimental results of the oil production in %OOIP and wettability of the reference cores during SI and FI. 72
Table 9 Experimental results of the oil production in %OOIP and wettability of the reference cores during SI and FI 80
Table 10 Summary of the experimental results during oil recovery tests 82
Table 11 Wetting index for cores exposed to polar components, reference cores has Aw=0.282 86
Table 12 Calculated absolute- and effective permeabilities to determine endpoint relative permeabilities. 87
Table 13 Output values from SENDRA for automatic history matching of experimental data of strongly water-wet reference cores and fractional-wet core. 88
Table 14 Output values from SENDRA for manual history match of experimental data for strongly water-wet reference cores and fractional-wet core. 89
Table 15 Chemicals for AN measurement 110
Table 16 Chemicals for BN measurement 110
Table 17 SI data, reference core SKR1 111
Table 18 SI data, reference core SKR2 111
Table 19 SI data, SKC1 112
Table 20 SI data, SKC4 113
Table 21 FI data, SKR1 114
Table 22 FI-data, reference core SKR2 115
Table 23 Combined oil recovery test (SI+FI). FI data, SKR2 116
Table 24 FI-data, SKC1 117
Table 25 Combined oil recovery tests (SI+FI). FI data, SKC4 118
Table 26 Chromatographic data reference core, SKR1 119
Table 27 Chromatographic data reference core, SKR2 119
Table 28 Chromatographic data SKC1 120
Table 29 Chromatographic data SKC4 120
Table 30 Input paramters for history matching in SENDRA 121

Nomenclature

Abbreviations

AN	Acid number [mgKOH/g]
BN	Base number [mgKOH/g]
a_o	Skjæveland exponent for oil, defining negative part of imbibition curve
a_w	Skjæveland exponent for water, defining positive part of imbibition curve
C_o	Skjæveland parameter for oil, defining negative part of imbibition curve [Pa]
C_w	Skjæveland parameter for water, defining positive part of imbibition curve [Pa]
CBR	Crude oil, brine and rock system
DI-water	Deionized water
E	Total displacement efficiency
E_D	Microscopic displacement efficiency
E_V	Macroscopic (volumetric) displacement efficiency
EOR	Enhanced oil recovery
EDAX	X-ray Energy Dispersive Spectroscopy
f_w	Fractional flow function of water
FI	Forced imbibition
FW	Formation water
I_{AH}	Amott Harvey index
I_o	Wettability index to oil
I_{USBM}	Wettability index (for USBM method)
I_w	Wettability index to water
I_w^*	Wettability index (for SI)
IFT	Interfacial tension
IOR	Improved oil recovery
$J(S_w)^*$	Leverett J-function scaling
K	Absolute permeability [mD]
$K_{eff,o}$	Effective permeability of oil [mD]
$K_{eff,w}$	Effective permeability of water [mD]
k_{ro}	Relative permeability of oil
k_{rw}	Relative permeability of water
KOH	Potassium hydroxide
M	Mobility ratio
N_o	Corey exponent for oil
N_w	Corey exponent for water
OOIP	Original oil in place [%]
P_c	Capillary pressure [Pa]
POC	Polar organic components
PV	Pore volume
S_{or}	Residual oil saturation

S_w	Water saturation
S_{wi}	Irreducible water saturation
S_w^*	Normalized water saturation
SEM	Scanning Electron Microscopy
SI	Spontaneous imbibition
SK	Stevns Klint
SW	Synthetic seawater
SW0T	Synthetic seawater without sulfate and tracer
SW½T	Synthetic seawater with equal amounts of sulfate and tracer
USBM	United states bureau of mines

Symbols

ϕ	Porosity
λ	Mobility
μ	Viscosity [mPa.s]
θ	Contact angle measured through the wetting phase
ρ	Density [g/cm^3]
σ	Interfacial tension between two phases [N/m]

1 Introduction

More than 50% of the proven oil resources are located in carbonate reservoirs, but the recovery factor is relatively low due to fractures and low permeabilities. The wettability of most carbonate reservoirs is believed to be neutral-wet to oil-wet (Høgnesen et al., 2005). However, the enhanced oil recovery (EOR) potential for these reservoirs can be very high. Several studies have been carried out to investigate the effect of wettability on oil recovery in carbonates According to studies by Puntervold (2008) the oil recovery will increase by altering the wettability from neutral-wet towards more water-wet. Injection of Smart Water, which is a water-based EOR method, will influence the wettability and significantly increase the oil recovery by improving the capillary forces. Oil will then be more easily displaced by spontaneous imbibition (SI) of water. Seawater can be used as a Smart Water and has been successfully injected into the fractured Ekofisk chalk field in the North Sea (Austad et al., 2007).

Oil recovery by waterflooding in carbonate reservoirs is an important and frequently used secondary recovery method, where water is injected into the reservoir and oil is produced. The waterflood behavior and relative permeability is strongly affected by the wettability of the system. It is documented that the wettability is a major factor that controls the location, flow and distribution of fluids in a reservoir, hence it will influence all types of core analyses (Anderson, 1986a, 1987c; Morrow, 1990). Wettability is defined as "the tendency of one fluid to spread on or adhere to a solid surface in presence of other immiscible fluids" (Craig, 1971), and it can range from strongly water-wet to strongly oil-wet in a porous system. The term neutral-wet is frequently used for mixed-wet and fractional-wet systems, which is defined for heterogenous systems where the surface is either preferentially water-wet or oil-wet. The main distinction between the wettability's is that the fractional wettability does not imply either specific locations for the oil-wet and water-wet surfaces (Donaldson & Alam, 2013). The wettability of a preferentially water-wet reservoir can be altered by the adsorption of polar organic components (POC) and deposition of organic material in the crude oil (Anderson, 1986a)

Displacement processes in capillary systems can be distinguished between drainage and imbibition. Drainage is defined when the non-wetting fluid displaces the wetting fluid, while

imbibition is the opposite process where the wetting fluid displaces the non-wetting fluid. Spontaneous imbibition (SI) of the wetting phase appears as the capillary forces declines to zero. SI is driven by the capillary forces in a system and is an important recovery method, especially in fractured carbonate reservoirs (Donaldson & Alam, 2013). Water will spontaneously imbibe into the pores in the matrix and displace the trapped oil.

Relative permeability is "a measure of the ability of the porous system to conduct one fluid when one or more fluids are present" (Craig, 1971), and it is important in the prediction of reservoir behavior (Brooks & Corey, 1964). Relative permeability data are usually obtained by steady- or unsteady state core flooding experiments in the laboratory (Lucia, 2007). Experimental data can be used to model relative permeability curves. The curves are well documented for strongly wetted system, and Craig (1971) has presented several general rules for these systems. For example, that a crossover saturation over 50% indicates a strongly water-wet system.

To describe the fluid flow for a reservoir that has been through a wettability alteration process, two sets of relative permeability curves are needed; one system for the initial wettability and one system for the altered wettability. Few studies have been conducted on relative permeability curves for wettability alteration processes. The main objective in this thesis is to construct relative permeability curves for a Smart Water EOR process. Waterflooding is performed on cores with different initial wettability. The wettability is changed by flooding the cores with crude oils containing different POC. The wettability alteration process towards a more oil-wet state is quantified by the acid and base numbers, (AN) and (BN) which are measured in mgKOH/g. Studies performed by Standnes and Austad (2000) have confirmed that the oil recovery will be influenced by the carboxylic material in the crude oil

1.1 Objectives

The main objective of this thesis is to study if the experimental data from oil recovery tests performed in the laboratory could be utilized as input data for modelling of relative permeability curves at different initial wettability. This will be done by the following procedure:

- Prepare outcrop chalk material to have different initial wetting, but with same initial water saturation, S_{wi} = 20%. Two chalk cores are prepared to be strongly water-wet and used as reference cores. Two other cores are prepared to be less water-wet, i.e. fractional-wet. The wettability of the cores is altered by introducing crude oil with polar organic components with acid number, AN=0.67 mgKOH/g. Finally, the crude oil is displaced with a mineral oil to ensure that all core flooding experiments are performed with an oil with the same properties and without the influence of adsorption of polar components during flooding experiments. The two fractional-wet cores are compared to four cores prepared by Harestad (2019) and Radenkovic (2019). The cores are saturated with two different crude oils with AN=0.34 mgKOH/g and AN=0.15 mgKOH/g, hence the cores are more water-wet than the cores in this experimental study.
- Oil recovery tests by spontaneous- and forced imbibition are conducted on the cores. Initially, a forced imbibition test followed by a spontaneous imbibition test. Afterwards, the experimental work is performed in the reverse order, a SI-test directly followed by a FI-test.
- Oil production and pressure-drop are measured, and the experimental data is presented versus time [PV injected]. The wettability is confirmed by spontaneous imbibition and the chromatographic wettability test for chalk.
- The core flooding simulator SENDRA is used for history matching of the experimental data. Relative permeability curves are constructed by the Brooks and Corey (1964) correlation based on the output data from the history matching.
- Capillary pressure curves and fractional flow curves are used to confirm the wettability and waterflood behavior of the systems.

2 Fundamentals of oil recovery

Oil production from reservoirs are mainly governed through different oil recovery mechanisms together with displacements forces. Originally, the displacement of oil results from energy naturally existing in the reservoirs. When no more oil can be naturally displaced anymore, other mechanisms must be used to mobilize the residual oil. There are several factors influencing the oil recovery, and in this section the various oil recovery mechanisms, displacement forces and important parameters during waterflooding is presented.

2.1 Oil recovery mechanisms

Oil recovery methods have traditionally been categorized into three different stages; primary, secondary, and tertiary. Historically, these processes describe the production from a reservoir in a chronological sense. However, many reservoir production operations are not conducted in these chronological orders, due to different reservoir characterization (Green & Willhite, 1998).

2.1.1 Primary recovery

Primary recovery is the initial production stage in an oil recovery process. The displacement of hydrocarbons is resulting from energy naturally existing in the reservoir. The main driving mechanism in these naturally stored energy sources are fluid and rock expansion, natural waterdrive, gas-cap drive and gravity drainage (Green & Willhite, 1998). During a primary recovery process, there can be a gradual and rapid decrease in the reservoir pressure. This disadvantage will lead to the development of a solution gas drive which will result in unacceptably low oil production rates and ultimate oil recovery (Zolotukhin & Ursin, 2000).

2.1.2 Secondary recovery

The second stage of production are the secondary recovery processes which are usually implemented after the primary production has declined. Traditionally secondary recovery methods are pressure maintenance, waterflooding and gas injection. The gas is injected into either a gas cap for pressure maintenance and gas-expansion, or into an oil-column well through an immiscible displacement of oil according to relative permeability and volumetric sweepout considerations. The water is injected into the production zone and it is a very efficient method (Green & Willhite, 1998). Waterflooding is almost synonymous with the secondary recovery classification and is the most frequently applied recovery technique in North Sea reservoirs. However, there are three factors that will lead to a low volumetric (macroscopic) sweep

efficiency during waterflooding; reservoir heterogeneity, problems relating to well siting and spacing, and an unfavorable mobility ratio between the displacing and displaced fluid (Zolotukhin & Ursin, 2000).

2.1.3 Tertiary recovery

The third stage of production is the tertiary recovery processes which are implemented after the secondary recovery processes have become uneconomical. Tertiary methods operate with chemicals, miscible gases, and thermal energy to displace the additional oil in the reservoir. In some situations, the chronological depletion sequences cannot be followed. Then the so-called tertiary process might be applied as a secondary operation. For example, if the waterflooding process will reduce the overall effectiveness, then the stage might be bypassed, and a tertiary recovery method can be applied right after primary recovery. Due to such situations, the term "tertiary recovery" is often replaced by "enhanced oil recovery" (EOR) or "improved oil recovery" (IOR). The latter includes EOR, but also an extensive range of activities, e.g., improved recovery management, reservoir characterization and infill drilling (Green & Willhite, 1998).

Oil recovery by EOR methods are injection of materials that are not normally present in a reservoir, the materials interact with the reservoir system and construct favorable conditions for oil recovery (Lake, 2010). In EOR processes, the main objective is to increase the volumetric (macroscopic) sweep efficiency and to enhance the displacement (microscopic) efficiency. There are two mechanisms that are aimed toward the EOR objective. The macroscopic efficiency is increased by reducing the mobility ratio between the displacing and displaced fluid. The effect of microscopic trapping is reduced by lowering the interfacial tension between the displacing and displaced fluid, which yields a lower residual oil saturation ($S_{or)}$ and hence higher oil recovery (Zolotukhin & Ursin, 2000). The most common EOR processes are listed in table 1.

Table 1 Classification of EOR methods (Taber et al., 1997; Thomas, 2008; Torrijos, 2017)

Chemical	Polymer Surfactant Alkaline Micellar ASP Emulsion
Thermal	Hot Water and steam injection In Situ Combustion Electrical Heating
Miscible	Slug process Enriched Gas Drive Vaporizing Gas Drive CO_2 Miscible N_2 Miscible Alcohol
Other	Microbial EOR Foam

Today, most of the oil reservoirs utilize waterflooding to improve oil recovery. Waterflooding has been characterized as a secondary recovery process, since no special EOR chemicals are introduced. However, it has been confirmed that the injected water, which are different in composition compared to the initial formation water (FW), can disturb the established equilibrium in the crude oil-brine-rock system (CBR). A new chemical equilibrium influencing the wetting properties will lead to an improved oil recovery. Injection of water with a different composition than the FW may change the wetting properties and act as a tertiary recovery process (Austad, 2013; Jadhunandan & Morrow, 1995). Wettability alteration towards more water-wet conditions increases the capillary forces and the microscopic sweep efficiency; hence it is suggested as a new EOR method. The wettability alteration methods are listed in table 2.

Table 2 EOR methods by water-based wettability alteration

Wettability alteration	Smart Water Low salinity Water Flooding (Sandstones) Seawater/Modified seawater (Carbonates)

2.1.4 Smart Water

During millions of years, a chemical equilibrium has been established in the CBR system. The distribution of crude oil and FW in the porous media are fixed at given saturations of oil and water. The distribution of oil and water in the porous media is linked to the wetting properties of the CBR system, hence the contact between the rock surface and the two fluids. Smart water consists of modified water injection, where the ion composition has been adjusted or optimized to change the wetting properties of the CBR system. The chemical equilibrium will change, and hence the wettability is altered. This has a favorable effect on the positive capillary forces which improve the spontaneous imbibition process in the bypassed pores in the core and hence a higher oil recovery is observed. The method is cost-efficient and environmentally friendly. No chemicals are needed, and no injection problems are observed. Smart water should be injected from the start of the waterflooding process, and in order to understand the EOR process, the chemical mechanism need to be understood since the method doesn't function in all types of oil reservoirs (Austad, 2013). Figure 2.1 illustrates the injection of Smart Water compared to FW, where Smart Water displaces oil from the bypassed pores.

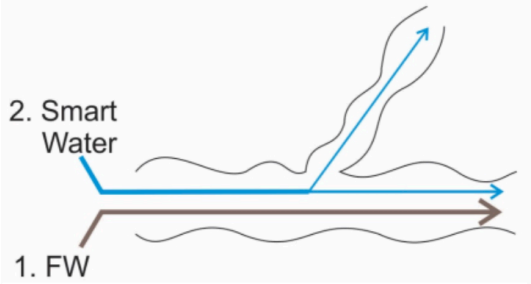

Figure 2.1 Illustration of wettability alteration by smart water (Smart Water EOR group spring 2019)

2.2 Displacement forces

The overall displacement efficiency of any oil recovery displacement process can be considered conveniently as the product of microscopic and macroscopic displacement efficiencies. The overall displacement efficiency (E) is given by the following equation:

$$E = E_D E_V \tag{2.1}$$

Where E_D is the microscopic displacement efficiency, and E_V is the macroscopic (volumetric) displacement efficiency, both expressed as fractions. Microscopic displacement relates to the

displacement or mobilization of oil at pore scale. For crude oil, E_D is reflected as the magnitude of S_{or} in places contacted by the displacing fluids. Macroscopic displacement relates to the effectiveness of the displacing fluid in contacting the reservoir in a volumetric sense. An alternative term for E_V is the sweep efficiency, which is a measure of how effectively the displacing fluid sweeps out the volume of a reservoir, and how effectively the displacing fluid moves the displaced oil toward production wells. The efficiencies are determined from mathematical- or 2D physical models and are fractions that varies from 0 to 1. If one of the calculated efficiencies is small, the overall recovery efficiency will be small. On the other hand, each of the factors can be large, but the recovery efficiency will still be small since it is a product of factors that are less than one. The vertical sweep effects are minimized by using homogenous, relatively thin porous media and fluids with matching densities (Fanchi, 2010; Green & Willhite, 1998).

The most important mechanisms causing transport in naturally occurring permeable media are gravity forces, viscous forces and capillary forces. Capillary and viscous forces control the phase trapping and mobilization of fluids in a porous media, and hence microscopic displacement efficiency. The driving force for capillary pressure and viscous forces is the pressure differences (Lake et al., 2014). The oil production usually occurs through two different processes; forced imbibition (FI) and spontaneous imbibition (SI). Capillary and gravity forces are the driving mechanism in spontaneous imbibition, while the viscous forces control the forced imbibition which is a viscous flooding process.

2.2.1 Gravity forces

Gravity forces influence the spontaneous displacement process of oil and may dominate the flow pattern in the porous media. The effect of gravity forces only exists if there is a density difference between the fluids in the porous media (Milter, 1996). The pressure gradient due to gravity is given by equation (2.2)

$$\Delta P_g = \Delta \rho g H \tag{2.2}$$

Where:

ΔP_g Pressure difference over the oil-water interface due to gravity [Pa]

$\Delta \rho$ Difference in density of the two phases [kg/m^3]

g Gravitational acceleration constant, 9.81 [m/s^2]

H Height of the fluid column [m]

2.2.2 Viscous forces

The viscous forces in a porous medium is reflected in the magnitude of the pressure drop that occurs during a fluid flow. The viscous forces can be determined by assuming a laminar flow through a porous system, which can be considered as a bundle of capillary tubes. The pressure drop across the core is given by Poiseuille's law, shown in equation (2.3) (Green & Willhite, 1998).

$$\Delta P = -\frac{8\mu L v_{avg}}{r^2 g_c} \tag{2.3}$$

Where:

Δp Pressure drop across the capillary tube [Pa]

L Capillary tube length [m]

r Capillary tube radius [m]

v_{avg} Average velocity in the capillary tube [m/s]

μ Viscosity of flowing fluid [mPa.s]

g_c Conversion factor

2.2.3 Capillary forces

Capillary forces are the most fundamental rock-fluid characteristic of a multiphase flow in a porous medium (Lake et al., 2014). They depend on the geometry and dimension of pore throats, wettability and the surface/interfacial tension created by the rocks and fluids of a given system. Capillary forces are the main driving force in a fluid flow and can act against or in favor of oil recovery, depending on the porous medium. In heterogenous reservoirs, spontaneous imbibition will lead to oil recovery due to capillary migration of water into the water-wet porous media (Donaldson & Alam, 2013). In homogenous reservoirs, the capillary forces during waterflooding can induce oil trapping, and high residual oil saturation can be observed (Anderson, 1987c).

Capillary pressure (P_c) is the pressure difference that exists across an interface between two immiscible fluids (Green & Willhite, 1998). P_c is given by the following equation:

$$P_c = P_{nw} - P_w \tag{2.4}$$

Where

P_{nw} Pressure of non-wetting phase at the interface

P_w Pressure of wetting phase at the interface

The capillary tube concept is used to describe the capillary pressure. The tube consists of two immiscible phases; a non-wetting phase and a wetting phase. The wetting phase wets the tube surface, because the contact angle θ, measured through this phase is less than 90°. If the interface between the phases in the tube are not flowing, then a higher pressure is required in the nonwetting phase than in the wetting phase to keep the interface from moving (Lake, 2010). This pressure difference causes a curvature between the fluids, and the interface will always be convex towards the wetting fluid which has the highest internal pressure. The curvature of the meniscal surface can be characterized by two radii, illustrated in figure 2.2 (Zolotukhin & Ursin, 2000). The pressure difference across the interface is given by equation (2.5)

$$P_c = \sigma\left(\frac{1}{R_1} + \frac{1}{R_2}\right) \tag{2.5}$$

Where

R_1 and R_2 Principal radii of the interface curvature

σ Interfacial tension

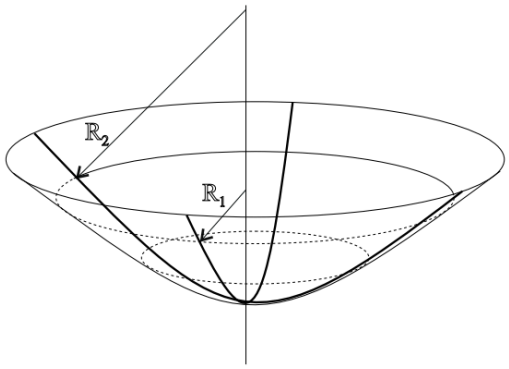

Figure 2.2 Radii R1 and R2 of the curvature of a meniscal surface (Zolotukhin & Ursin, 2000)

For a hemispherical meniscus, or a spherical oil droplet equal to the pore size, the radii is said to be $R_1 = R_2 =$ r, and the pressure difference then become, $\Delta p = 2\sigma/r$ (Zolotukhin & Ursin, 2000). If a capillary tube is filled with two immiscible fluids, oil and water, where water is the wetting fluid, then the capillary pressure is given by equation (2.6) and illustrated in figure 2.3.

$$P_c = \frac{2\sigma_{ow}cos\theta}{r} \tag{2.6}$$

Where

Pc Capillary pressure [Pa]

σ_{ow} Interfacial tension (IFT) between the non-wetting and wetting fluid [mN/m]

θ Contact angle

r Radius of the cylindrical pore channel

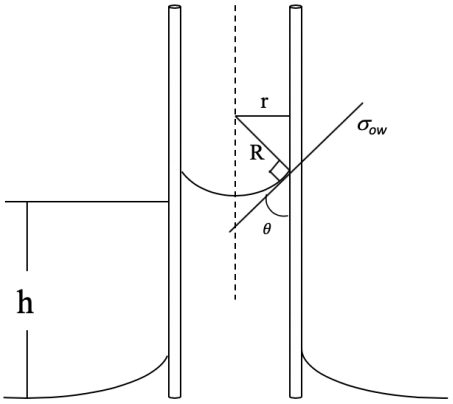

Figure 2.3 Capillary pressure resulting from interfacial forces in a capillary tube. Redrawn after Green and Willhite (1998)

Capillary pressure is related to the interfacial tension between fluids, the relative wettability of the fluids (through θ), and the size of the capillary, r. P_c can be positive or negative, and the sign expresses which phase that has the lowest pressure. The phase with the lowest pressure will preferentially wet the capillary (Green & Willhite, 1998). If the pore channel is narrower the capillary pressure is stronger and the displacement of oil by water will be greater (Zolotukhin & Ursin, 2000).

2.2.3.1 *Capillary entry pressure*

Spontaneous imbibition in heterogenous reservoirs is an important oil recovery mechanism, and the efficiency is controlled by the wettability of the reservoirs. The imbibing fluid must overcome a capillary entry pressure in the porous media to produce oil. The Leverett's capillary pressure function is used for correlation of P_c data, which reflects the pore size distribution, radius of the largest pores, wettability and interfacial tension of the fluids in the system. The capillary entry pressure decreases with reduced IFT, and the imbibing fluid can enter several pores. The entry pressure is calculated by the Leverett J-function, which correlating capillary pressure to water saturation and rock properties, given in equation (2.7) (Craig, 1971; Fanchi, 2010)

$$P_c = \sigma\sqrt{\frac{\phi}{k}}J(S_w)^* \tag{2.7}$$

Where

P_c Capillary pressure [Pa]

σ Interfacial tension [N/m]

ϕ Porosity

k Permeability [m^2]

$J(S_w)^*$ Leverett dimensionless entry pressure ($J^* \approx 0.25$ for a complete water-wet system)

2.2.4 Interfacial tension

When two immiscible fluids coexist in a porous medium the surface energy related to the interface between the fluids is called the interfacial tension (IFT). The term relates to the liquid/liquid and solid/liquid phase boundaries. The interfacial tension will influence the saturations, distributions, and displacement of the fluids (Green & Willhite, 1998). Two fluids are immiscible if the molecules of each fluid are more strongly attracted to their own molecules. This will give a positive interfacial tension ($\sigma > 0$) and the contact area between the fluids are minimized. The magnitude of IFT represents the energy or work required to keep the two fluids separate from each other in a pressure equilibrium state. Stronger intermolecular attractions within a fluid phase, will require more work to bring the molecules to the fluid phase's surface and hence the IFT will be greater (Zolotukhin & Ursin, 2000). The work required to create a new surface area is expressed by equation (2.8):

$$W = \sigma dA \tag{2.8}$$

Where

W Force applied to surface [N]

dA New surface area [m^2]

σ Interfacial tension [N/m]

The interfacial tension will influence the oil recovery. Several EOR processes utilize fluids that are not completely miscible with the oil phase, and the interfacial forces need to be examined to determine their significance for oil recovery (Green & Willhite, 1998).

2.3 Important parameters during waterflooding

Waterflooding is a frequently used injection method and is a significantly reason for the high oil recoveries in many of the largest oilfields. It is important to understand some basic properties of the reservoirs to get a better understanding of the waterflood performance. Porosity, permeability, surface area and pore size distribution are properties of the rock's skeleton, while capillary pressure and relative permeability characteristics are combined rock-fluid properties (Craig, 1971)

2.3.1 Sweep efficiency

Oil recovery in all displacements processes depends on the reservoir volume that is in contact with the injected fluid. Volumetric displacement or sweep efficiency is a quantitative measure of the contact and is donated E_V. The sweep efficiency is a function of time in a displacement process and is defined as the fraction of reservoir pore volume that is invaded by the injected fluid. There are four factors that normally controls how much of the reservoir that will be affected by a displacement process: properties of the injected fluid, i.e. displacing fluid, properties of the displaced fluid, properties and geological characteristics of the reservoir rock and geometry of the injection and production well pattern (Green & Willhite, 1998).

2.3.2 Porosity

Porosity of a reservoir rock is the rock's fluid-storage capacity. Defined as the void part of the total volume of the rock, unoccupied by the rock grains and mineral cement. Absolute porosity is defined as the fraction of the total void volume V_{pa} over the bulk volume V_b, independent of

the distribution of the voids, whether they are interconnected or not. The effective porosity is the ratio of the total volume of interconnected voids V_p to the bulk volume. The porosity is given by equation (2.9), where V is for either absolute or effective porosity.

$$\phi = \frac{V}{V_b} \tag{2.9}$$

Effective porosity is dependent on several factors, including rock type, grain size distribution, packing and orientation, cementation and weathering. Porosity is a static parameter, in comparison to permeability which defines the rock's fluid transmission capacity and relates to conditions where the fluid is moving through the porous media (Zolotukhin & Ursin, 2000).

2.3.3 Permeability

Permeability of a porous media is the media's capacity to transfer fluids through its network of interconnected pores. Permeability is related to the permeable pores of a media and hence directly related to porosity. All factors controlling permeability will also control the porosity and several reservoir rocks have a good correlation between these two properties. Permeability is a constant property of a porous media only if there is a single fluid flowing through the media, hence absolute permeability. When there are more than one fluid present in the system (water, oil, gas), each phases permeability is referred to as their effective permeability. Relative permeability of a fluid is the ratio of its effective permeability to the absolute permeability. (Donaldson & Alam, 2013; Zolotukhin & Ursin, 2000).

The permeability in reservoir rocks can vary from high values in well-sorted sandstones reservoirs (100 to 1000 mD), to low values in tight carbonate reservoirs (1 to 10 mD). An example of a reservoir with even lower permeabilities being exploited commercially for oil production is the Ekofisk field. The fractures in the chalk matrix controls the permeability and increase the oil recovery (Bjørlykke, 2015).

The reservoirs are far from homogenous. The permeability and porosity can be measured in a core plug at the laboratory, but it's not sure that these values are representative for a field scale. Fractures can occur at varying intervals and range in size in a reservoir. Rocks with low permeability and porosity may fracture and sufficiently increase their porosity and especially the permeability, which can form large oil reservoirs. Hence, oil reservoirs can have high

recovery due to low permeability values (Bjørlykke, 2015). Darcy's law describes the laminar flow of fluid through a porous media exposed to a pressure difference, and is used to determine the absolute and effective permeability, given by equation (2.10):

$$q = \frac{KA}{\mu}\frac{dP}{dx} \tag{2.10}$$

Where

q Fluid flow [m^3/s]

K Absolute permeability [m^2]

A Cross-sectional area [m^2]

μ Viscosity [Pa.s]

$\frac{dP}{dx}$ Pressure gradient [Pa/m]

2.3.4 Mobility ratio

Mobility of a fluid flowing through a porous media is defined from the basis of Darcy equation (2.10). For a multiphase fluid flow, it is the effective permeability of the flowing phase, which is a function of the saturation of the phase. For a waterflood, where a piston-like displacement is assumed, the mobility ratio is defined as the mobility of the displacing fluid at average residual oil saturation divided by the mobility of the displaced fluid at irreducible water saturation (Green & Willhite, 1998). The mobility ratio is given by equation (2.11):

$$M = \frac{\lambda_D}{\lambda_d} = \frac{\lambda_w}{\lambda_o} = \frac{\left(\frac{k_{rw}}{\mu_w}\right)_{S_{or}}}{\left(\frac{k_{ro}}{\mu_o}\right)_{S_{wi}}} \tag{2.11}$$

Where

M Mobility ratio

λ_D Mobility of the displacing fluid [m^2/Pa.s]

λ_d Mobility of the displaced fluid [m^2/Pa.s]

λ_w Mobility of water [m^2/Pa.s]

λ_o Mobility of oil [m^2/Pa.s]

k_{rw} Relative permeability of water [m^2]

μ_w Water viscosity [Pa.s]

k_{ro} Relative permeability of oil [m^2]

μ_o Oil viscosity [Pa.s]

S_{or} Residual oil saturation

S_{wi} Irreducible water saturation

Mobility ratio describes the rate and efficiency of oil displacement by other immiscible fluids and is an important parameter in displacement processes. A favorable mobility ratio is generally considered for values less than one, $M < 1.0$. An unfavorable mobility ratio is considered for increasing values, $M > 1.0$. The mobility ratio affects the stability of the displacement process. The flow becomes unstable, and viscous fingering can occur when M is increasing (Donaldson & Alam, 2013; Green & Willhite, 1998). Figure 2.4 illustrates a favorable mobility ratio and an unfavorable mobility ratio.

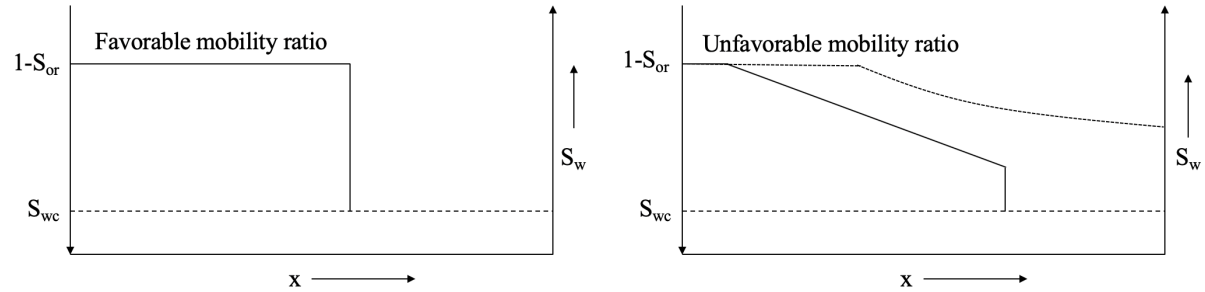

Figure 2.4 (left) a favorable mobility ratio, displacement of oil by water in a water-wet system. A mobile oil bank will develop ahead of the advancing water. (right) an unfavorable mobility ratio, water is capable to travel faster than oil, which will result in discontinuities in the water saturation. Redrawn after Apostolos et al. (2016)

2.3.5 Flow regimes

Flow regimes is related to different boundary conditions, and is identified as: steady-state, pseudo-steady state and transient state, also called unsteady-state. The different flow regimes are identified by the change in pressure with time. At steady state, the mass flow rate and the pressure in the system is constant with respect to time *(dP/dt = 0).* The boundary conditions are given at the constant pressure boundary. Pseudo steady state is applied to a system where the average reservoir pressure and wellbore pressure changes with time. The pressure changes at a constant rate (*dP/dt = constant).* The system is closed, and there is no fluid flow through the boundaries. In the unsteady-state, the pressure changes as a function of time *(dP/dt = f(t)).* The systems have no restrictions for fluid flow and boundary conditions (Fanchi, 2010)

3 Wettability

Wettability is defined as “the tendency of one fluid to spread on or adhere to a solid surface in the presence of other immiscible fluids” (Craig, 1971). A petroleum reservoir, with porous rocks saturated with more than one fluid, is a complex system of mutual static interactions between water, oil, gas and the porous rock. The saturation distribution is controlled by the combined effect of these phenomena, and the fluid contacts in a reservoir are of primary importance during reservoir evaluation and production (Zolotukhin & Ursin, 2000). The wettability is a major factor that controls the location, distribution and flow of fluids in a reservoir, hence it will affect almost all types of core analyses, including relative permeability, capillary pressure, waterflood behavior, electrical properties and simulated tertiary recovery (Anderson, 1986a).

3.1 Wettability classification

In a CBR system the wettability is a measure of which fluid the rock has a preference for, oil or water. It controls the location, flow and distribution of fluids in a reservoir. In a reservoir system that is in equilibrium, the wetting fluid exists in a continuous phase and occupies the smallest pores and the surface of the rock. The non-wetting fluid will be in the middle of the larger pores and form globules that will extend over several pores. The wettability in a reservoir system can change from strongly water-wet to strongly oil-wet, dependent on the specific interactions of rock, oil and brine (Anderson, 1986a).

In a strongly water-wet system, the water will have a tendency to occupy the smallest pores and contact the majority of the rock surface. Oil will be present in the center of the larger pores as droplets resting on a film of water. If the system is waterflooded, the oil will quickly become discontinuous and trapped as droplets in the larger pores. Hence, the reducible oil saturation, S_{or} will increase (Donaldson & Alam, 2013). The strongly water-wet system is illustrated in figure 3.1a.

In a strongly oil-wet system, the location of the fluids is reversed from the water-wet system, hence the oil will occupy the smallest pores and contact the majority of the rock surface. Water will be present in the center of the larger pores. If the water saturation increases during a waterflooding, the water will be located as a continuous phase in the center of the larger pores. If the water saturation decreases, the water droplets will be isolated in the center of the larger

pores resting on a film of oil (Donaldson & Alam, 2013). The strongly oil-wet system is illustrated in figure 3.1b.

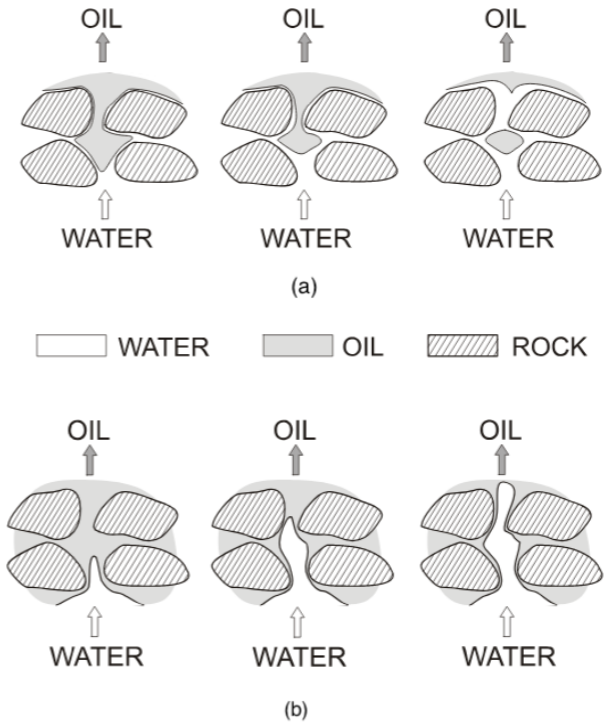

Figure 3.1 Displacement of oil by water for a (a) water-wet rock, and (b) oil-wet rock. Modification of Raza et al. (1968)

The system is said to be of neutral or intermediate wettability if neither of the fluids has a strong tendency to occupy the small pores and contact the majority of the rock surface. Intermediate wettability assumes that all portions of the surface of the rock have a slight but equal preference to be water- or oil-wet. Strongly and intermediate wettability is classified to be homogenous (uniform) wettability (Anderson, 1986a).

There is also a third type of wettability called fractional wettability. Different areas of the rock core have different wetting preferences (Anderson, 1986a). Fractional wetting characterizes heterogenous wetting of the surface in a porous rock where the preferential wetting is randomly distributed throughout the porous media. The random distribution of minerals exposed to the surface in the pores causes the system to be either preferentially water-wet or oil-wet, and there are no continuous oil networks through the rock (Donaldson & Alam, 2013). Another term of wettability which implies specific locations for the oil-wet surface are the mixed wettability, which was first defined by Salathiel (1973). The smallest pores in the porous rock are water-wet, while the larger pores are oil-wet and filled with a continuous oil-phase which are in

contact with the pore walls. During waterflooding, the oil in the larger pores would be displaced and no or little oil would be held by capillary forces in the small pores due to the water-wet state. Hence, very low residual oil saturations are observed in mixed-wet systems (Salathiel, 1973).

3.2 Wettability measurements methods

Reservoir wettability is not a simply defined property, and characterization of the wettability in a system is complex. Several methods for measuring the wettability from strongly water-wet to strongly oil-wet have been proposed. They include quantitative- and qualitative methods. Morrow (1990) pointed out that the relationship between wettability and capillary displacement pressures are complicated by the inhomogeneous pore structure and the effect of adsorbed organic components in the crude oil (Morrow, 1990)

3.2.1 Contact angle

The wettability in a reservoir rock can be estimated by measuring the contact angle between the two immiscible fluids interface and the rocks surface. The contact angle ranges from 0-180°. Wettability measurements with contact angle is a quantitative method and is the best method when there are only pure fluids and artificial cores, then no other compounds like surfactants can altering the wettability. Contact angle measurements is also used to determine if crude oil can alter the wettability and check the effect of pressure, temperature and brine chemistry on wettability. There are several methods of contact-angle measurements, such as vertical rod method, sessile drops or bubbles, tilting plate method, tensiometric method, cylinder method and capillary rise method. The sessile drop method is most common in the petroleum industry (Anderson, 1986b).

The contact angle is measured through the water. The system is preferentially water-wet if the contact angle is less than 90°. Hence, if the angle is greater than 90°, then the system is preferentially oil-wet. The system is neutral-wet when the contact angle is equal to 90°. Figure 3.2 illustrates wettability of the oil/water/rock system. The surface energies in the system are related to Young's equation, given by equation (3.1):

$$\sigma_{ow} cos\theta = \sigma_{os} - \sigma_{ws} \qquad (3.1)$$

Where

σ_{ow} Interfacial tension between the oil and water

σ_{os} Interfacial tension between oil and solid

σ_{ws} Interfacial tension between water and solid

θ Contact angle, the angle of the water/oil/solid contact line

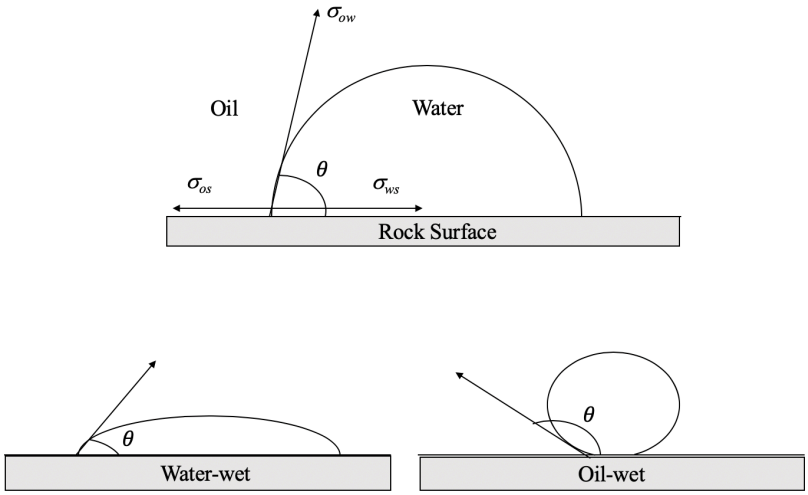

Figure 3.2 Wettability of the oil/water/rock system. Redrawn after Anderson (1986b)

3.2.2 Amott method

The Amott method presented by Amott (1959), combines imbibition and forced displacement to measure the average wettability of a core sample. Reservoir core samples and reservoir fluids can be used in the test. The wetting fluid will spontaneously imbibe into the core and displace the non-wetting fluid. The relationship between spontaneous and forced imbibition is used to reduce the influence of other considerations, like relative permeability, viscosity and the initial saturation of the core (Anderson, 1986b).

The test results are described by two different wettability indices. The wettability index to water I_w, "displacement-by-water ratio" is given as the ratio of oil volume displaced by spontaneous imbibition of water to the total volume displaced by spontaneous and forced imbibition. Likewise, the wettability index to oil I_o, "displacement-by-oil ratio" is given as the ratio of water volume displaced by spontaneous imbibition of oil to the total volume displaced by spontaneous and forced imbibition (Anderson, 1986b). In a strongly preferentially water-wet

core the water wettability index will approach one, and the oil wettability index will approach zero. For a strongly preferentially oil-wet core, the results will be reversed (Amott, 1959). The two indices are represented by equation (3.2) and (3.3):

$$I_w = \frac{\Delta S_{ws}}{\Delta S_{ws} + \Delta S_{wf}} \tag{3.2}$$

$$I_o = \frac{\Delta S_{os}}{\Delta S_{os} + \Delta S_{of}} \tag{3.3}$$

Where

ΔS_{ws} Saturation change during spontaneous imbibition of water

ΔS_{wf} Saturation change during forced imbibition of water

ΔS_{os} Saturation change during spontaneous imbibition (drainage) of oil

ΔS_{of} Saturation change during forced imbibition (drainage) of oil

The Amott-Harvey method is a modification of the Amott wettability test. Figure 3.3 illustrates a complete test cycle for the Amott-Harvey method which are divided into five segments:

1. Primary drainage of water by oil to establish initial water saturation, S_{wi}.
2. Spontaneous imbibition of water
3. Forced imbibition of water
4. Spontaneous imbibition (drainage) of oil
5. Forced imbibition (drainage) of oil

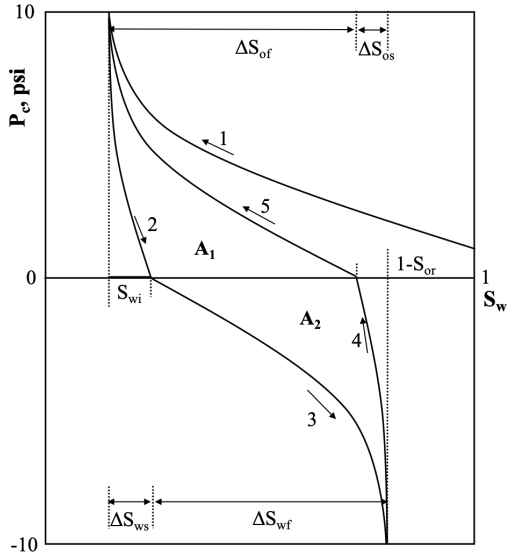

Figure 3.3 Capillary pressure curves for different wettability tests; Amott and USBM. Redrawn after Morrow (1990)

The Amott-Harvey method gives a relative displacement index I_{AH}, which characterize the wettability by a single number (Morrow, 1990). The relative displacement index is the difference between the two indices, I_w and I_o, shown in equation (3.4):

$$I_{AH} = I_w - I_o \tag{3.4}$$

The wettability index, I_{AH} varies from +1 for a complete water-wet system, to -1 for a complete oil-wet system. Cuiec (1984) supplemented the index range, by stating that the system is water-wet when $+0.3 \leq I_{AH} \leq 1$, intermediate wet when $-0.3 \leq I_{AH} \leq 0.3$, and oil-wet when $-1 \leq I_{AH} \leq -0.3$. The major disadvantages by using the Amott wettability test and its modification is that they are insensitive to near neutral wettability. The test measures the wettability easily for strong wettability's, but for a neutral-wet system neither of the fluids will easily spontaneously imbibe and displace the other fluid when the contact angle varies roughly from 60 to 120° (Anderson, 1986b).

3.2.3 United states bureau of mines (USBM) method

The USBM method is a quantitative wettability test which measures drainage and imbibition capillary pressures, usually by centrifuge (Morrow, 1990). The test can also measure the average wettability of the core. The method compares the work required for one fluid to displace the other fluid. The necessary work for the wetting fluid to displace the non-wetting fluid in a core sample is less than the work required for the reversed displacement, because of the favorable free-energy change. For a water-wet core, the area under the water-drive capillary pressure curve, i.e. when water displace oil, is smaller than the area under the capillary pressure curve for the opposite displacement. The water-wetting is strong enough, and the water will imbibe spontaneously into the core, hence the area under the water-drive curve will be very small.

The method is based on the ratio of areas under the two capillary pressure curves to calculate a wettability index I_{USBM}, given by equation (3.5):

$$I_{USBM} = \log\left(\frac{A_1}{A_2}\right) \tag{3.5}$$

Where A_1 and A_2 are the areas under the oil- and water-drive curves, respectively. The areas are illustrated in figure 3.3. The core is water-wet when I_{USBM} is greater than zero, and when I_{USBM} is less than zero, the core is oil-wet. The wettability index is close to zero for a neutral-wet system. The larger absolute value of the wettability index, the greater the wetting preference (Anderson, 1986b). Compared to the Amott test, the USBM test is sensitive near neutral wettabilities, which is a major advantage. But the test cannot determine if the system is either fractional- or mixed-wet. A major disadvantage is that the wettability index can only be measured at core plug sample sizes, due to measurements by centrifuge (Anderson, 1986b).

3.2.4 Spontaneous imbibition

Spontaneous imbibition is the most frequently used qualitative wettability measurement method. The test gives an instantaneous but rough idea of the wettability, and do not require any complicated equipment (Anderson, 1986b). The method measures the rates of a spontaneous imbibition, and the driving force for the rates are proportional to the imbibition capillary curves (Morrow, 1990). The core is strongly water-wet if a great volume of water rapidly imbibes into the porous media and produce the oil. The water saturation increases until the capillary pressure becomes zero (Milter, 1996). Lower rates and smaller volumes imply a less water-wet core. For a strongly oil-wet core, the oil will imbibe into the core and produce water. The preference of oil-wetness is indicated by the rate and volume of oil imbibition. The core is neutral-wet if there is no imbibition of water or oil. Some cores will imbibe both water and oil and are said to have either fractional or mixed wettability. In addition to wettability, the imbibition rates also depend on viscosity, relative permeability, pore structure, IFT and the initial saturation of the core. The dependency is reduced by comparing the measured imbibition rate with a reference rate measured for a strongly water-wet core (Anderson, 1986b).

The water wetness by spontaneous imbibition could be quantified for a specific core when the results from a completely very water-wet reference core exists. Equation (3.6) represents a simplified wetting index that is only based on SI experiments (Torrijos et al., 2019).

$$I_w^* = \frac{\%R}{\%R_{ww}} \tag{3.6}$$

Where

$\%R$ Recovery by SI for specific case

$\%R_{ww}$ Recovery by SI for a very water-wet reference core

The degree of water wetness is specified by the wetting index. If I_w^* approaches 1, the core is said to be strongly water-wet, but if it approaches 0 the core is said to be fractional/neutral wet.

3.2.5 Chromatographic wettability test

The chromatographic wettability test method was developed by Strand et al. (2006) for measuring the fraction of water-wet surface area of chalk cores. The method is based on the chromatographic separation between two-water soluble components, sulfate (SO_4^{2-}) and tracer (thiocyanate, SCN^-) during core flooding. The sulfate ions adsorb on the surface of the water-wet core due to higher affinity towards the water-wet surface. While the tracer will act as a non-adsorbing agent due to no affinity for the water-wet surface. Initially, the oil-saturated chalk core is flooded to residual oil saturation (S_{or}) with a seawater brine without SO_4^{2-} and SCN^-. Then, a seawater brine containing equal amounts of SO_4^{2-} and SCN^- is injected into the core. The effluent is sampled in fractions and analyzed for ionic compositions of SO_4^{2-} and SCN^-. Relative concentration of SO_4^{2-} and SCN^- is plotted against pore volume injected. Figure 3.4 illustrates the chromatographic separation between SO_4^{2-} and SCN^-.

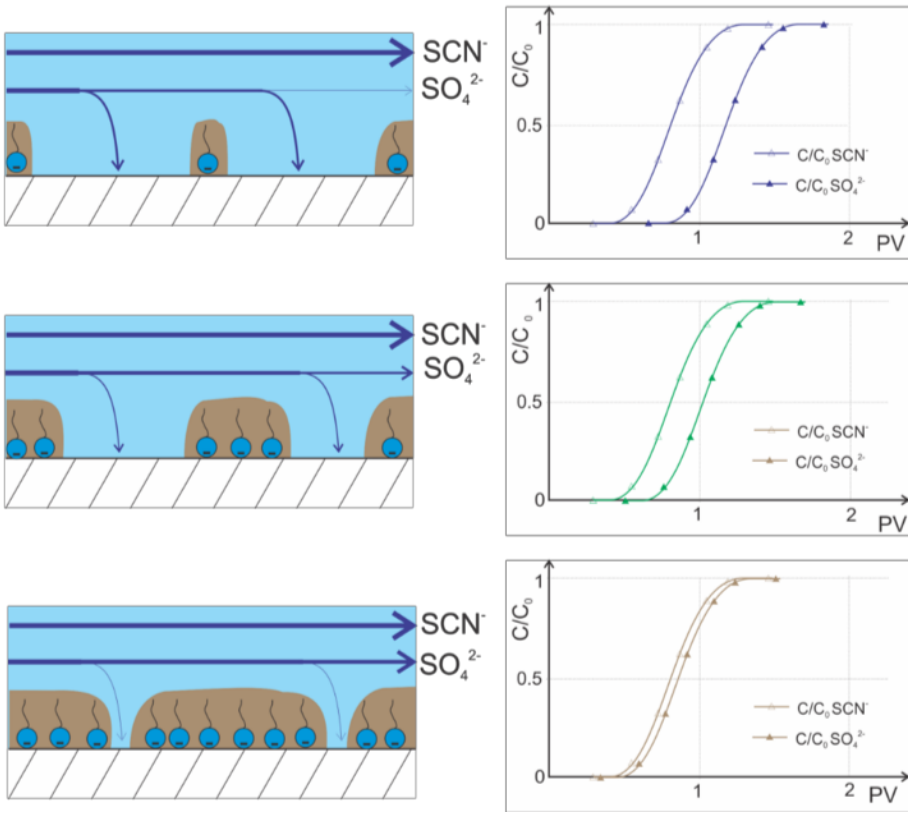

Figure 3.4 Illustration of the chromatographic separation of SO_4^{2-} and SCN^- for a preferential water-wet, mixed-wet and oil-wet core (Strand et al., 2006b)

The area between the effluent ion concentration curves, $A_{Wett,}$ is proportional to the area for the water-wet surface, $A_{Heptane}$, and defines the wetting index, (WI). The wetting index is given by equation (3.7):

$$WI = \frac{A_{Wett}}{A_{Heptane}} \tag{3.7}$$

Where

A_{Wett} Area between the thiocyanate and sulfate curves generated by flooding a core aged in crude oil

$A_{Heptane}$ Reference area between thiocyanate and sulfate curves generated by flooding a core assumed to be strongly water-wet (saturated with heptane)

According to the definition of WI, the wettability is classified as:

$WI = 1.0$ represents a completely water-wet system

$WI = 0.5$ represents a neutrally wetted system

$WI = 0.0$ represents a completely oil-wet system

The area between the two curves is determined by subtraction of the area under each curve which are calculated by the trapeze method. The chromatographic wettability test method is time efficient and excellent for neutral wetting conditions, which will give a wetting index of 0.5, and is often the case for carbonates. A disadvantage is that one need a representative water-wet core as reference, which was available when the method was developed and verified on outcrop chalk cores (Strand et al., 2006b).

3.3 Effect of wettability on core analyses

Anderson (1986a) have performed several studies about the effect of wettability on core analyses. He observed that the wettability will affect relative permeability, capillary pressure and waterflood behavior, because wettability is an important factor that controls the location, flow and distribution of fluids in a porous system (Anderson, 1987a; Anderson, 1987b; Anderson, 1987c).

3.3.1 Effect of wettability on relative permeability

The concept relative permeability is introduced when there are more than one fluid present in the porous media, and is a "direct measure of the ability of the porous system to conduct one fluid when one or more fluids are present" (Anderson, 1987a; Craig, 1971). Relative permeability relates absolute permeability of a porous media, to the effective permeability of a particular fluid that only occupies a fraction of the total pore volume in the system. The relative permeabilities for water and oil is shown in equation (3.8) and (3.9)

$$k_{rw} = \frac{k_w}{k} \tag{3.8}$$

$$k_{ro} = \frac{k_o}{k} \tag{3.9}$$

Where

k_{rw} Relative permeability of water [m^2]

k_w Effective permeability of water [m^2]

k Absolute permeability of a porous media [m^2]

k_{ro} Relative permeability of oil [m^2]

k_o Effective permeability of oil [m^2]

Relative permeability is a strong function of the wetting phase saturation. Wettability affects relative permeability by regulating the distribution of immiscible fluids. When the wettability in a system is varied from water-wet to oil-wet, the relative permeability of oil will increase while the relative permeability of water will decrease. The crossover saturation illustrated in figure 3.5 will move from lower to higher water saturations (Donaldson & Alam, 2013). In general, there is no correlation between relative permeability and fluid properties, but when certain properties change, like IFT, then the relative permeability can be affected. Relative permeabilities for a water-oil system is illustrated in figure 3.5. The left figure illustrates a strongly-water wet system, and the right figure illustrates a strongly oil-wet system (Zolotukhin & Ursin, 2000).

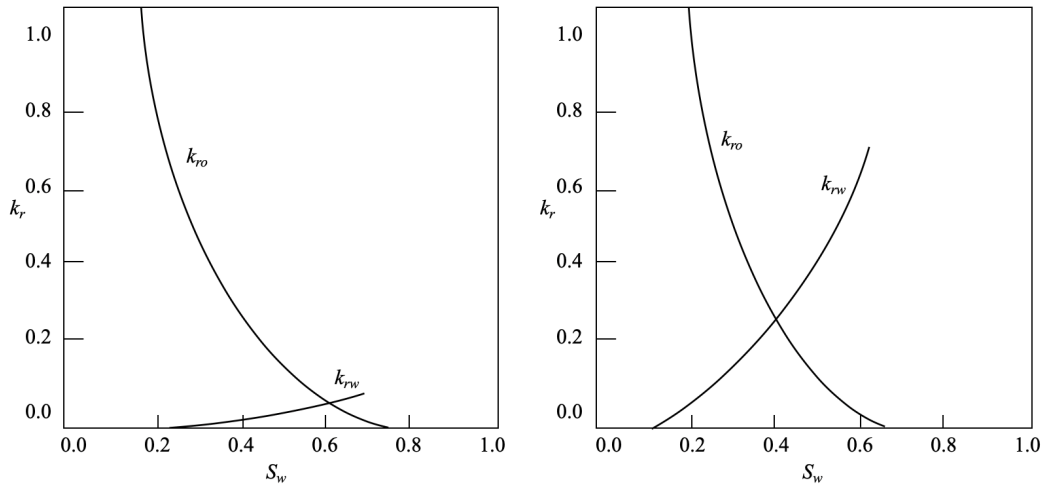

Figure 3.5 Characteristics of typical relative permeability curves for a two-phase flow, where S_w is the wetting phase. (Left) a strongly water-wet formation and (right) a strongly oil-wet formation. Redrawn after Craig (1971)

Craig (1971) introduced general rules to differentiate between the strongly water-wet and strongly oil-wet systems. The three rules are as follows:

1. Connate water saturations are usually greater than 20-25% PV (pore volume) in a water wet-rock and less than 10% PV in an oil-wet rock.
2. Water saturation (S_w) at which water relative permeability (k_{rw}) and oil relative permeability (k_{ro}) are equal (crossover saturations) are usually greater than 50% for water-wet cores and less than 50% for oil-wet cores.
3. The relative permeability to water at maximum water saturation (i.e. floodout) is usually less than 30% in water-wet rocks, but from 50-100% in oil-wet rocks.

The endpoint saturations for the relative permeability curves are generally less than one and are the measures of the wettability. For water, the endpoint saturation is the irreducible water saturation, S_{wir}. For oil, the endpoint saturation is the residual oil saturation, S_{or}. The non-wetting phase is trapped in isolated globules in the center of the pores, while the wetting phase occupies the cavities between the rock grains and cover the surface of the rock. The trapped non-wetting phase is a bigger disincentive for the wetting phase than vice versa. Hence, the wetting phase endpoint relative permeability is less than the non-wetting phase endpoint. For example, water relative permeability is higher in an oil-wet system than in a water-wet system, as shown in figure 3.5. The ratio between the phases is a good indication of the wettability of the system (Anderson, 1987a; Fanchi, 2010; Zolotukhin & Ursin, 2000).

3.3.2 Effect of wettability on capillary pressure

There are two fundamental displacement processes in a capillary system; drainage and imbibition. During a drainage process, the non-wetting phase displaces the wetting phase, while for an imbibition process the reverse occur, the wetting phase displaces the non-wetting phase. An example of an imbibition process is waterflooding of oil in a water-wet reservoir. When the saturation changes in a core, a hysteresis in capillary pressure will occur and the drainage and imbibition curves become different. A drainage curve is established by reducing the maximum saturation of the wetting fluid to irreducible minimum by increasing the capillary pressure from zero to a great positive value. An imbibition curve is established by increasing the saturation of the wetting fluid (Anderson, 1987b; Donaldson & Alam, 2013) Figure 3.6 illustrates the capillary pressure curves in a (left) strongly water-wet system and (right) strongly oil wet system. The area under the curves represents the work required for the displacement of oil and water.

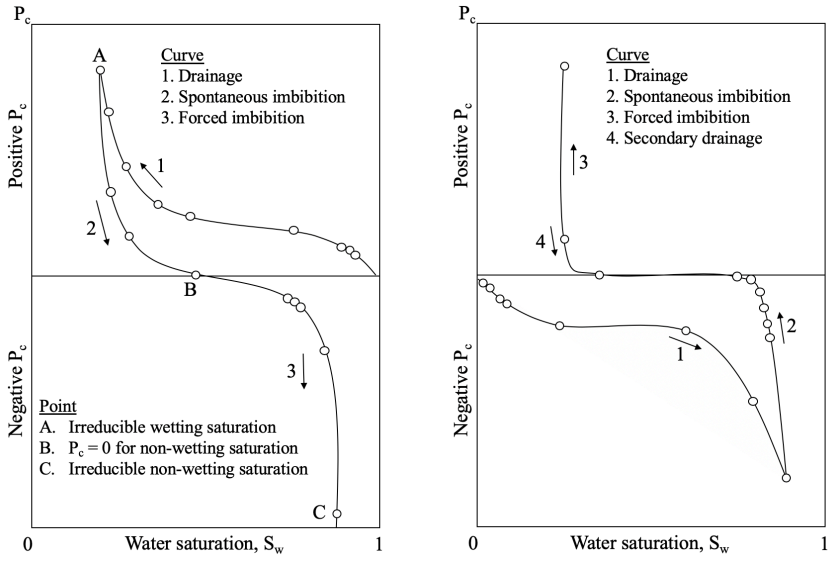

Figure 3.6 Oil/water capillary pressure curves measured in a (left) strongly water-wet system and (right) strongly oil-wet system. Redrawn after Anderson (1987b)

Figure 3.6 (left) represents a water-wet system. Curve number one, a drainage curve, is first measured by gradually increasing P_c from zero to a large positive value, and hence the water saturation is reduced. The imbibition curve (two and three) is divided into two distinctly different portions. First a spontaneous imbibition curve is measured after the drainage curve. P_c at a high positive value decreases to zero, and the wetting fluid is allowed to imbibe. The residual saturation of the non-wetting fluid is reached at $P_c = 0$. Little or no work must be done during an imbibition process when the wetting fluid displaces the non-wetting fluid, due to the

favorable free energy change. A forced imbibition curved is followed after the SI-curve. $P_c = P_o - P_w$ decreases from zero to a negative value, hence the pressure in wetting phase is larger than the pressure in the non-wetting phase which will force water into the system.

Figure 3.6 (right) represents an oil-wet system, where oil is the strongly wetting fluid. The performance of water and oil are reversed from the strongly water-wet system. Oil will spontaneously imbibe into the core. During forced imbibition, P_c is increased to a large positive value, and additional oil is forced out of the core. The drainage and SI capillary curves have negative P_c values, while the forced imbibition curve is positive. Also and additional secondary drainage curve is added to the system which illustrates that no water is imbibed to the system since the capillary pressure is reduced to zero (Anderson, 1987b).

3.3.3 Effect of wettability on waterflooding

Waterflooding is a frequently used secondary recovery method where water is displacing oil. However, it behaves very differently in water-wet and oil-wet reservoirs and is more efficient in water-wet reservoirs, due to the wetting fluid. A waterflood in a strongly water-wet reservoir will give high oil recoveries before water breakthrough, and little residual oil. The water will imbibe into small and medium sized pores and displace the oil into larger pores where it is easily recovered. In the pores where both water and oil are flowing, the oil will either exists in continuous channels or trapped in discontinues globules. When the displacing waterfront has passed almost all of the remaining oil becomes immobile. In a strongly oil-wet system, the water breakthrough will occur earlier and the oil production is less efficient with simultaneously production of oil and water (Anderson, 1987c).

McDougall and Sorbie (1995) have studied the effect of waterflooding in fractional-wet and mixed-wet systems. In these systems, the small pores are water-wet while the larger pores are oil-wet and filled with oil droplets. This situation may occur when oil migrates into systems that were initial water-wet and whereas the oil fills the larger pores. Wettability is altered to be less water-wet due to adsorption of polar organic components and making the larger pores oil-wet. During the study, it was found that the most efficient displacement takes place in a system that contains 50% oil-wet pores, i.e. mixed-wet systems. Compared to the other two classical strong wettability systems, the water breakthrough will be later than for an oil-wet system but earlier than for a water-wet system. However, the overall oil production is largest in a mixed-wet system, due to the distribution of oil and water in the pores. A larger volume of water will

imbibe into the pores, compared to a water-wet system, and displace the oil. A forced displacement is followed after the imbibition and hence water is forced into the larger oil-wet pores (Donaldson & Alam, 2013; McDougall & Sorbie, 1995). Figure 3.7 illustrates oil recovery with different wettability.

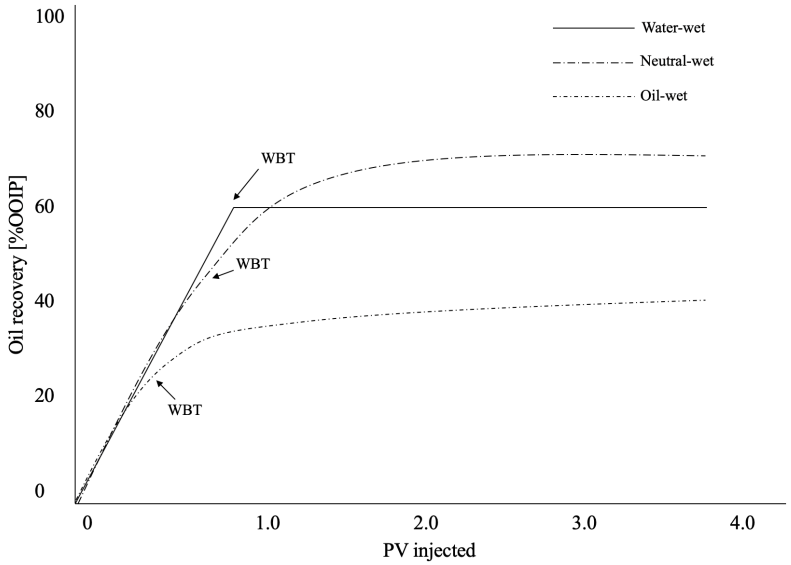

Figure 3.7 Idealized production from three different conditions of wettability. Redrawn after Donaldson and Alam (2013)

The effect of wettability on oil production can be summarized by having three different conditions of wettability. The water-wet system has a piston-like displacement before water breakthrough which occurs approximately at 1 PV of water injected. The neutral-wet or mixed-wet system will have an earlier water breakthrough, due to fingers of water in front of the production. However, the production of water and oil continues, and the residual oil saturation is less than for the water-wet system. For the oil-wet system, the water breakthrough occurs almost immediately compared to the water-wet system, and the residual oil saturation is also greater (Donaldson & Alam, 2013)

4 Carbonate reservoirs

Carbonate reservoirs accounts for approximately 50% of the world proven reserves. However, the average oil recovery factor is less than 30% worldwide, which is significantly less than for sandstones (Austad et al., 2007; Bjørlykke, 2015). Carbonate reservoirs are characterized as naturally fractured and heterogenous, due to a wide variation in permeability and porosity (Lucia, 2007). According to literature data, many of the carbonate reservoirs have a negative capillary pressure, i.e., they are preferentially oil-wet. The oil recovery factor is improved by two main mechanisms; wettability alteration and interfacial tension reduction. The most important phenomenon in oil recovery is spontaneous imbibition, and especially in fractured reservoirs. Water may imbibe spontaneously into the porous media in water-wet to mixed-wet formations, and the capillary forces are increased due to improved water wetness. In the oil-wet formations, the process may not be possible due to the negative capillary forces. The injected water will flow in the high permeable fractures which will cause early water breakthrough and low oil recovery. However, the comprehensive IOR potential of these reservoirs is very high (Alotaibi et al., 2010; Austad, 2013; Høgnesen et al., 2005). Waterflooding is a widely used IOR method, but an increased oil recovery is strongly dependent on the wetting properties of the rock (Puntervold et al., 2007b).

4.1 Carbonate rocks

Carbonates are sedimentary rocks composed of organic materials which consists of altered plankton remains or plant debris. Sedimentary rocks consist of fragments, also called clastic materials. The fragments are derived from weathering or erosion processes of older rocks. A sedimentary rock that consists of fragments of skeletal parts or shells of dead organisms which has not been fully homogenized by chemical processes are introduced as bioclastic (Zolotukhin & Ursin, 2000). The most common carbonate rocks are limestone and dolomite (Marshak, 2011).

The carbon sediments are a component of the carbon cycle and consist of the anion complex CO_3^{2-}, and one or more cations. Carbon dioxide (CO_2) from the atmosphere dissolves in water (H_2O) and forms carbonic acid (H_2CO_3). The carbonic acid reacts with for example calcium (Ca^{2+}) or magnesium (Mg^{2+}) and precipitate the sediments, calcite ($CaCO_3$) and magnesite ($MgCO_3$). The rate of sedimentation is globally controlled of the extent of cations (mostly Ca^{2+} and Mg^{2+}) into oceans from rivers, which again are controlled of the weathering of Ca^{2+} bearing

silicate minerals like plagioclase. The most common forming carbonate minerals are calcite ($CaCO_3$), aragonite ($CaCO_3$), siderite ($FeCO_3$), magnesite ($MgCO_3$), anhydrite or gypsum ($CaSO_4$), dolomite ($CaMg(CO_3)_2$) and ankerit ($Ca(Mg,Fe)CO_3)_2$) (Bjørlykke, 2015).

Most of the limestones are of bioclastic source, and chalk is classified as a bioclastic limestone (Zolotukhin & Ursin, 2000). Chalk is an important reservoir rock in the southern part of the North Sea, and it is identified as fine-grained with low permeability (1-4 mD) and high porosity (35-50%) (Korsnes et al., 2008). Chalk consist of small calcareous skeletal parts of pelagic coccolithophorid algae, called coccoliths and a small percentage of foraminiferal material (Milter, 1996). The coccolithophorid algae consists of numerous spherical coccospheres. These are built up of coccolithis ring structures which consists of ring fragments or platelets composed of calcite crystals. The diameter of the coccolithophorid algae and coccospheres ring varies from 2-20 µm and 3-15 µm (Puntervold, 2008). Figure 4.1 (a) is a Scanning Electron Microscopy (SEM) photo, which illustrates coccolithis ring and ring fragments, (b) presents pore size distribution in Stevns Klint (SK) outcrop chalk material.

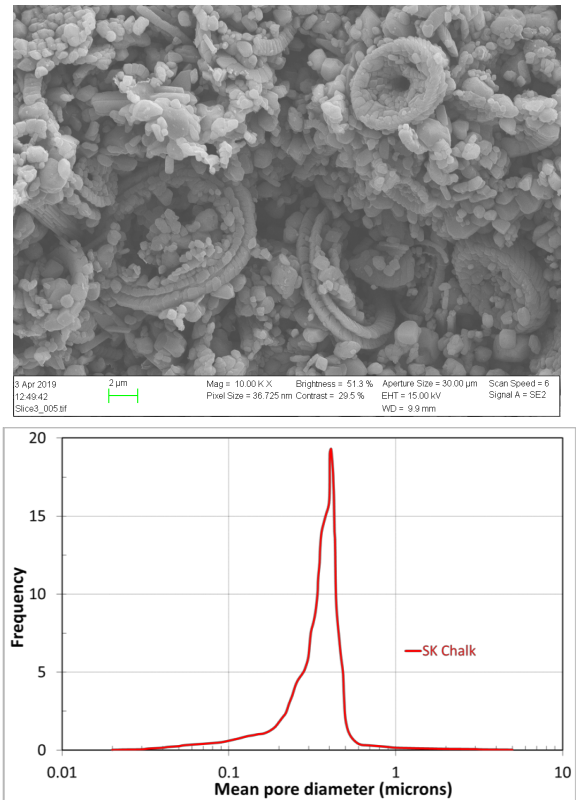

Figure 4.1 (a) Scanning Electron Microscopy (SEM) picture of Stevns Klint outcrop material (Smart Water EOR group spring 2019). (b) Pore size distribution in SK chalk, redrawn from (Milter, 1996)

4.1.1 Smart Water EOR processes in carbonates

When water with a different composition from the formation water is injected into a carbonate reservoir, the established equilibrium in the CBR system will change. Hence, the oil recovery may increase significantly. Seawater is an excellent injection fluid for EOR processes in heterogenous chalk reservoirs. The ion composition is adjusted or optimized in such a way that it will change the equilibrium of the initial CBR system and modify the initial wetting conditions to a more water-wet state. The microscopic sweep efficiency will increase, and more oil is recovered. Smart Water EOR processes has a positive effect on the capillary forces and relative permeability of oil and water during oil recovery processes (Austad, 2013; Zhang et al., 2007). Figure 4.2 illustrates the increased oil recovery by Smart Water injection compared to spontaneous imbibition and viscous flooding (VF) of formation water.

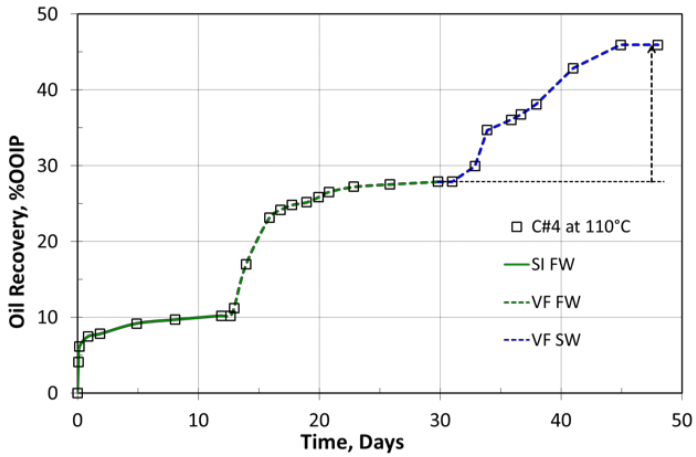

Figure 4.2 Oil recovery from a chalk core by spontaneous imbibition of FW, viscous flooding using FW and finally viscous flooding using SW (Strand et al., 2008)

Seawater contains the potential determining ions Ca^{2+}, Mg^{2+} and SO_4^{2-} which is reactive against the chalk surface. The ions are important for wettability alteration processes in carbonates. Sulfate present in seawater will adsorb on the positively charged carbonate surface and lower the positive surface charge. Then, Ca^{2+} can react with the adsorbed negatively carboxylic group which are bonded to the positive carbonate surface, and release some of the organic material from the rock surface. At high temperatures, Mg^{2+} will be more active and can substitute Ca^{2+} at the surface, which will react with the carboxylic group. (Austad, 2013; Fathi et al., 2011). The surface charge in the chalk cores will become less positive and hence become more water-wet. Positive capillary forces will be developed, and water will spontaneously imbibe into the

cores and produce oil (Zhang & Austad, 2006). Figure 4.3 illustrates the wettability alteration process in chalk cores by smart water.

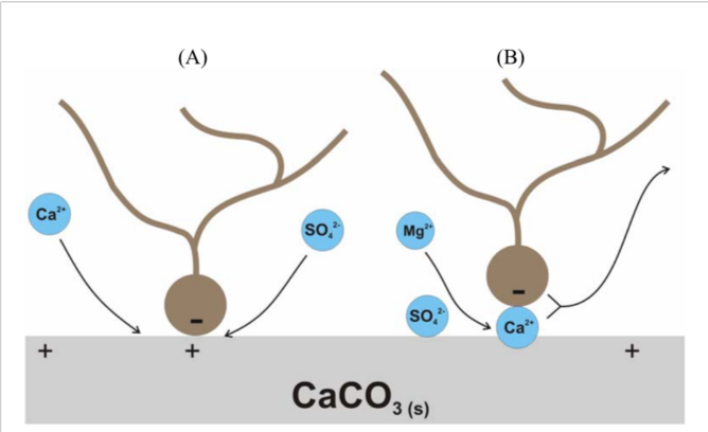

Figure 4.3 Schematic model of the mechanism for the wettability alteration induced by seawater. (A) Ca^{2+} and SO_4^{2-} are active at lower temperature. (B) Mg^{2+}, Ca^{2+} and SO_4^{2-} are active at higher temperatures (Zhang et al., 2007)

The amount of non-active salt (NaCl) present in the injected seawater also have an impact on the oil recovery processes. Studies showed that both the imbibing rate and the ultimate recovery changed dramatically by removing NaCl from the synthetic seawater compared to the ordinary seawater. When the NaCl concentration in the injected seawater is reduced, the access of the active ions (SO_4^{2-}, Ca^{2+} and Mg^{2+}) on the rock surface will increase and hence the wettability alteration process will be improved (Austad et al., 2011; Fathi et al., 2011).

4.1.2 Initial wetting in carbonates

Initially in a reservoir, a thermodynamic equilibrium has been established between the rock, formation water and oil through millions of years (RezaeiDoust et al., 2009). The surface charge is dependent on the ion composition in the formation water. At reservoir conditions, the carbonate rocks have a positively charged surface due to a large concentration of Ca^{2+} in the formation water (Høgnesen et al., 2005). Some formation waters contain also the ion SO_4^{2-}. Sulfate is for example found in formation waters in carbonate reservoirs which contain the rock mineral anhydrite. Ca^{2+} and SO_4^{2-} are strong potential determining ions towards the chalk surface, and they will have a great influence on the surface charge of the rock. Figure 4.4 presents the zeta potential, the surface charge of the Stevns Klint chalk cores with Ca^{2+} and SO_4^{2-} present in the equilibrium brine.

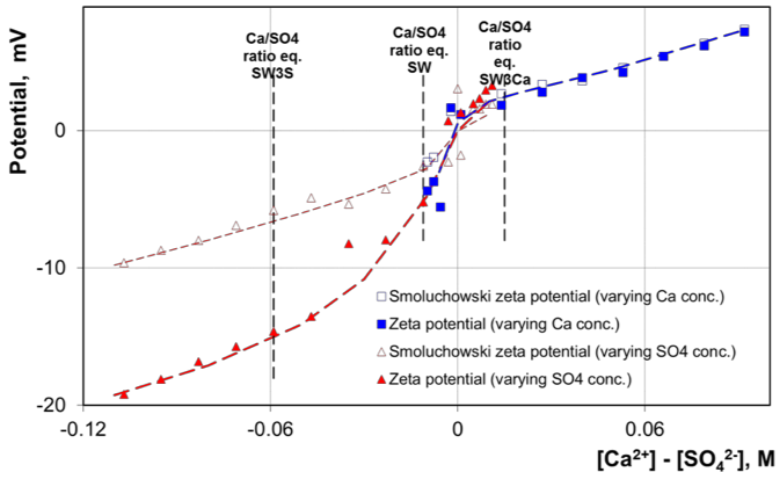

Figure 4.4 Zeta potential of the chalk core with potential determining ions present in the seawater (Strand et al., 2006a)

High concentrations of SO_4^{2-} will give a negatively surface charge while high concentrations of Ca^{2+} will give a positively surface charge. If the concentrations are equal, the surface charge will most likely be neutral (Strand et al., 2006a).

The carboxylic material in crude oil is the most important wetting parameter for carbonate CBR systems. The crude oil components with the negatively charged carboxyl group, $-COO^-$ will adsorb to the carbonate surface. The bond between the positively charged carbonate surface and the negatively charged carboxyl group $-COO^-$ is very strong, and the large molecules will cover the surface of the carbonate rock (Austad, 2013). Figure 4.5 presents a study of Mjøs et al. (2018) about adsorption of polar components in SK chalk material.

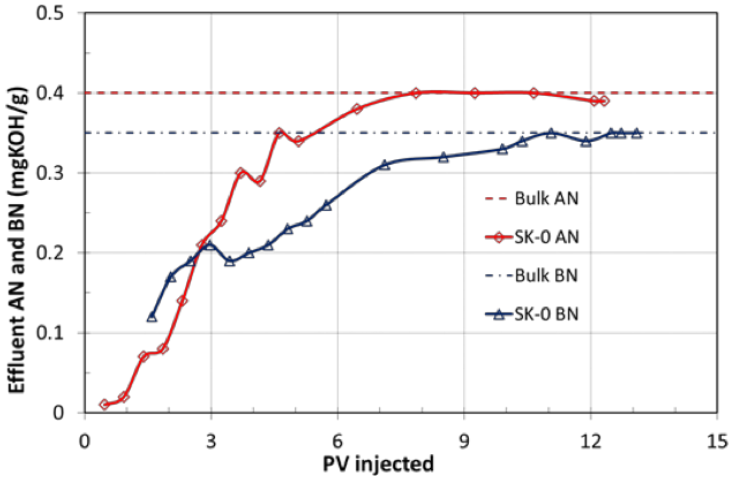

Figure 4.5 AN and BN measurements of effluent crude oil samples during 15 PV of Res 40-0.4 flooding of SK chalk core at Swi=0%. The core is flooded in one direction at rate of 4 PV/day (Mjøs et al., 2018)

With no brine initially in the system, the surface accessibility of negatively charged polar components are high, and they adsorb almost immediately. After 8 PV injected an equilibrium plateau of flowing crude oil and adsorbed crude oil on the chalk surface has been reached. At this point the carbonate surface is then believed to have mixed wettability or to be oil-wet (Alotaibi et al., 2010; Mjøs et al., 2018). Clean outcrop SK chalk cores are naturally water-wet, but the crude oil may fracture the water-film and the surface-active components of the crude oil ($-COO^-$) will adsorb to the rock surface resulting in a less water-wet rock.

Wettability is dependent on the nature of the solid and the fluid properties, both oil and initial formation water. Carbonate rocks also becomes more water-wet as the temperature in the reservoir increases, but the most important factor for the wetting properties is the acid content (Høgnesen et al., 2005). The carboxylic material in the crude oil is determined by the acid number (AN) and the polar organic bases are determined by the base number (BN) in mgKOH/g. The wettability of carbonate rocks is strongly related to the acidic material present in crude oil. When the AN of the crude oil increases, the imbibition rates and oil recovery decreases. Higher AN will result in more adsorption of carboxylic components onto the chalk surface and decrease the water-wetness of the rock (Puntervold et al., 2007b). Figure 4.6 illustrates lower oil recovery with increasing AN of the crude oils.

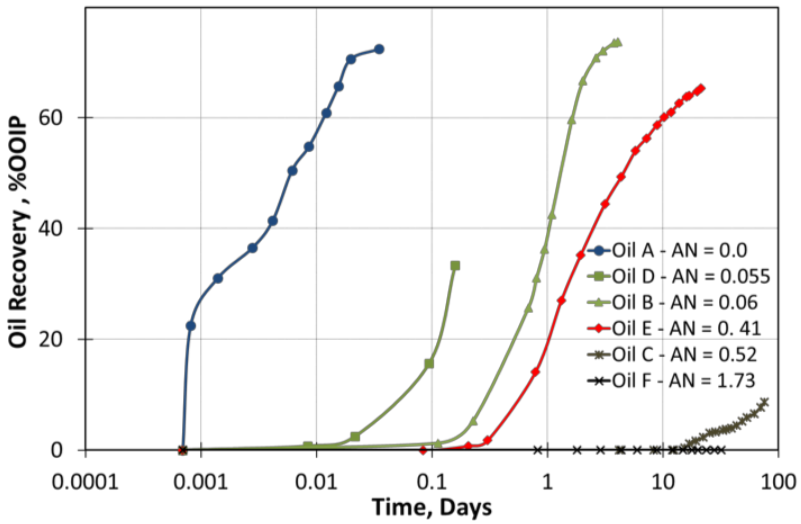

Figure 4.6 Spontaneous imbibition of brine into chalk cores saturated with crude oils with different AN number at 40°C (Standnes & Austad, 2000)

Puntervold (2008) studied the effect of basic components on chalk wettability. In order to study the effect, a varying AN:BN ratio was utilized where BN was varied while the AN was kept constant during the experimental work. When the base content in the oil increased, the water-wetness of the rock slightly increased. Acid-base complexes is formed on the rock surface which will prevent adsorption of carboxylic material, resulting in a more water-wet rock. Figure 4.7 illustrates increased oil recovery versus time with increasing BN.

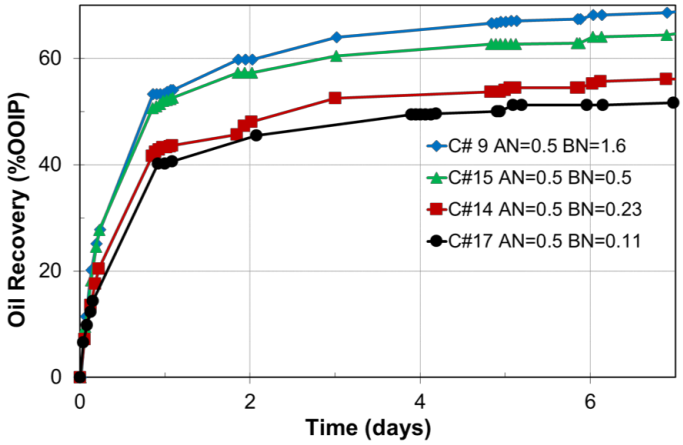

Figure 4.7 Spontaneous imbibition experiments with the effect of bases in crude oil. Increasing oil recovery versus time with increasing BN (Puntervold, 2008)

Shariatpanahi et al. (2016) studied the effect of DI-water (deionized water) as both formation water and brine imbibition fluid in waterflooding experiments. Highest adsorption of polar components by using DI-water was observed, hence the water-wetness is reduced with DI-water. Figure 4.8 presents oil recovery by spontaneous imbibition from SK chalk cores with injection brines with different cation concentration.

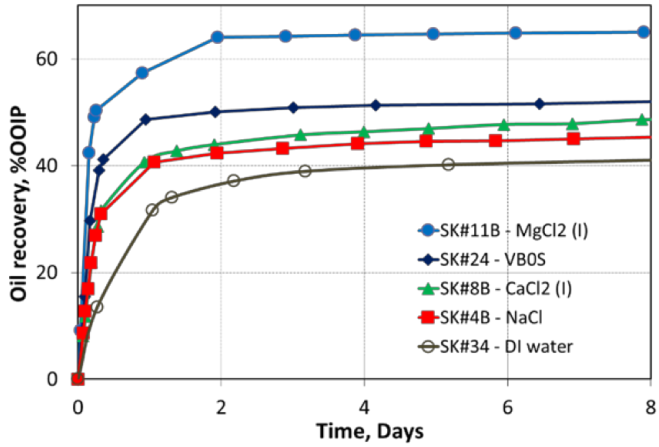

Figure 4.8 Oil recovery by SI from SK chalk cores with Swi = 10% with formation brines with different types of cations. The formation brine was also the imbibing brine, oil with AN=0.17 mgKOH/g was used. (Shariatpanahi et al., 2016)

Based on Shariatpanahi et al. (2016) experiments figure 4.9 was developed, which presents the chemical model describing the initial wetting in carbonates.

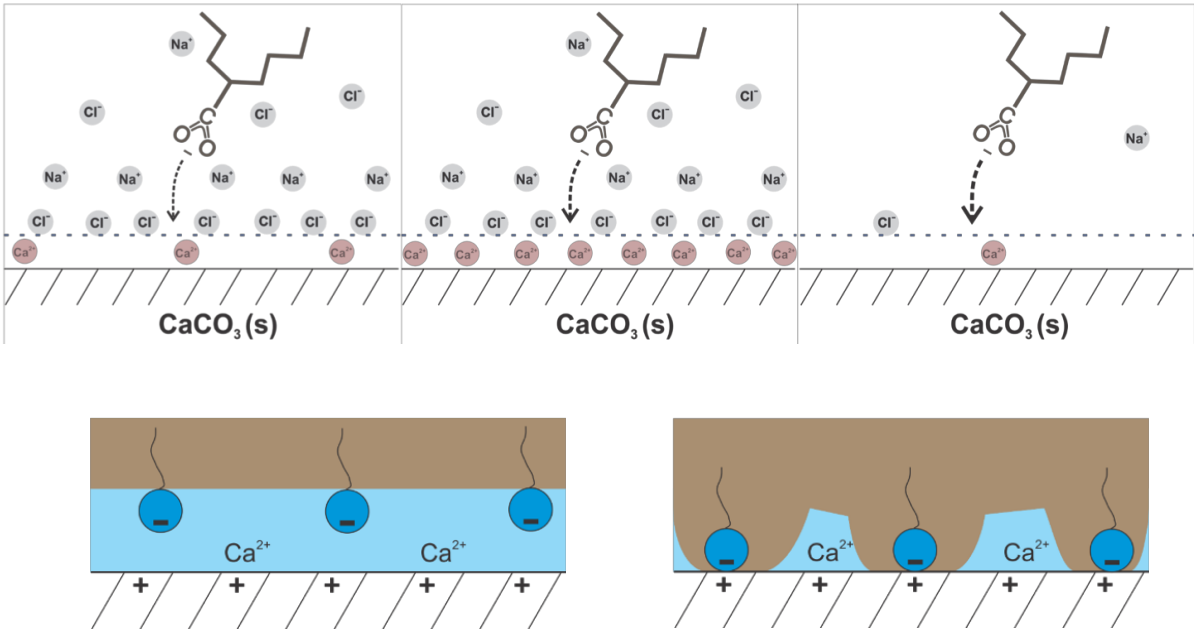

Figure 4.9 Chemical model describing initial wetting in carbonates. Figures based the experimental work done from (Shariatpanahi et al., 2016)

The initial wetting in carbonates are influenced by the formation water composition in the system. Figure 4.9 presents three systems with different initial wettings. Left figure illustrates a system with FW, where there is adsorption of polar organic components. Middle figure illustrates a system with seawater, where the adsorption of polar components increases when the Ca^{2+} concentration increases, due to the adsorption of sulfates on the rocks surface. Right figure illustrates a system with DI-water where there is adsorption of polar components on the rocks surface.

pH of the formation water will also influence the wettability of the carbonate rocks by affecting the surface charge (Anderson, 1986a). The carboxylic material act as a surface-active material when the pH is close to neutral or slightly alkaline, and the oil-water interface becomes negatively charged due to dissociation of the acid. The water-solid interface is still positively charged due to a large concentration of the potential determining ion Ca^{2+}, which is present in the initial formation water (Høgnesen et al., 2005). The chemical equation 4.1 shows the dissolution of carbonates, which results in an excess of OH^- increasing the pH. When the environment is slightly alkaline, the carboxylic group (RCOOH), which is pH dependent, will

become negatively charged, while the basic components (R_3NH^+) are neutrally charged. Equations (4.2) and (4.3) shows the chemical reactions.

$$CaCO_3 + H_2O \leftrightarrow Ca^{2+} + HCO_3^- + OH^- \quad (4.1)$$

Low pH		**Alkaline environment**	
$RCOOH$	$\leftrightarrow$	$RCOO^- + H^+$	(4.2)
R_3NH^+	$\leftrightarrow$	$R_3N + H^+$	(4.3)

The negatively charged carboxylic acids will then adsorb to the positively charged carbonate rock, hence the wettability of the rock is less water-wet. The last two figures in figure 4.9 illustrates the negative oil-water interface and positive water-solid interface, and the negative carboxylic acid attached to the positively charged carbonate surface.

5 Modelling of relative permeability curves during waterflooding

Relative permeability curves can be simulated based on experimental waterfloods. Several studies have been conducted on very strongly water-wet and very strongly oil-wet reservoir systems. However, most reservoirs have a mixed wettability, and there are very few studies reported on these conditions. Craig (1971) have presented fundamental characteristics of the relative permeability curves of the classic strongly wet systems and defined several rules to describe the systems. The rules have been confirmed by several subsequent experimental studies, and the features is used as fundamental theory for pore-scale simulations. According to McDougall and Sorbie (1995), when a model like that is anchored, further investigations at different wettability conditions can be conducted.

Smart Water EOR processes in reservoirs is aiming to improve oil recovery by a wettability alteration from a fractional-wet to a more water-wet system. Because of the wettability alteration process, the Smart Water system needs two different sets of relative permeability cures. The relative permeability curves for the fractional-wet system represents the initial wettability, before the wettability alteration. While the relative permeability curves for the strongly water-wet system represents the reservoir after waterflooding with Smart Water. Laboratory measurements can be used to model these curves at different initial wettabilities.

5.1 Laboratory measurements of relative permeability

Relative permeability can be measured by various techniques in the laboratory, and two of them are the steady-state and unsteady-state methods. During the steady-state method, water or oil is injected into the core at constant rates until the saturations reach equilibrium values. Pressure-drop across the core is measured and used to determine the relative permeabilities. The method is time consuming and expensive since it includes simultaneously injection of water and oil until the output rates match the input rates.

The unsteady-state method is less accurate but more rapid and common to use. The cores at S_{wi}=20% are saturated with 80% oil and flooded with water to residual oil saturation. Water is injected at one end at constant rates. The volumes of oil and water are measured at the other end of the core, and the pressure-drop over the core is measured. During waterflooding, steady state is not reached and hence Darcy's law is not applicable. Then, often the Johnson-Bossler-Naumann (JBN) method is used for calculating of the relative permeabilities from unsteady-

state method. The measured pressure-drop over the core is also used for relative permeability measurements. The period of the two-phase production is increased by using viscous oils, because the flow before water breakthrough will give no information about the relative permeability. If low-viscous oils are used in a water-wet core, only the endpoint relative permeabilities at S_{wi} and S_{or} can be determined (Anderson, 1987a; Apostolos et al., 2016; Lucia, 2007). Figure 5.1 illustrates the unsteady-state and steady-state methods of measuring two-phase oil and water relative permeability.

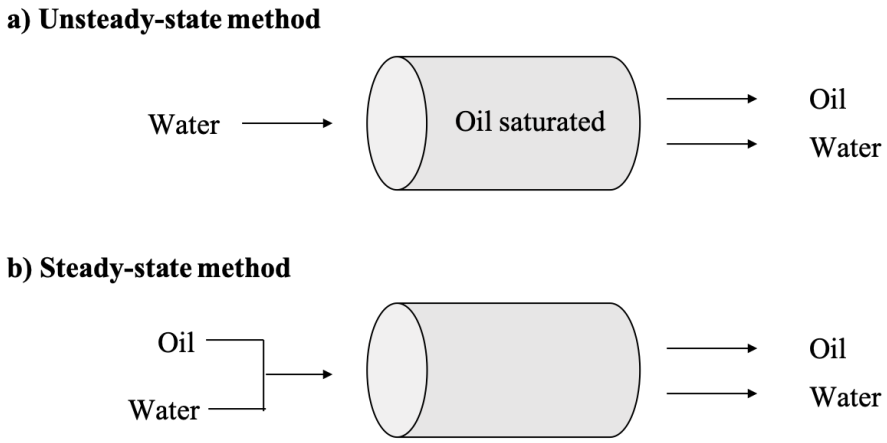

Figure 5.1 Illustration of measuring relative permeability for water and oil at (a) Unsteady-state method and (b) Steady-state method. Redrawn after Lucia (2007)

The experimental data conducted form waterflooding experiments can then be used to model relative permeability curves. In this experimental study, the simulator program SENDRA is used to simulate relative permeability curves based on history matching between experimental and simulated data.

5.2 Relative permeability curves with Corey correlations

The shape of the relative permeability curves is dependent on its history, and saturation history is indicated by two terms; drainage and imbibition. A drainage curve results from when the non-wetting phase saturation increases while the wetting phase saturation decreases, i.e. oil displaces water in a water-wet system. An imbibition curve results from the reverse procedure, the non-wetting phase saturation decreases while the wetting phase saturation increases, i.e. waterflood in a water-wet reservoir (Fanchi, 2010; Standing, 1975).

The relative permeability curves are history matched using the Brooks and Corey (1964) correlation given in equation (5.1) and (5.2).

$$k_{rw} = k_{rw}^{0}(S_w^*)^{N_w} \quad (5.1)$$

$$k_{ro} = k_{ro}^{0}(1 - S_w^*)^{N_o} \quad (5.2)$$

Where

k^o_{rw} Relative permeability of water at residual oil saturation (S_{or})

k^o_{ro} Relative permeability of oil at initial water saturation (S_{wi})

The shape of the relative permeability curves is achieved by the Corey exponents, N_w and N_o. The curves are constructed by changing the exponents, while the endpoints are kept constant at S_{wi} and S_{or}. The normalized water saturation (S_w^*) is given by equation (5.3)

$$S_w^* = \frac{S_w - S_{wi}}{1 - S_w - S_{or}} \quad (5.3)$$

The residual oil saturation is a measure of pore volume occupied by oil in the end of the displacement process. This property signifies the ultimate recovery and represents the endpoint of the relative permeability curve of water in reservoir modelling. The residual oil saturation is the ratio of immobile residual oil over the effective porosity, and is calculated by equation (5.4) (Zolotukhin & Ursin, 2000).

$$S_{or} = \frac{V_{oi} - V_o}{V_p} \quad (5.4)$$

Where

V_{oi} Initial volume of oil in the core

V_o Displaced (recovered) oil volume

V_p Pore volume

5.3 Two-phase capillary pressure curves with Skjæveland correlations

The Skjæveland et al. (1998) correlation is used to make representative capillary pressure curves in numerical simulation of reservoirs with different wettability and to model waterflooding experiments. The design idea for the correlation is a combined symmetrical correlation based on two limiting expressions, since neither of the fluids dominates the wettability. The correlation which is valid for a completely water-wet system, with the index *w*

for water, and a correlation which is valid for a completely oil-wet system, where the index *o* is for oil (Skjæveland et al., 1998). The correlation equation for a mixed-wet system comprises the imbibition capillary pressure curve in figure 5.2

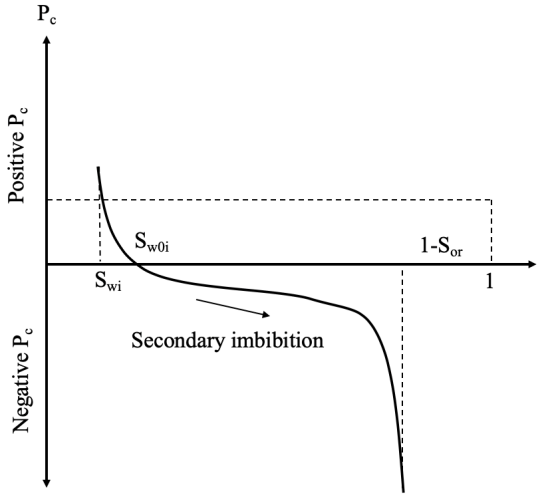

Figure 5.2 Schematic of bounding curve, capillary pressure P_c as function of water saturation S_w, secondary imbibition, redrawn after Skjæveland et al. (1998).

The symmetrical correlation for imbibition curve is given by equation (5.5).

$$P_{ci} = \frac{C_w}{(\frac{S_w - S_{wi}}{1 - S_{wi}})^{a_w}} - \frac{C_o}{(\frac{1 - S_w - S_{or}}{1 - S_{or}})^{a_o}} \qquad (5.5)$$

Where

P_{ci}	Capillary pressure for imbibition curve [Pa]
S_w	Water saturation
S_{wi}	Initial water saturation
S_{or}	Residual oil saturation
C_w, a_w, C_o, a_o	Constants for imbibition curve from S_{wi} to S_{or}.

The constants with the index for oil, C_o and a_o is used to define the negative term of the imbibition curve, while the constants with the index for water, C_w and a_w is used to define the positive term of the imbibition curve. At initial water saturation, the negative term has $S_o = 1\text{-}S_{wi}$, and the value is not zero. Hence, both terms are needed to produce a capillary pressure equal to zero. At S_{w0i} the imbibition curve crosses zero capillary pressure (Skjæveland et al., 1998).

5.4 Prediction of waterflood performance

The Buckley-Leverett displacement theory or often called the fractional flow theory demonstrates the effects of relative permeability and viscosity ratio on waterflooding, where the capillary effects are neglected, and the core is assumed to be horizontal. The fractional flow equation is given in equation (5.6)

$$f_w(S_w) = \frac{1}{1+\frac{\mu_w k_{ro}}{\mu_o k_{rw}}} \tag{5.6}$$

Where

f_w	fractional flow of water
S_w	water saturation
μ_o, μ_w	oil and water viscosities, respectively [cp]
k_{ro},k_{rw}	oil and water relative permeabilities

From equation (5.6) it is clear that at a given saturation, f_w is increased when the water/oil viscosity ratio is decreased. This will cause an earlier breakthrough and lower oil production. Similarly effect will happen if the relative permeability ratio increases (Anderson, 1987c; Zolotukhin & Ursin, 2000). The relative permeability curves can be used for predictions of how the displacement efficiency will be influenced by wettability in a porous system. The fractional flow curves for a strongly water-wet and oil wet system is illustrated in figure 5.3.

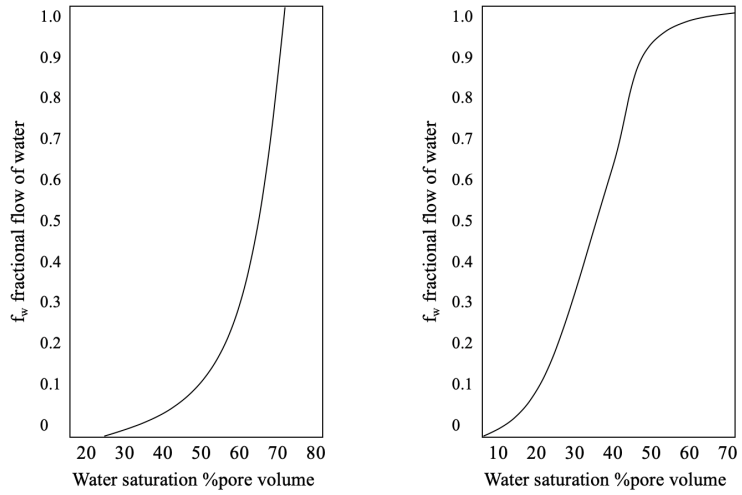

Figure 5.3 Fractional flow curves. (left) Strongly water-wet rock, (right) strongly oil-wet rock. Redrawn after Craig (1971)

The efficiency of a waterflood has a strong dependency on the mobility ratio of the displacing fluid to the displaced fluid. The displacement becomes more efficient if the ratio is low, and

hence the curve is shifted to right. The highest recovery efficiency is obtained when the ratio is so low that there are no S-shape of the curves, as illustrated in figure 5.3 (left), i.e. piston-like displacement in the strongly water-wet system (Kleppe, 2017).

The waterflood performance can be determined from the f_w-curves by tangent of the f_w -curve drawn with the line from f_w=0 at S_{wi}. The point of tangency indicates the water saturation at the front of the waterflood. When the tangent is extrapolated to f_w=1, then the average water saturation at water breakthrough is given. f_w increases as the system becomes more oil-wet and hence do the slopes of the corresponding tangents. This is based on the fact that waterfloods of strongly water-wet systems are most efficient at water breakthrough. As the efficiency decreases, the system becomes more and more oil-wet (Craig, 1971; McDougall & Sorbie, 1995). Figure 5.4 illustrates the front saturation of water and average water saturation at water breakthrough.

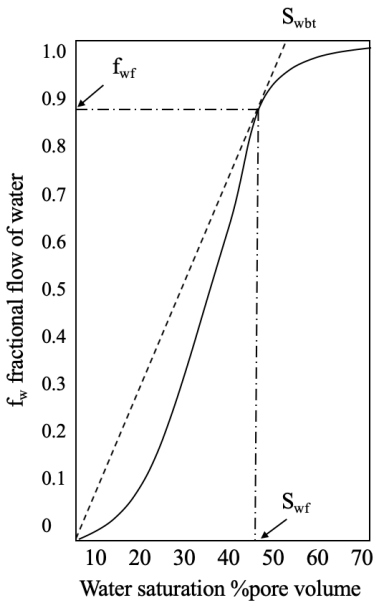

Figure 5.4 Determination of front saturation S_{wf} and average water saturation S_{wbt} at water breakthrough from S_{wi}. Redrawn after Craig (1971)

6 Experimental work

In this experimental study the effect of wettability on oil recovery in chalk materials are investigated. This chapter will include the materials and the methods used to perform the experimental work for evaluating the effect of wettability on relative permeability estimations.

Before the experimental work started, there was an introduction about the materials and fluids used in the laboratory. All experiments were performed following the HSE-regulations. Risk assessments were performed before every measurement to ensure that everyone in the laboratory had the same knowledge about potential accidents, and how they could be prevented. Specified security equipment, laboratory coat, googles, gloves and mask were used during the experimental work.

6.1 Materials

The materials and fluids utilized in the experimental work is listed in this section.

6.1.1 Core materials

Outcrop of carbonate chalk cores from Stevns Klint (SK), near Copenhagen in Denmark were utilized as the porous media in this study. The material is similar to some of the North Sea chalk reservoirs. Stevns Klint is of Maastricthian age, has high porosity between 47 to 52% and low permeability around 3-5 mD. The chalk is mainly composed of fine graded matrix, whereas larger bioclasts (mostly uncemented foraminifera) constitute the remaining part of the rock (Milter, 1996). The cores were cropped from the same block in the same direction. The diameter was cut to 3.79 cm, and the length varied from 6.94 – 7.12 cm with an average length of 7.06 cm.

Eight chalk cores with nominally identical properties, but with different initial wetting states were used in the experimental work. Two of the cores were prepared to be reference cores, SKR1 and SKR2. The reference cores were strongly water-wet and was used for comparison with the six other cores (SKC1-SKC6), which had an initial fractional wetting. SKC1-SKC6 were divided on the three students in the relative permeability group, and the experimental results were compared to strengthen the results. This thesis concerns core SKC1 and SKC4, and the results are compared with the results from Harestad (2019) and Radenkovic (2019). Properties of all cores utilized in the study are presented in table 3.

Table 3 Core properties

Core	**SKR1**	**SKR2**	**SKC1**	SKC2	SKC3	**SKC4**	SKC5	SKC6
Dry weight [gr]	109.10	107.68	104.10	107.15	106.19	108.33	105.36	105.97
Length [cm]	7.06	7.07	6.94	7.12	7.10	7.09	7.03	7.08
Diameter [cm]	3.78	3.79	3.79	3.79	3.79	3.79	3.79	3.79
Pore volume [ml]	37.53	39.17	38.34	39.80	37.99	38.51	39.90	39.91
Porosity [%]	47	49	49	50	47	48	50	50
Permeability [mD]	4.02	4.09	4.12	4.16	4.25	4.97	4.30	4.33

Initially, the cores are cleaned and prepared as described in section 6.3.1, and the properties of the cores are determined during this process. Pore volume is determined based on the weight difference between a dry core and a core fully saturated with FW. Porosity is calculated as PV over the bulk volume of the core. The weight of the core is measured by a Mettler Toledo scale, while the porosity of the FW is measured by a densitometer (described in section 6.2.2). Equation (6.1) and (6.2) is used for calculation of PV and porosity. The absolute permeability is calculated as described in section 6.3.1.1.

$$PV = \frac{w_{sat.} - w_{dry}}{\rho_w} \tag{6.1}$$

$$\phi = \frac{PV}{V_{bulk}} \tag{6.2}$$

Where

PV Pore volume [cm^3]

$w_{sat.}$ Weight of the saturated core [g]

w_{dry} Weight of dry core [g]

ρ_w Density of the formation water [g/cm^3]

ϕ Porosity of the core [fraction]

V_{bulk} Bulk volume of the core [cm^3]

6.1.2 Oils

In this experimental work performed together with Harestad (2019) and Radenkovic (2019) there were utilized different types of oils; crude oils and a mineral oil (m-oil). Three different types of crude oils were prepared with different acid numbers. OIL A, B and C, respectively. The crude oils were used for saturation of the six cores to establish an initial fractional wetting. Standnes and Austad (2000) have studied how the wettability of the cores are affect by saturation of crude oils with different AN. The cores become less water-wet when AN of the crude oil is increased. The cores were then flooded with the mineral oil to displace the crude oil to ensure that the following core flooding experiments were performed without the influence of further adsorption of polar components. The mineral oil was also used for saturation of the reference cores; hence the mineral oil is used during the whole experiment. The viscosity, density and acid and base number of the oils are presented in table 4. The details about the analysis are presented in section 6.2.

Heidrun

The biodegraded Heidrun crude oil is a base crude oil that is used to establish the crude oil RES 40. The polar organic components in the Heidrun oil is measured to be: AN=1.93 mgKOH/g and BN=0.84 mgKOH/g, and the oil is sampled from a real well during a well test.

RES 40

RES 40 was prepared by diluting Heidrun crude oil with n-heptane in a volume ratio of 60:40 to reduce the viscosity. Then the oil was filtrated using a 5µm filter.

RES 40-0

RES 40-0 was prepared by adding silica gel to RES 40. The silica gel is added to remove most of the polar organic components in the crude oil which controls the wettability of the porous media. 20wt% of the silica gel was added twice and left on a magnetic stirrer for one week each time. Hence a total of 40wt% of silica gel is added to RES 40. The mixture was then centrifuged and filtrated with a 5µm filter.

OIL A, B, C

The crude oils A, B and C were prepared by mixing RES 40 with RES 40-0. The purpose was to make three different oils with three different acid numbers. AN of the crude oil are decreasing

by adding more of the RES 40-0 to the RES 40. The target AN can be calculated by equation (6.3).

$$Target\ AN = AN_{RES40} \cdot \frac{V_{RES40}}{V_{RES40}+V_{RES40-0}} + AN_{RES40-0} \cdot \frac{V_{RES40-0}}{V_{RES40}+V_{RES40-0}} \quad (6.3)$$

Oil A has the lowest acid number, while oil C has the highest acid number. In this experimental work oil C is utilized. The experimental results are compared with the results for the other cores were oil A and B are used, presented by Harestad (2019) and Radenkovic (2019).

Mineral oil

The mineral oil is a mixture of Marcol 85 and n-heptane and does not contain any polar organic components. The m-oil was established by making a mixture that has the same viscosity as the above mention oils. A mixing ratio was determined to be 58% Marcol 85 and 42% n-heptane. M-oil was prepared by weight since it is more accurate than by volume. The preparation of m-oil and the viscosity measurements are presented in section 7.2.1 in the results.

Table 4 Properties of the oils utilized in this experimental work.

Oil	**Heidrun**	**RES 40**	**RES 40 0-0**	**OIL A**	OIL B	OIL C	**Marcol 85**	**n-heptane**	**Mineral oil**
Density [g/cm^3]	0.684	0.820	0.809	0.818	0.814	0.817	0.847	0.684	0.783
Viscosity [mPa•s]	3.9	2.7	2.4	2.9	3.5	2.9	28.3	0.4*	2.7
AN [mgKOH/g]	1.93	2.40	0.06	0.15	0.34	0.67	-	-	-
BN [mgKOH/g]	0.84	0.90	0.01	0.18	0.26	0.34	-	-	-
IFT [mN/m]	34	14	27	26	23	18	45	34	41

* Theoretical value

6.1.3 Brines

The brines were synthetically prepared in the laboratory by dissolving the correct amount of salts in DI-water. All chemicals used were reagent graded. To avoid precipitation during mixing, sulfate and carbonate salts were dissolved separately. The salts were then mixed together and diluted to 1L on a magnetic stirrer and left for approximately 2 hours to secure that the solution was properly dissolved. At last, the brines were filtrated using a VWR vacuum

gas pump with a 0.22µm millipore membrane filter. Table 5 shows the composition of the seawater brines.

A brief explanation on the different brines used in this work is listed below:

- **SW**, synthetic seawater brine used as reference for the chromatographic wettability test.
- **SW0T**, synthetic seawater brine without sulfate (SO_4^{2-}) and tracer (SCN^-), used initially for the chromatographic wettability test.
- **SW½T**, synthetic seawater brine with equal amounts of sulfate (SO_4^{2-}) and tracer (SCN^-), used secondary for the chromatographic wettability test after S_{or} is reached with SW0T.

Table 5 Synthetic Seawater for Chromatographic tests

Brine Ions	**SW mM**	**SW0T mM**	**SW½T mM**
HCO_3^-	2.0	2.0	2.0
Cl^-	525.0	583.0	583.0
SO_4^{2-}	24.0	0.0	12.0
SCN^-	0.0	0.0	12.0
Mg^{2+}	45.0	45.0	45.0
Ca^{2+}	13.0	13.0	13.0
Na^+	450.0	460.0	427.0
Li^+	0.0	0.0	12.0
K^+	10.0	10.0	22.0
Density [g/cm^3]	1.022	1.022	1.022
TDS [g/l]	33.39	33.39	33.39
pH	7.64	7.62	7.61

6.1.4 Chemicals

Following chemicals was used during the experimental work:

- Silica gel was used in the desiccator to dry the chalk cores to initial water saturation at 20%.
- n-heptane was used to make the mineral oil, and to clean the equipment that has been in contact with crude oil, such as piston-cells and the lines in the experimental setups.
- Chemicals was used for measuring of acid- and base numbers for the crude oils. The chemicals are listed in Appendix A.

6.2 Analyses

The various analyses utilized in this experimental work is explained in this section.

6.2.1 pH measurements

The pH in brines and produced water was measured using the pH meter seven compact™ from Mettler Toledo, with the electrode semi-micro pH. There were taken several measurements to quantify the results and the repeatability was ±0.01 pH units at room temperature.

6.2.2 Density measurements

The densities of the brines and oils were measured using an Anton Paar DMA-4500 density meter at room temperature. Initially, the density meter was cleaned with white spirit, acetone and DI-water. Then a small amount of fluid was injected into the glass tube and the density was determined. There were taken several measurements to quantify the results, and the repeatability was ±0.001 g/cm^3.

6.2.3 Viscosity measurements

The viscosities of the brines and oils were measured using an Anton Paar rotational rheometer Physica MCR 302. Approximately 0.650 ml fluid was placed on a metallic surface, and a metal plate was lowered towards the fluid and the position between the two surfaces were measured. The viscosities of the oil and brines were determined through shear stress/shear rate relation. The repeatability was 0.01 mPa.s. Figure 6.1 presents a viscosity measurement of RES 40-0. Three equal and stable measurements are done before the viscosity is confirmed.

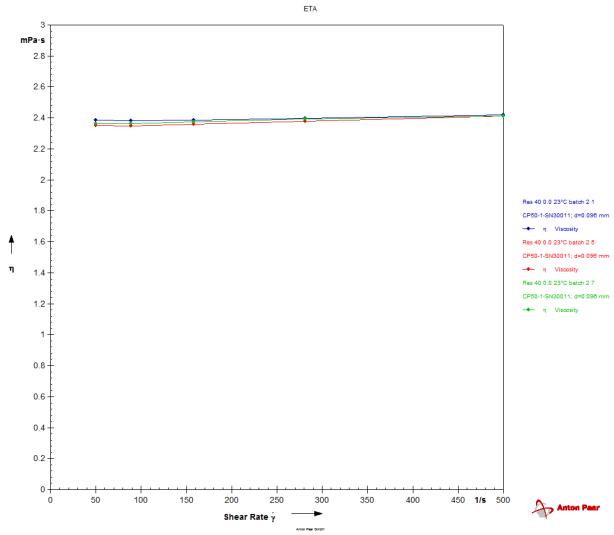

Figure 6.1 Example of viscosity measurements by Anton Paar rotational rheometer

6.2.4 Interfacial tension measurements

The IFT between a liquid-liquid interface was measured using a Krüss tensiometer with the Du Noüy ring method. Initially, liquid one was placed in a glass container, and a platinum-iridium ring was lowered into the glass container, then liquid two was introduced. The ring was moved from liquid phase one to liquid phase two. A lamella was produced when the ring moved through the phase boundary, and the force acting on the optimally wettability ring was measured in mN/m (du Noüy, 1925). Figure 6.2 illustrates measurement of IFT between DI-water and oil with the Du Noüy ring method.

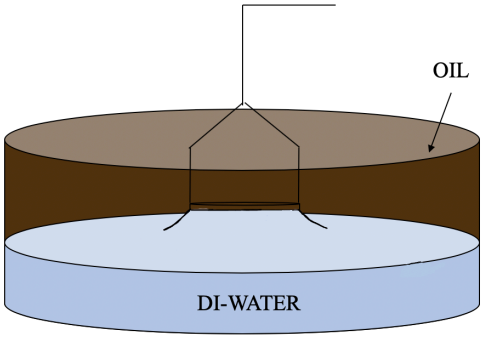

Figure 6.2 Illustration of IFT measurement between oil and DI-water with the Du Noüy ring method. A lamella is produced between the two immiscible fluids.

6.2.5 Determination of AN and BN

The crude oils were analyzed for the amount of acidic and basic polar components, in mgKOH/g. The AN (Acid number) and BN (base number) for the oils were measured using a Mettler Toledo T55 auto-titrator with an international standard developed by (Fan & Buckley, 2007). The standard is a modified version of ASTM D664 for acid number titration and ASTM 2895 for basic number titration. The instrument is using a blank test as a reference during potentiometric titration of oil samples, where measurements of electronic potential is converted to equivalent acid numbers. Each measurement of the oil samples requires a titration solvent and a spiking solution, the composition of these two solvents are listed in appendix A. To quantify the measurements, the weight of the samples was taken with a Mettler Toledo weight instrument with an accuracy of ±0.0001 g. Calibrations and blank samples were done regularly to compensate for changes in the electrode properties when it was exposed to air. The reproducibility of the analyses was better than 0.02 mgKOH/g oil added.

6.2.6 Ion chromatography

The effluent samples from the chromatographic wettability test were diluted 1000 times with DI-water using the trilution™ LH system from a Gilson GX-271 liquid handler. The diluted samples were then placed in a Dionex ICS-5000^{+} Ion Chromatograph, and chemical analyses of cations and anions was determined. The software controlling the chromatograph used retention time, which is travelling time through the columns, and plotted conductivity versus the retention time. The area below each peak corresponds to the ion's relative concentrations, and the concentrations of each ion was measured using external standard methods.

6.2.7 Scanning Electron Microscopy (SEM), EDAX

Small samples from the chalk outcrop material was analyzed with a Scanning Electron Microscopy (SEM). Images was taken by scanning a focused electron beam over the rock surface. The electrons in the beam interact with the sample, and various signals is produced which can be used to obtain information about the surface topography and composition. The material was prepared with assistance of an Emitech K550. The rock samples were exposed to vacuum and coated with palladium in an argon atmosphere. The coating will reduce the thermal damage, enhance secondary electron emission and increase the electrical conductivity of the sample which is important for Scanning Electron Microscopy (Emitech, 1999; Instruments).

Elementary analyses were also taken of the rock samples with Energy Dispersive X-ray Spectroscopy (EDAX). The analyses are used to obtain quantitative results of chemical composition of a specific location within the rock sample. The technique can detect elements from carbon and uranium with a capacity as low as 1.0 wt%. When SEM and EDAX is combined, elemental analyses of the specific area for a given sample can be adjusted based on the magnification the sample is being observed (Marickar et al., 2009)

6.2.8 Simulating with SENDRA

The two-phase core flooding simulator SENDRA was used to history match experimental data. Relative permeability curves at different initial wettings were created based on the output data from the history match. SENDRA utilize a fully implicit black-oil formulation which is based on Darcy's law and the continuity equation with a fully automated history matching routine and a forward simulation of an experimental performance (Chukwudeme et al., 2014). Experimental pressure-drop data and oil production profiles was implemented in the program, and the

simulated curves was determined from an automated history matching approach (Prores). Initially, a water-oil experiment and imbibition displacement were chosen, then experimental core data and recovery test data was implemented into the program, and finally a SENDRA analyses were done.

The initial water saturation was S_{wi}=20% and the residual oil saturation, S_{or} was calculated by equation (5.4) in section 5.2, and the endpoint relative permeabilities was calculated by equation (3.8) and (3.9) in section 3.3.1. Relative permeability of water (k_{rw}) was calculated at S_{or}, and relative permeability of oil (k_{ro}) was calculated at S_{wi}. The initial saturation and endpoint relative permeabilities were used as input data in SENDRA. Capillary pressure curves and fractional flow curves were also constructed based on the output data and relative permeability curves from the history match in SENDRA.

6.3 Methods

The various experimental methods utilized in this experimental work are explained in this section.

6.3.1 Core preparation

The core preparation process for the chalk cores were done following a cleaning procedure described by Puntervold et al. (2007a). Initially the cores were placed in a Hassler cell (figure 6.3) in a Hassler core holder and flooded with DI-water with a rate of 0.100 ml/min, at room temperature (23°C). The cores were flooded with DI-water without SO_4^{2-} to remove sulfate that may be present initially. SO_4^{2-} in FW would affect initial wettability during core restoration (Puntervold et al., 2007a). The removal of sulfate was confirmed by a batch test of the effluent by adding Ba^{2+}, where $BaSO_4$ precipitated when SO_4^{2-} was still present. Equation (6.4) represents the chemical reaction in the batch test.

$$Ba^{2+}\,(aq) + SO_4^{2-}\,(aq) \leftrightarrow BaSO_4\,(s) \qquad (6.4)$$

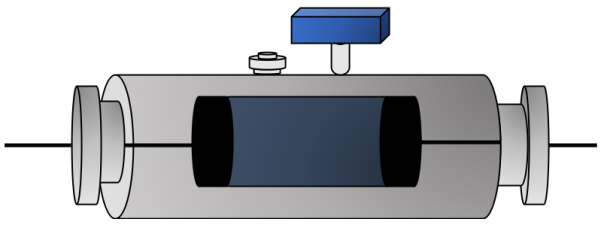

Figure 6.3 Illustration of the Hassler cell used in the experimental work.

6.3.1.1 *Permeability measurements*

The absolute permeability of the cores was determined during the core cleaning process, when DI-water was flowing through the core in the Hassler core holder. Two pressure gauges were used to measure the differential pressure between the inlet and outlet of the core holder. One measured the small range of differential pressure up to 600mbar, while the other measured a higher range up to 2.5 bar. The back and confining pressure of the setup was 10 and 20 bar, respectively. The injection rate was changed three times (0.05 ml/min, 0.15 ml/min, 0.10 ml/min). The differential pressure was measured at a specific rate, and a linear regression of ΔP versus rate was plotted. The absolute permeability of the cores was then calculated with Darcy's law. The empirical correlation is presented in equation (2.10) from section (2.3.3). Figure 6.5 illustrates the experimental setup, where DI-water was the imbibing fluid inside the piston cell.

The effective permeabilities k_{eff} of water and oil were calculated to determine the endpoint relative permeabilities of water and oil. The calculation is the same as for absolute permeability. $k_{eff,w}$ was calculated during the forced imbibition test when a recovery plateau was reached at constant ΔP and injection rate. $k_{eff,o}$ was calculated during the end of the oil saturation at constant ΔP and injection rate.

6.3.2 Core restoration

6.3.2.1 *Establishing initial water saturation*

The chalk cores are saturated with DI-water to establish initial water saturation. Using DI-water as FW will not significantly affect the adsorption of POC and the initial wettability established in the cores. The chalk cores were dried in an oven at 90°C after they were cleaned, and saturated with FW in a desiccator. The gas in the desiccator was removed using a vacuum pump, and the FW was introduced into the cores during vacuum and left there for an hour. Then they were placed into a new desiccator onto a porous plate to establish initial water saturation. The desiccator contained a silica gel that vaporize the water from the cores to the weight corresponding to initial water saturation (S_{wi}) at 20%. The cores where then stored in a sealed container to equilibrate for 72 hours to establish an even ion distribution. The process is done following a procedure described by Springer et al. (2003). Figure 6.4 illustrates the experimental setup for the saturation of the cores.

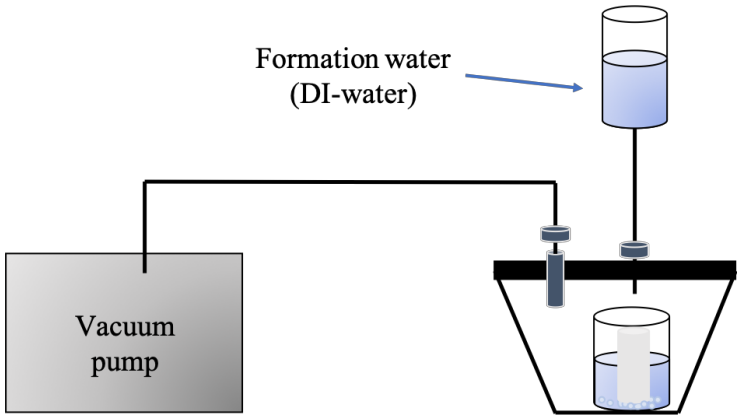

Figure 6.4 Illustration of saturation of the chalk cores with FW in a desiccator under vacuum to establish initial water saturation.

6.3.2.2 *Oil saturation*

All oil recovery experiments were performed with the mineral oil to secure the same oil viscosity in both the water-wet reference cores, and in the cores exposed to crude oil to reduce water wetness.

First, the oil recovery experiments were performed on the water-wet cores, i.e. the reference cores. After establishing initial water saturation (S_{wi}=20%), the reference chalk cores were saturated with the mineral oil in the desiccator. The gas was removed using a vacuum pump, and the m-oil was introduced into the cores during vacuum and left there for an hour, illustrated in figure 6.4. The chalk cores were then placed in a protective rubber sleeve and mounted into a Hassler core holder with a back and confining pressure of 10 and 20 bar, respectively. The cores were flooded with the mineral oil for 5 PV, and the pressure-drop was measured during the flooding process at S_{wir}=0.2.

After the reference cores, six other chalk cores are prepared to have a fractional wetting. The cores utilized in this experimental work were saturated with crude oil C, with highest acid number (AN=0.67 mgKOH/g). First the initial water saturation (S_{wi}=20%) was established. Then the cores were saturated with oil C in a desiccator. The gas was removed using a vacuum pump, and oil C was introduced into the cores during vacuum and left there for an hour, illustrated in figure 6.4. The chalk cores were then placed in a protective rubber sleeve and mounted into a Hassler core holder with a back and confining pressure of 10 and 20 bar, respectively. The cores were flooded with the crude oil, 2 PV in each direction, at a constant

rate and room temperature (23°C). The crude oil was introduced to the cores to decrease the water wetness. At the end, the cores were flooded with the m-oil to displace oil C present in the pores. The mineral oil was flooded for 5 PV and the pressure drop was measured to calculate the effective permeability of oil, to determine the endpoint relative permeability of oil (k_{ro}) at S_{wir}. Effluent oil samples were sampled during m-oil injection to compare the displacement efficiency of the mineral oil. The color difference was compared, and after 5 PV injected the mineral oil was hardly polluted by crude oil. Figure 6.5 presents the effluent oil sampled after each PV injected. The experimental set-up is illustrated in figure 6.6.

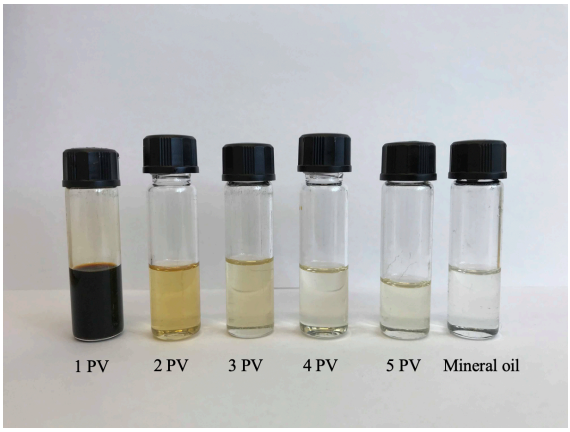

Figure 6.5 Effluent oil samples after each PV injected to compare with the 100% mineral oil to the right.

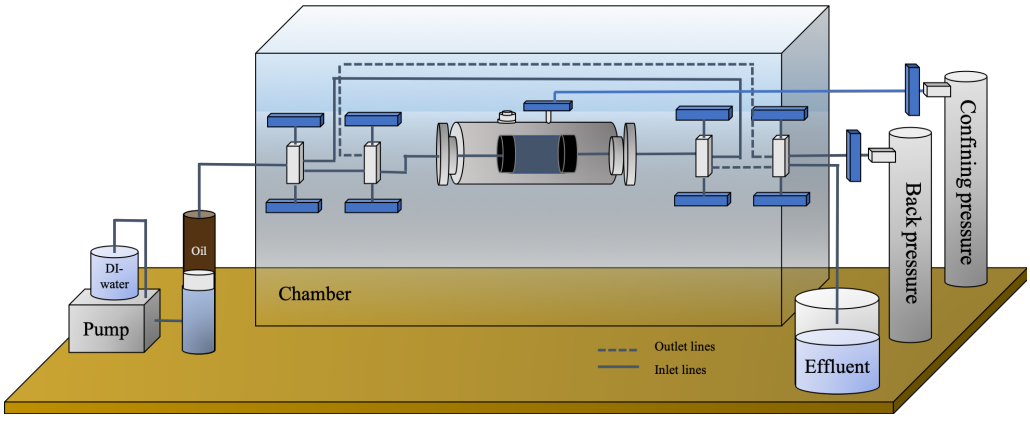

Figure 6.6 Illustration of the experimental set-up for oil saturation

6.3.2.3 *Aging*

According to Hopkins et al. (2016) the oil will adsorb to the cores almost immediately during oil saturation, so there is no need for the aging process were the cores are stored in an aging cell. The cores were stored in the Hassler core holder after the oil saturation for 72 hours before mineral oil displacement.

6.3.3 Oil recovery tests

Two different oil recovery tests were conducted on the chalk cores. The tests were performed to evaluate the effect of wettability on oil recovery, and the experimental data from the tests were used to model relative permeability curves. Figure 6.7 illustrates the experimental procedure in this study.

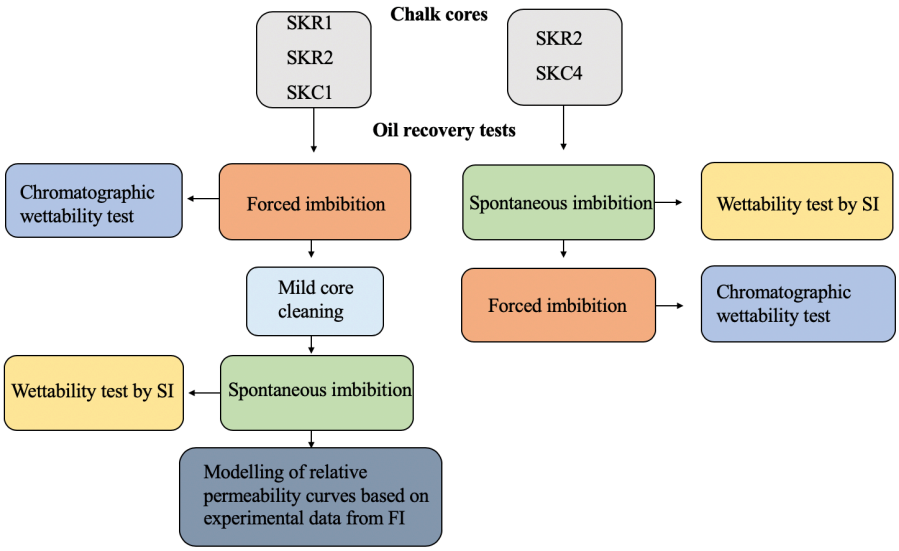

Figure 6.7 Procedure of the experimental work in this study

Initially, two strongly water-wet reference cores (SKR1 and SKR2) and one less water-wet core (SKC1) produced oil by forced imbibition and spontaneous imbibition. Between the two oil recovery tests, a mild core cleaning procedure of the cores had to be done. Relative permeability curves were then modelled with SENDRA based on the experimental data from FI.

Then, the reverse test procedure was performed. One strongly water-wet reference core (SKR2) and one less water-wet core (SKC4) produced oil by spontaneous imbibition, followed directly by forced imbibition. There was no need for a cleaning procedure of the cores between these two tests. Wettability tests were also performed to confirm the wettability of the systems, chromatographic wettability test after the forced imbibition test and wettability test by SI. The experimental work performed on the oil recovery tests are described in the sections below.

6.3.3.1 *Oil recovery by forced imbibition*

The restored chalk cores saturated with oil at S_{wi} = 20% were placed in a Hassler core holder and flooded with the formation water to produce the cumulative oil. The back and confining pressure were still 10 and 20 bar, respectively. The imbibing fluid was flooded through the cores at the rate of 1 PV/day at room temperature (23°C) until the oil production and pressure drop had stabilized at a plateau. The pressure-drop was measured to calculate the effective permeability of water to determine the endpoint relative permeability of water (k_{rw}) at S_{or}. Then the rate was increased to 4 PV/day to investigate if there was any extra oil production. The cumulative oil produced was collected in a burette and measured to determine oil recovery (% of OOIP) vs time. The experimental set-up is equal to the one illustrated in figure 6.6, but the imbibing fluid is the formation water (DI-water). The injection rates are presented in table 6.

Table 6 Determined PV and injection rates of cores during forced imbibition.

Core	**SKR1**	**SKR2**	**SKC1**	SKC2	SKC3	**SKC4**	SKC5	SKC6
PV [ml]	37.53	39.17	38.34	39.80	37.99	38.51	39.90	39.91
1PV/day [ml/min]	0.026	0.027	0.027	0.028	0.026	0.027	0.028	0.028
4PV/day [ml/min]	0.104	0.109	0.107	0.111	0.106	0.107	0.111	0.111

6.3.3.2 *Oil recovery by spontaneous imbibition*

The restored chalk cores saturated with oil at S_{wi} = 20% were placed in a glass Amott imbibition cell surrounded by the imbibing FW at 23°C. The cumulative oil production (%OOIP) was measured and plotted against time until a recovery plateau was reached. The experimental set-up is illustrated in figure 6.8.

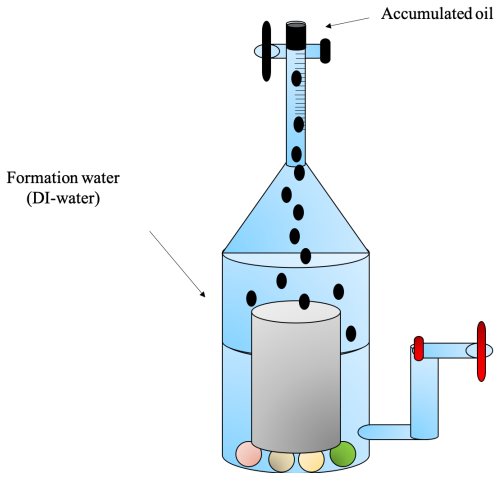

Figure 6.8 Illustration of the Amott imbibition cell

Between the forced imbibition and spontaneous imbibition for the first cores, a mild cleaning procedure had to be performed, described in section 6.3.3.3. After the mild cleaning, the cores were dried to initial water saturation (S_{wi}=20%) in a desiccator with silica gel. Then the cores were saturated with the m-oil in a desiccator where gas was removed using a vacuum pump. The m-oil was introduced and left there for an hour, illustrated in figure 6.4. For the other cores, the spontaneous imbibition test was performed first, and the forced imbibition test followed directly.

6.3.3.3 *Mild core cleaning*

During a mild core cleaning procedure most of the adsorbed acidic components are preserved (Hopkins et al., 2015). Brine, oil and the easily dissolved salts in the porous media of the rock are removed out of the core. The cores were first flooded for 4 PV with n-heptane to displace the mineral oil from the pores. The cores were clean when the effluent samples were clear. Then DI-water were flooded for 5 PV to displace n-heptane, easily dissolved salts and SW½T brine from the chromatographic wettability test conducted after the forced imbibition test. The cores were flooded at a constant rate of 0.100 ml, respectively.

6.3.4 Chromatographic wettability test

Chromatographic wettability tests were performed after the forced imbibition in the Hassler core holder. The process is done following a procedure described by Strand et al. (2006b). Initially, the cores were flooded at a constant rate of 0.200 ml/min with SW0T brine, which doesn't contain any sulfate and tracer, to ensure that the cores were at residual oil saturation (S_{or}). Continued by flooding with SW½T which contains equal amounts of sulfate and tracer. Effluent brine samples during SW½T flooding were collected with an auto-sampler and analyzed for SO_4^{2-} and SCN^- separation. Effluent curves of SO_4^{2-} and SCN^- were plotted against PV injected. The observed results of the water-wet surface for the six cores were compared to the water-wet surface for the strongly water-wet reference cores. The area between SCN^- and SO_4^{2-} for all the cores were calculated using trapezoidal method. The WI was calculated using equation (3.7) from section (3.2.5). Figure 6.9 illustrates the experimental set-up for the chromatographic wettability test.

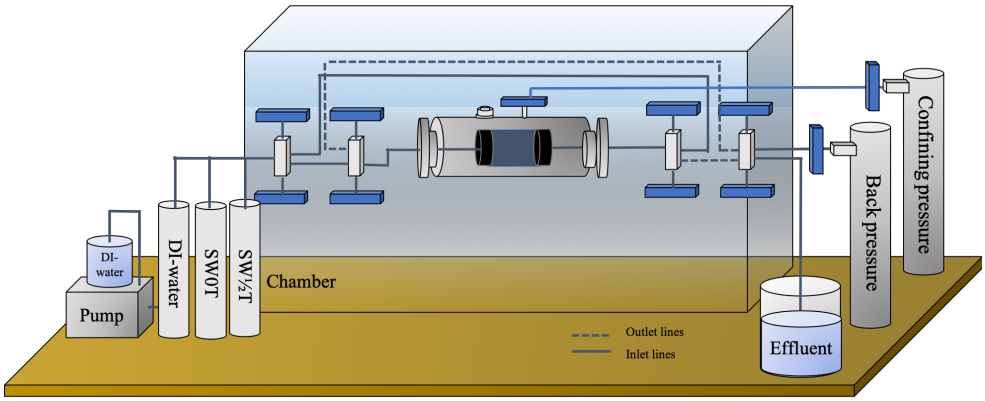

Figure 6.9 Illustration of the experimental set-up for sampling effluent to the chromatographic wettability test at 23°C

7 Results and discussion

Experimental data and field observations have confirmed that Smart Water EOR processes are wettability alterations towards more water-wet conditions increasing the oil recovery. No chemically induced wettability alteration is taking place during formation water injection. Seawater behaves as a Smart Water in chalk and significant increased oil recovery are observed, both during forced imbibition and spontaneous imbibition core experiments.

In this experimental work, oil recovery tests on outcrop chalk material is performed. The effect of wettability on oil recovery is tested, both during spontaneous and forced imbibition processes. Relative permeability curves at different initial wettings are modelled based on the experimental data from the oil recovery tests. The objective is to verify if reliable relative permeability curves could be produced from oil recovery profiles and pressure-drop data to explain the wettability alteration observed during Smart Water injection. The strongly water-wet cores represent the wettability alteration by Smart Water injection, while the fractional-wet cores represent the initial condition, before the wettability alteration.

7.1 Core characterization

Small rock samples of the Stevns Klint outcrop material were analyzed using a Scanning Electron Microscopy in collaboration with Andreassen (2019) and Lindanger (2019). The samples were first exposed to vacuum and coated with palladium in an argon atmosphere before the samples were placed in a Zeiss Supra 35VP Scanning Electron Microscopy (SEM). Photos of the mineral surface were taken at different magnifications. Figure 7.1 presents SEM analysis of the chalk material at 1000 times magnification. There is little change in the grain fragments, and the system looks fairly homogenous at a macroscopic scale.

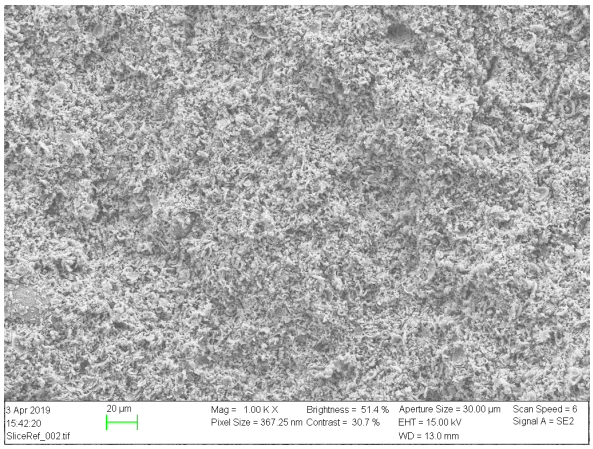

Figure 7.1 Scanning electron microscopy (SEM) photo of the chalk outcrop material, magnification 1000 times.

Figure 7.2 presents SEM analyses of the chalk material when the magnification was increased to 10 000. Coccolithic rings and ring fragments in the chalk is easy recognized, and the dark spots between the grains indicates the pore system. We observe different grain structures, and at a microscopic scale the rock looks relatively heterogenous.

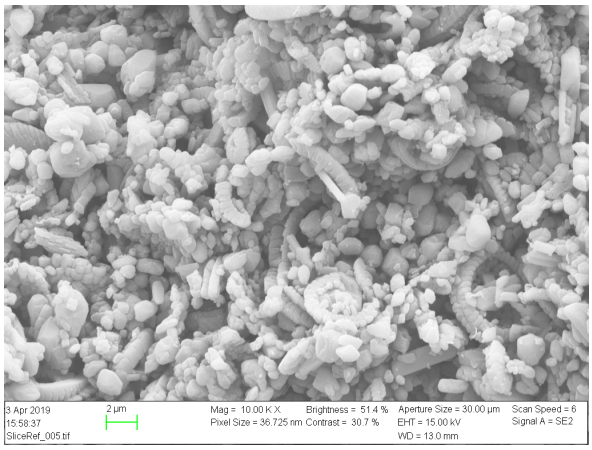

Figure 7.2 Scanning electron microscopy (SEM) photo of the chalk outcrop material, magnification 10 000 times.

7.1.1 Energy dispersive x-ray spectroscopy (EDAX)

The elementary distribution analyses (EDAX) shows the chemical composition of the Stevns Klint outcrop material. The analysis was done in combination with SEM to get a total understanding of the materials morphology. Results of the analysis showed that the atomic weight (At %) for Ca^{2+} were 98% which indicates the mineralogy of limestone. Tracers of Mg^{2+} could be linked to dolomite/magnesite or clays. Small contents of Al^{3+} could be linked to clay, or feldspar minerals. Small amount of Sulfur (S) can be linked to anhydrite or gypsum minerals,

but the extent of other atoms than calcium is negligible (Guan et al., 2003). Table 7 shows the elemental analysis of the outcrop chalk material.

Table 7 Element analysis of outcrop chalk material with EDAX

Element	Atomic weight, At [%]
Ca^{2+}	97.66
Mg^{2+}	0.31
Al^{3+}	0.47
S	0.58

7.1.2 Pore size distribution

The pore size distribution in Stevns Klint outcrop material was studied by Milter (1996). Figure 7.3 (left) presents the results of the pore size distribution. The smallest pores are less than 100nm, while the largest pores are close to 1000nm or 1µm. Stevns Klint chalk have a heterogenous pore size distribution, and the main pore diameter is close to 500nm. Studies have also shown that the Stevns Klint outcrop material has the same pore size distribution as the Valhall field in the North Sea (Webb et al., 2005) figure 7.3 (right).

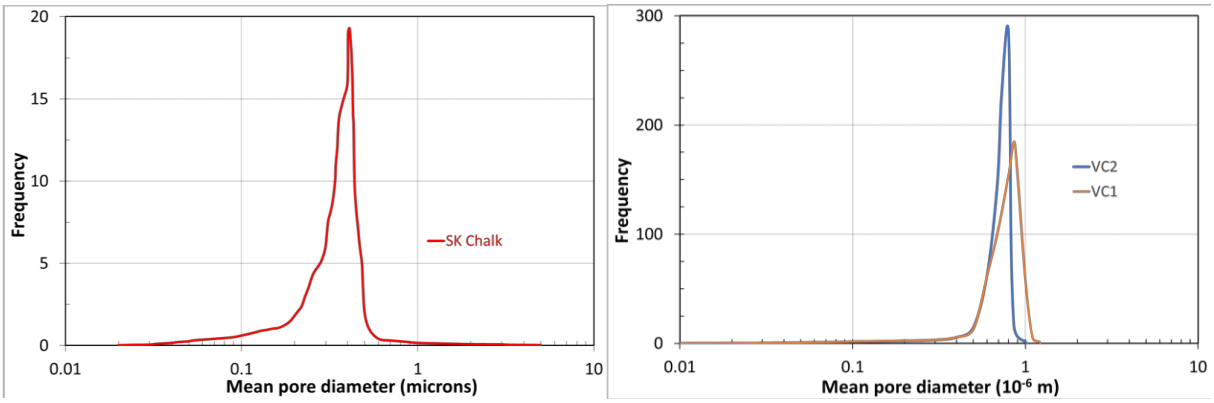

Figure 7.3 (Left) Pore size distribution for Stevns Klint Chalk material, redrawn after (Milter, 1996). (Right) pore size distribution in Valhall reservoir chalk. Redrawn after (Webb et al., 2005).

7.1.3 pH analyses

During the forced imbibition tests of the cores, pH measurements of effluent samples from the produced formation water were taken. The pH is controlled by the carbonate equilibrium in equation (4.1) in section 4.1.2. Dissolution of $CaCO_3$ causes an excess of OH^- and the

environment become slightly alkaline. The carboxylic group (RCOOH) in crude oil is pH dependent, and at alkaline pH, the carboxylic acids are negatively charged ($RCOO^-$), while the basic components are neutrally charged, as shown in equation (4.2) and (4.3) in section 4.1.2. The pH measurements of the produced water (FW) effluents confirm that the environment was slightly alkaline, and the polar components were negatively charged. Figure 7.4 (left) presents the pH measurements of the effluent FW samples during oil recovery, while figure 6.4 (right) presents reference core SKR1, where oil production and pH are plotted versus time. It is observed that the environment was slightly alkaline during the whole oil recovery experiment.

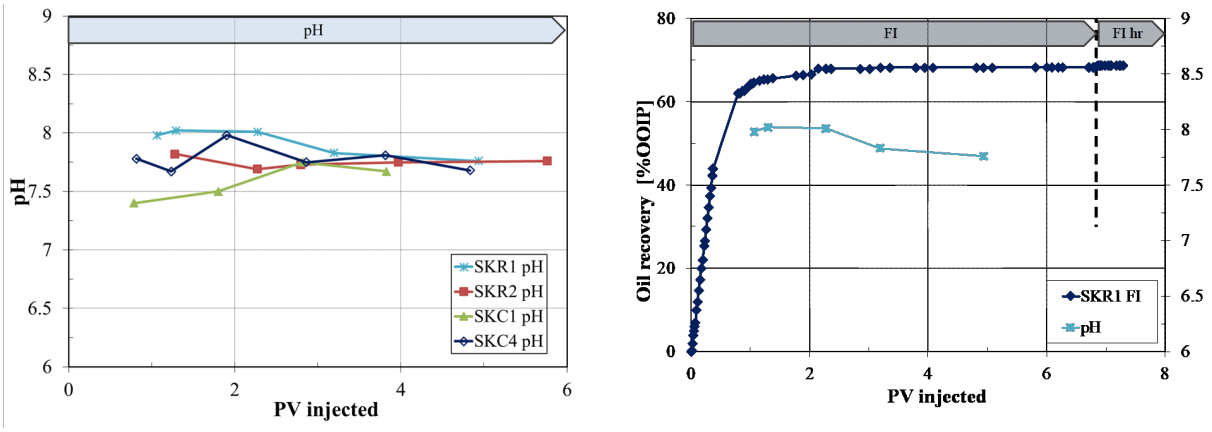

Figure 7.4 (Left) pH measurements of effluent samples from the produced formation water of the reference cores (SKR1 and SKR2) and the fractional-wet cores (SKC1 and SKC4). (Right) oil production and pH versus time for core reference core SKR1.

7.1.4 Permeability measurements

The absolute permeability of all cores was calculated during the core preparation process described in section 5.3.1.1. According to Darcy's equation, the injection rate is proportional to the pressure-drop. The pressure-drop versus injection rate is calculated by linear regression and Darcy's law is used to determine the absolute permeability. The empirical correlation is given in equation (2.10) in section 2.3.3. An example of determination of absolute permeability for core SKC1 is illustrated in figure 7.5. (Left) illustrates the proportional injection rate and pressure-drop and (right) the linear regression of ΔP versus injection rate for core SKC1.

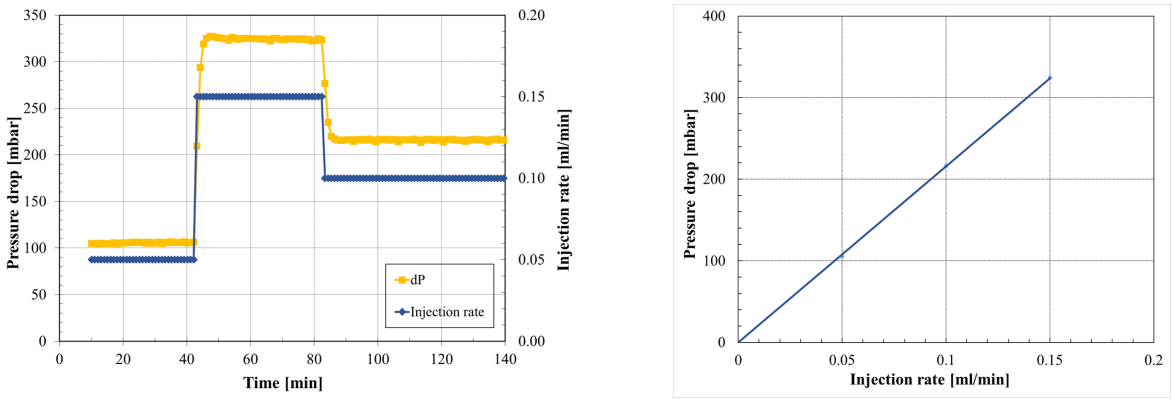

Figure 7.5 (left) injection rate proportional to pressure-drop, (right) linear regression of dP used for calculation of absolute permeability. The experimental data is for core SKC1

The effective permeabilities are determined with the same method as the absolute permeability and are used for calculation of endpoint relative permeabilities. The effective permeability of oil, ($K_{eff,o}$) was determined based on ΔP and injection rate data from oil saturation process, while the effective permeability of water, ($K_{eff,w}$) was determined at the end of the forced imbibition, when the oil production have reached a recovery plateau and ΔP had stabilized. The permeabilities calculations can be found in section 7.7.1, table 12. Where the endpoint relative permeabilities are used in the SENDRA simulation.

7.2 Oil characterization

To be able to compare the experiments with different core wettability, there was need for an oil phase with the same properties in all experiments. Mineral oil without polar components was used for completely water-wet cores, and a viscosity close to the crude oils was designed.

7.2.1 Mineral oil: Marcol 85 mixture

The mineral oil was prepared by mixing Marcol 85 and n-heptane in different ratios. The mixing ratio was determined by measuring the viscosity of the crude oils, and then try to prepare a mixture of Marcol 85 and n-heptane that matched the viscosity of the crude oils. The mean viscosity of the crude oils was 3.0 mPa.s, and the 58% Marcol 85 42% n-heptane mixture had a viscosity of 2.7 mPa.s. The Marcol 85 and n-heptane mixture with the 58:42 ratio was utilized in this experimental work, and the mixture was prepared by weight [g] which is more accurate than volume [ml]. Figure 7.6 presents the viscosity measurements for crude oils and the mineral oils.

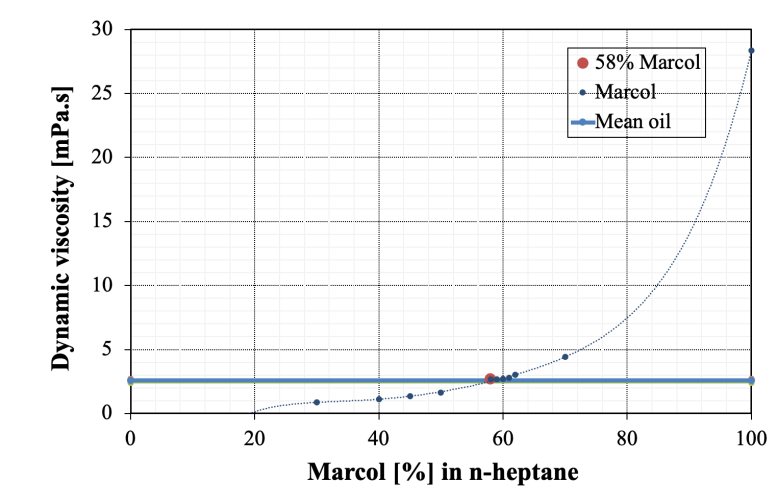

Figure 7.6 Viscosity measurements for preparation of the mineral oil

7.2.2 Effect of crude oil acids on interfacial tension

The interfacial tension was measured for the utilized crude oils and for the mineral oil. The six cores were exposed to three different crude oils with different acid numbers. The crude oils are oil A, B and C, where A has the lowest acid number and C the highest. After the forced imbibition tests, the IFT between the oils and FW was measured with the Du Noüy ring method at 23°C. The IFT results are plotted versus acid number of the oils. Figure 7.7 presents the measured IFT versus AN for the oils.

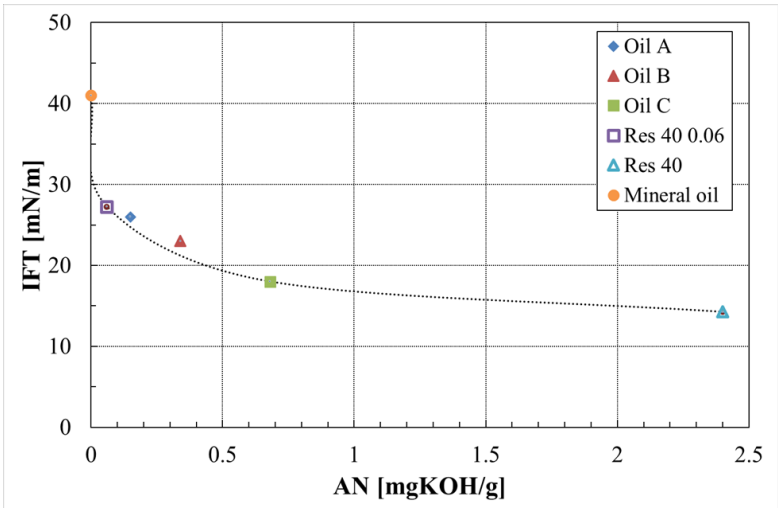

Figure 7.7 Measured IFT at 23°C between oil and DI-water versus measured acid number of the oils.

The mineral oil had an IFT of 41 mN/m. For the crude oils, it was observed that IFT decreased when AN increased which corresponds to Buckley and Fan (2007). Oil A has the lowest acid number and oil C has the highest acid number, and it is clear from figure 7.7 that the IFT decreases with increasing AN. Capillary forces will decrease when IFT decreases, according to

equation (2.6) in section 2.2.3. The oil recovery tests performed in this experimental work, could be affected by the increased IFT in the mineral oil compared to the modified crude oils. Only small contaminations of the mineral oil could also have significant effects on the IFT.

7.3 Oil recovery tests on water-wet cores

The cores SKR1 and SKR2 are used as reference cores and were prepared to be initially water-wet. First the cores were cleaned with distilled water to remove easily dissolvable salts and sulfate ions initially in the outcrop material. SO_4^{2-} has a strong affinity for the chalk surface and can affect the initial wetting established during core restoration. Then the cores were restored with 20% formation water saturation, and saturated and flooded with the mineral oil in a Hassler core holder.

7.3.1 Oil recovery by FI

Forced imbibition tests was performed on the cores. The restored cores were flooded at 23°C with FW at injection rate of 1 PV/day until a recovery plateau was reached and until the pressure-drop had stabilized. Then the injection rate was increased to 4 PV/day to lower S_{or} by increasing the viscous forces. The pressure drops and oil recovery in %OOIP was measured and plotted versus time. The results of the forced imbibition test for the two reference cores are presented in figure 7.8. FI hr in the figures represents the forced imbibition at higher injection rates (4 PV/day).

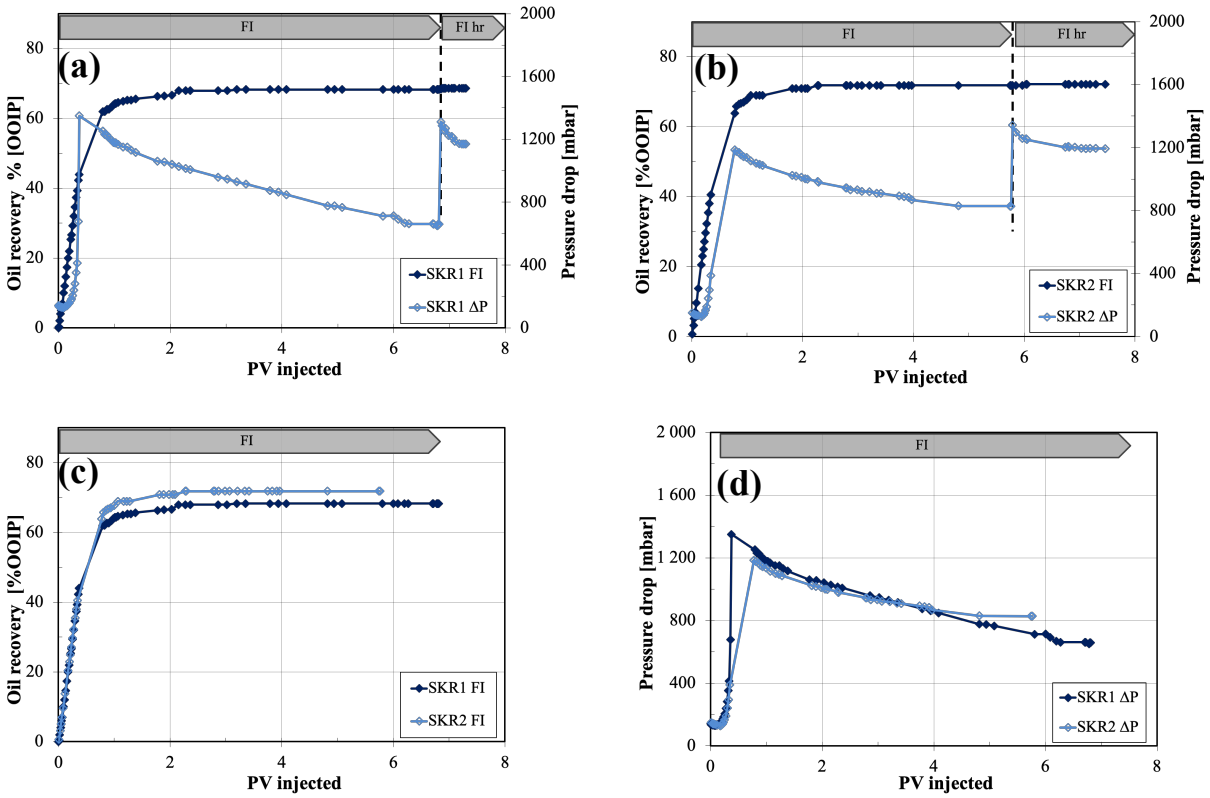

Figure 7.8 Oil production profile and pressure drop for two water-wet reference cores. (a) reference core (SKR1) and (b) reference core (SKR2) during forced imbibition with FW. The cores with S_{wi}=20% were flooded at a rate of 1 PV/day at 23°C. At the end, the injection rate was increased to 4 PV/day. Figure (c) compare oil production and (d) compare ΔP for the two cores.

The oil production profiles for the two oil recovery tests have the same trend and more than 40% of the oil is produced before water breakthrough. After 1 PV injected, more than 60% of the oil is recovered. The recovery plateau is reached after 2.5 PV injected (68-72 %OOIP). Hence, there is favorable mobility conditions for high displacement efficiency for the water-wet system. The pressure-drop profiles for the cores shows also the same trend. The pressure build-up is delayed and reach a maximum after 0.5 PV. The delay in the pressure-build up is due to the strong capillary forces in the core. Water imbibes immediately and starts to displace the oil. The pressure-build up peaks at water breakthrough, and ΔP decreases with increasing amount of FW injected. The pressure-drop will be influenced by positive capillary forces, which becomes zero when the pressure drop is stabilized at the plateau. When the oil recovery plateau is reached after 2.5 PV injected, the ΔP is still decreasing for more than 2 PV injected and stabilizes after 5-6 PV injected. This is significantly delayed compared to the plateau of recovery. Redistribution of oil in the pores, and water flows more easily in the core. There is a slightly difference between the two reference cores. SKR2 produce only slightly more oil

compared to SKR1. The pressure build-up is lower for SKR2, and it also stabilize one day earlier. However, the trend is equal and the experimental results for the two strongly water-wet reference cores are reproduced within a normal uncertainty for the two cores.

When the injection rate is increased to 4 PV/day, an immediately pressure build-up is observed, but only a maximum of 1% extra oil is produced. The pressure-drop stabilizes after 1 PV injected. The capillary forces are gone, and the recovery is controlled by the viscous forces. Later in this experimental study, relative permeability curves are modelled based on history matching of experimental data, and the increased rate data is not taken into consideration.

7.3.2 Oil recovery by SI

After the FI-test, the two reference cores were cleaned and restored to S_{wi}=20% and saturated with the mineral oil again. A spontaneous imbibition test was performed to confirm the wettability of the cores. Figure 7.9 presents the results of the SI tests.

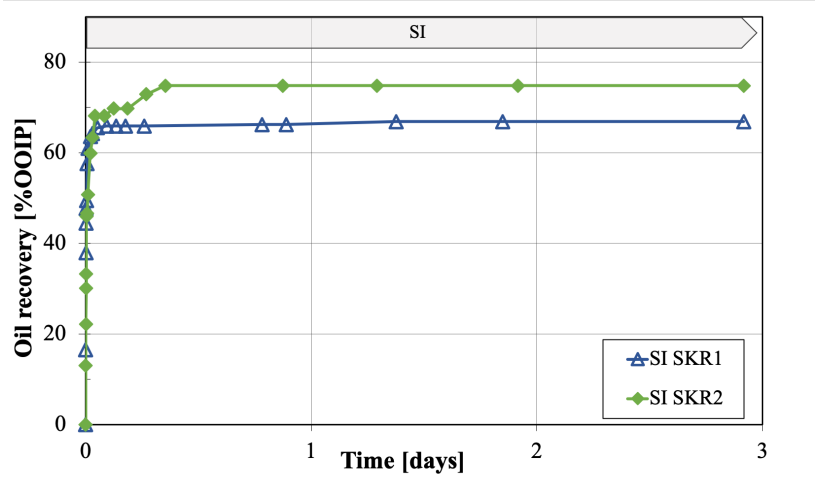

Figure 7.9 Oil production profiles for two strongly water-wet reference cores (SKR1 and SKR2) during spontaneous imbibition with FW at 23°C.

The spontaneous imbibition tests confirm that the two reference cores are strongly water-wet. Hence, water occupies the small pores and contact the majority of the rocks surface. With strong positive capillary forces, water imbibes rapidly into the cores, reaching the recovery plateau after only a few hours. The oil production profiles for the two cores have the same trend, and ultimate recovery is 67 %OOIP for SKR1 and 75 %OOIP for SKR2. This is close to the recovery observed during the forced imbibition experiments, which was 68 %OOIP for SKR1 and 72 %OOIP for SKR2. The Amott wetting index, I_w and the simplified wetting index I_w^* can

be calculated for the fractional-wet cores with the mean oil production during SI for the reference cores, $\%R_{ww} = 71\%$.

7.3.3 Oil recovery by SI+FI

After the spontaneous imbibition test on SKR2, the core was placed in the Hassler core holder, and a forced imbibition test was performed. Figure 7.10 presents the test results, first a spontaneous imbibition test followed directly by forced imbibition test where oil production and pressure-drop are plotted versus time.

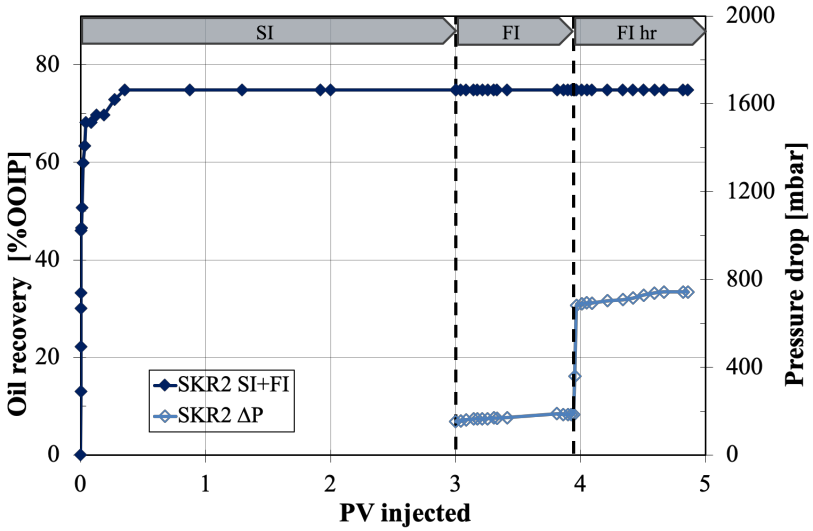

Figure 7.10 Oil production profile for a water-wet reference core (SKR2) during a spontaneous imbibition test followed by a forced imbibition test with FW at 23°C.

The production profile for the reference core during spontaneous imbibition followed by forced imbibition shows that the oil is rapidly produced during SI, which confirms the wettability of the core to be strongly water-wet. No more oil is produced during the forced imbibition test. The capillary forces are most likely gone, and water has imbibed and probably occupied most of the pores, hence no more oil can be produced. The pressure-drop data from the forced imbibition test shows that the pressure stabilize quickly and confirms that the capillary forces are gone. No more oil is produced after the injection rate is increased four times, and the pressure also stabilizes.

7.3.4 Chromatographic wettability test for water-wet core

The fraction of water-wet surface area was measured by a chromatographic wettability test. The test was performed after the forced imbibition test. Effluent brine samples during SW½T flooding were collected with an auto-sampler, and the areas between SCN^- and SO_4^{2-} were

determined by ion chromatography analysis of the ion concentration. The chromatographic separation between SCN^- and SO_4^{2-} for the reference cores are presented in figure 7.11

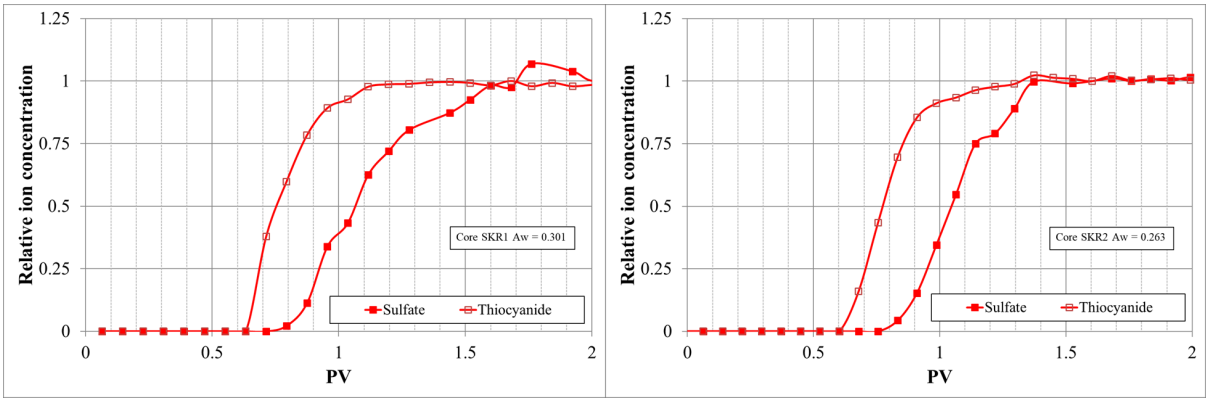

Figure 7.11 Chromatographic separation between tracer and sulfate for initially strongly water-wet cores. (Left) reference core (SKR1) and (right) reference core (SKR2)

Tracer curves shows the same trend for both cases containing the same type of pore distribution. The mean area between the SCN^- and SO_4^{2-} curves are A_w=0.282. The wetting index *WI* can be calculated for the fractional-wet cores by using A_w=0.282 as reference water-wet surface area.

7.3.5 Summary oil recovery tests for water-wet systems

There were observed almost the same recovery and recovery profiles during SI and FI for the water-wet cores. Active capillary forces during forced imbibition was observed in the delayed pressure build-up, after ½ PV injected and the delayed stabilization of ΔP at recovery plateau. Hence, the capillary forces affect the recovery for water-wet systems. The wettability of the reference cores was confirmed by the chromatographic wettability test and spontaneous imbibition test to be strongly water-wet. Table 8 summarize the experimental results from the tests.

Table 8 Experimental results of the oil production in %OOIP and wettability of the reference cores during SI and FI.

Core	SKR1	SKR2	Average results
%R by SI [%OOIP]	67	75	71
%R by FI [%OOIP]	68	72	70
A_{wett}	0.301	0.263	0.282

7.4 Oil recovery tests on fractional-wet cores

Two SK outcrop cores were prepared to have a reduced water wetness by introducing crude oil with polar components. Initial, the cores were cleaned with distilled water (5 PV injected) to displace easily dissolved salts and initial water saturation, S_{wi}=20% was established. Then the cores were exposed to 4 PV of crude oil C. The crude oil is used to wet the surface of the cores. At last, 5 PV of mineral oil was introduced to the cores to displace the crude oil in the pores without removing adsorbed polar organic components from the mineral surface. Hence, mineral oil with a constant viscosity was utilized for all cores during the whole experiment.

7.4.1 Oil recovery by FI

Forced imbibition test was performed on the initial fractional-wet core (SKC1) at 23°C. Oil recovery and pressure data was measured and plotted versus time. Figure 7.12 presents the results for the FI-test of SKC1.

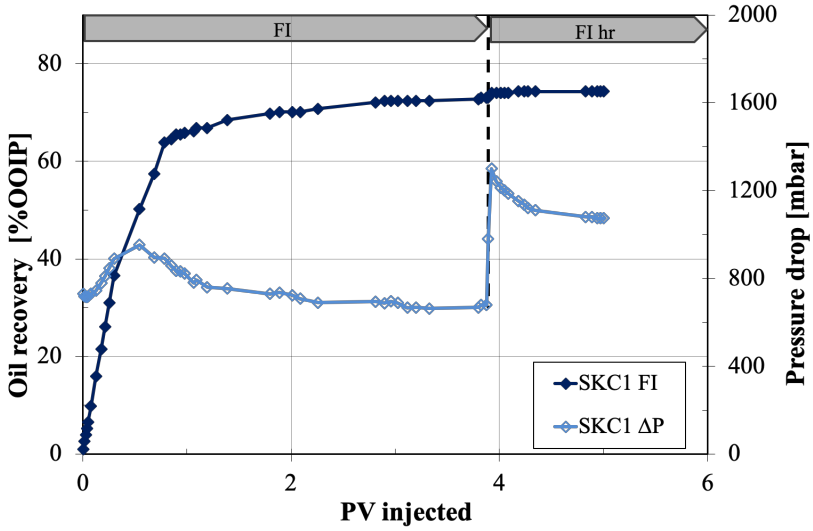

Figure 7.12 Oil production profile and differential pressure for a core exposed to POC (SKC1, AN=0.67mgKOH/g) during forced imbibition with FW at S_{wi}=20%.

The initial fractional-wet core (SKC1) which are exposed to oil C with AN=0.67 mgKOH/g has the same oil production profile trend as the reference cores (SKR1 and SKR2). Pure oil production is observed until more than 35 %OOIP is produced. After 1 PV injected, more than 60% of the oil is recovered. The recovery plateau is reached after 3 PV injected. There is a favorable mobility ratio between the two fluids. The observed oil recovery profile correspond to results obtained by McDougall and Sorbie (1995) where the maximum recovery is achieved in weakly oil-wet systems containing a mixture of oil- and water-wet pores. Figure 7.13

presents oil recovery profiles and pressure-drop for core SKC1 compared to reference core SKR2.

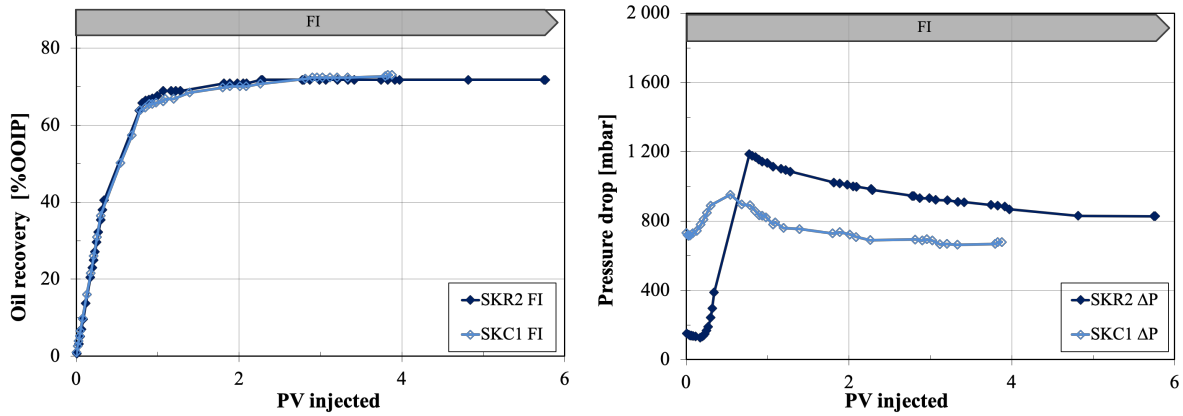

Figure 7.13 Less water-wet core SKC1 (AN=0.67 mgKOH/g) compared to reference core SKR2. The oil production profiles are identical, while the pressure-drop is lower and stabilize more quickly for the fractional-wet core.

The lowest ΔP plateau is reached when the core has a reduced water-wetness. However, the oil recovery results indicate that there is still contribution of positive capillary forces. The introduction of mineral oil, which will increase the IFT compared to oil C, will increase the capillary forces in the core according to equation (2.6) in section 2.2.3. The purpose of the experiment was to change the wetting in the cores i.e. increase the contact angle θ. However, as observed in figure 6.11, the oil production is approximately the same compared to the reference cores, and this is probably due to the IFT which is more dominant in this case. The IFT of the produced oil were measured to be 32 mN/m. Then it is clear that the IFT of the produced oil has decreased due to the contamination of polar organic components in oil C. IFT of mineral oil is 41 mN/m and IFT of oil C is 18 mN/m, respectively.

The pressure-drop profile shows a lower initial pressure build-up and the ΔP stabilize more rapidly compared to the reference cores. Confirming less positive capillary forces. The rate of imbibition will be reduced at less water-wet conditions, but the ultimate recovery is dependent on pressure/magnitude of P_c. Increased injection rate of 4 PV/day produced less than 2% extra oil. Confirming that most of the oil is produced at low injection rates and are less dependent on pressure drop and viscous forces.

7.4.2 Oil recovery by SI

The forced imbibition test was followed by a spontaneous imbibition test. Before the test, the core was mild cleaned and dried to S_{wi}=20% and saturated with the mineral oil again. The SI-test confirms the wettability of the less water-wet core. Figure 7.14 presents the results for the SI-test of SKC1 compared to reference core SKR2.

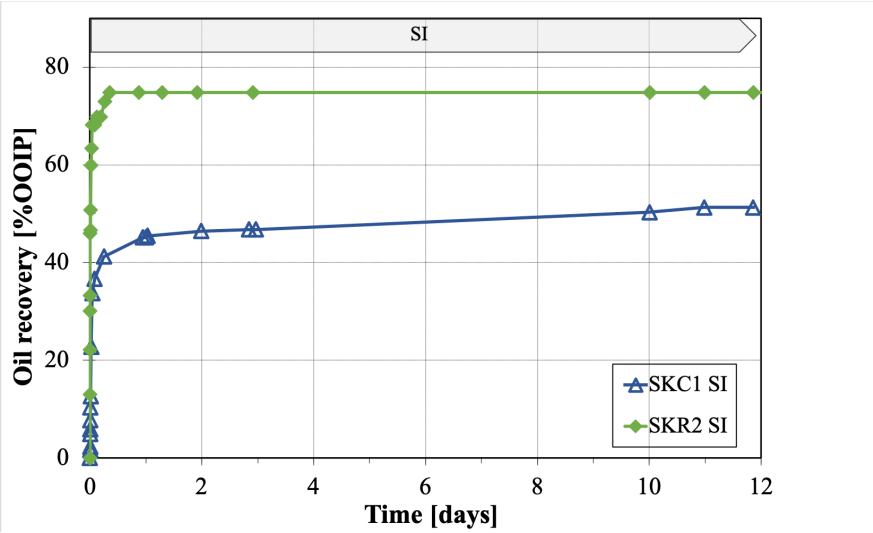

Figure 7.14 Oil production profile for a core exposed to crude oil (SKC1, AN=0.67 mgKOH/g) and a water-wet reference core (SKR2) during spontaneous imbibition with FW. The less water-wet core has a reduced imbibing rate and the production is lower compared to the water-wet core.

The spontaneous imbibition test for SKC1 showed a maximum recovery of 51.3 %OOIP. Compared to the reference cores the production is lower, and the imbibition rate is significantly reduced compared to the water-wet core SKR2. Hence, oil will occupy more of the small pores and contact more of the rock surface. However, over 40% of the oil is produced during the first day. Introduction of crude oil significantly reduces the water-wetness, and hence reduce the available capillary forces. Though, the core is still on the water-wet side. During the mild core cleaning process in front of SI, some of the polar components may have been removed and the water-wetness is slightly increased.

7.4.3 Oil recovery by SI+FI

For the second core (SKC4) exposed to oil C, reversed experimental procedure was performed at 23°C. A spontaneous imbibition test to confirm the initial wettability, followed by a forced imbibition test. Oil production profiles and pressure drop versus time was measured and plotted. There was no need for a mild cleaning process of the core between the recovery tests. Figure 7.15 presents the SI-test for one reference core and for the two cores exposed to oil C.

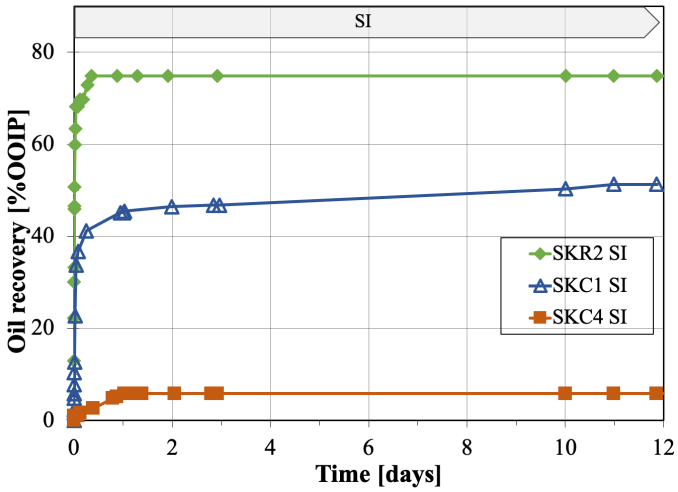

Figure 7.15 Spontaneous imbibition tests of one core exposed to crude oil (SKC4, AN=0.67 mgKOH/g compared to one reference core (SKR2) and one core exposed to the same crude oil (SKC1, AN=0.67 mgKOH/g) at 23°C. The less water-wet core, SKC4 produced lower volumes of oil and the imbibition rate was low compared to the other two cores. SKC1 has been through a mild cleaning process before SI, and there is less contamination of POC in the core.

The spontaneous imbibition test shows a maximum recovery of 5.8 %OOIP after 3 days. The low oil recovery implies a less water-wet core, and significantly lower than for SKR2. Hence, more oil is occupying the small pores, while water is located in the larger pores. Imbibition of water could take place when we have positive capillary forces nearly controlled by wettability and IFT. Core SKC4 indicates the initial wetting of the fractional-wet system compared to core SKC1. For core SKC1 a forced imbibition test and a mild core cleaning were conducted before SI. This would lead to less contamination of polar organic components in the porous system. The IFT of the system will increase due to the cleaning but also because of the m-oil. A higher IFT in the system is favorable for SI, and hence more water is imbibed to produce the oil.

Figure 7.16 (left) presents the results for SKC4, the SI test followed by the FI test at 1 PV/day and increased injection rate, 4 PV/day. (Right) forced imbibition test, where oil production and pressure drop are measured. Figure 7.17 compares the results for all cores. (left) oil production and (right) pressure-drop.

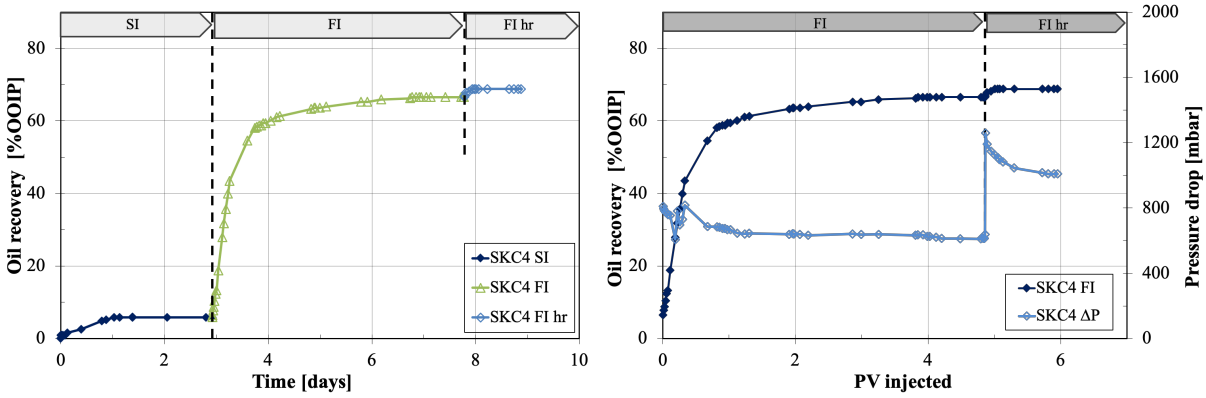

Figure 7.16 Oil production profiles for a core at S_{wi}=20% exposed to crude oil (SKC4, AN=0.67 mgKOH/g) during (left) spontaneous imbibition test followed by a forced imbibition test with FW at 23°C, and (right) forced imbibition test with FW at 23°C, oil production and pressure drop is plotted versus time.

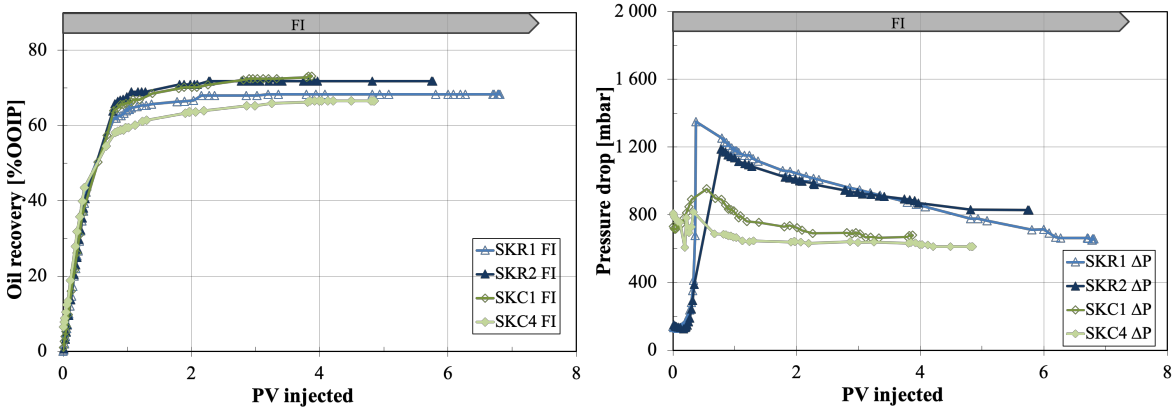

Figure 7.17 (left) Oil recovery compared for all cores and (right) pressure drop compared for all cores

The oil production profile for the forced imbibition test has the same trend but an earlier water breakthrough compared to the other tested cores, illustrated in figure 7.17. 60 %OOIP is produced after 1 PV injected and the recovery plateau is reached after 4 PV. The pressure-drop profile shows lower pressure build-up, confirming low water mobility, around 800 mbar compared to 1000 mbar for SKC1. The pressure stabilizes after 1 PV injected when 60% of the oil is recovered. Some oil is still produced after the pressure-drop has stabilized, and this can be due to viscous forces. The IFT of the produced oil were measured to be 30 mN/m. The IFT is slightly lower compared to the oil produced form core SKC1. The IFT of the mineral oil has decreased due to contamination of polar organic components. IFT of mineral oil is 41 mN/m and IFT of oil C is 18 mN/m, respectively.

The two cores exposed to oil C produced almost the same amount of oil. The total production for SKC1 was 74 %OOIP and for SKC4 the total production was 69 %OOIP. Compared to the reference cores, the oil production is approximately the same. During forced imbibition, positive capillary forces and viscous forces contribute to oil recovery. SK cores with pore radius below 1 μm could develop strong positive capillary forces, especially at high IFT. The introduction of the mineral oil will also contribute to higher IFT compared to if it was only crude oil in the pores. The oil recovery profiles also show that the production is capillary driven. Water imbibes immediately into the core and displace the oil in the pores, which also results in delayed pressure-build up. When the capillary forces are gone, the viscous forces will displace the oil. In this case, almost all of the oil is displaced by water, whether if the cores are strongly water-wet or less water-wet.

The wettability of core SKC4 can be investigated by calculating the The Amott water index, I_w with equation (3.2) from section 3.2.2. The calculation is shown in equation (6.1).

$$I_{w,SKC4} = \frac{0.06}{0.06+0.61} = 0.09 \tag{6.1}$$

The simplified wetting index, I_w^* for SI experiments could also be used to determine the initial wettability of cores which has been exposed to crude oil. The calculations are based on the total recovery during SI divided by a very water-wet reference core, equation (3.6) from section 3.2.4. The mean oil production during SI for the reference cores were, $\%R_{ww}$ = 71%. Equation (6.2) and (6.3) represents the calculation of the wetting index.

$$I^*_{w,SKC1} = \frac{0.51}{0.71} = 0.72 \tag{6.2}$$

$$I^*_{w,SKC4} = \frac{0.06}{0.71} = 0.08 \tag{6.3}$$

The wetting index confirms the wettability of the cores. SKC4 is less water-wet, i.e. neutral-wet or fractional-wet as it approaches 0, while SKC1 is more water-wet as it approaches 1. SKC1 is more water-wet due to the mild core cleaning procedure before the spontaneous imbibition test. The wettability measurements by SI is best to perform right after the first core

restauration, when the wettability is established in the core. Hence, not followed after a forced imbibition or a second restauration, i.e. mild core cleaning.

7.4.4 Chromatographic wettability tests for fractional wet cores

The fraction of water-wet surface area for the fractional-wet cores (SKC1 and SKC4) was investigated by a chromatographic wettability test. The procedure is the same as for the reference cores. Figure 7.18 presents the results.

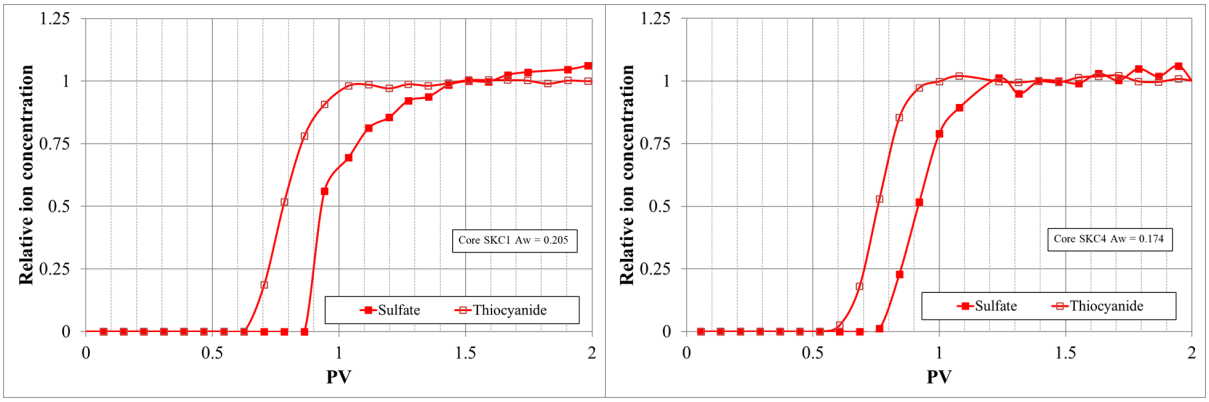

Figure 7.18 Chromatographic separation between tracer and sulfate for core exposed to crude oil, (AN=0.67 mgKOH/g), i.e. initially fractional-wet. (Left) fractional-wet core (SKC1) and (right) fractional-wet core (SKC4)

The area between the curves for the two cores is significantly less compared to the reference cores. This implies that the cores are less water-wet, but still on the water-wet side. The wetting index for the cores can be calculated with equation (3.7) from section 3.2.5. The wetting index for fractional-wet core SKC1 is calculated to be $WI = 0.73$ and for core SKC4 $WI = 0.62$. The calculations are shown in equation (6.4) and (6.5)

$$WI_{SKC1} = \frac{0.205}{0.282} = 0.73 \tag{6.4}$$

$$WI_{SKC4} = \frac{0.174}{0.282} = 0.62 \tag{6.5}$$

The calculated wetting index indicates that the systems are less water-wet compared to the reference cores and have a more fractional wetting as the values are closer to 0.5 which identifies a neutral-wet system. Core SKC1 has a higher wetting index compared to core SKC4. This can be due to that they are different cores, and that there are some diverse in their

properties. The chromatographic wettability test is performed after the forced imbibition test, and no cleaning process has been conducted on the cores.

7.4.5 Summary oil recovery tests for fractional-wet system

There were observed a slightly difference in the oil production for the two less water-wet systems. Core SKC4 had an earlier water breakthrough compared to SKC1 and the two reference cores. This can be due to that some of the oil had already been produced during SI, and also some of the capillary forces were gone. However, the differential pressure started at a peak before it dropped and build up again. This indicates that there were still capillary forces left in the core during FI, and together with viscous forces the oil was produced. Active capillary forces were also observed in core SKC1 which had a delay in pressure build-up. The ΔP stabilized after 3 PV for SKC1 and only after 1 PV for SKC4 and the recovery plateau was reached after 3 PV and 4 PV, respectively. This indicates that the viscous forces also contribute to oil recovery. IFT measurements of the produced oil signalized that the IFT of the m-oil had decreased due to contamination of oil C. However, the introduction of m-oil compared to only pure crude oil will contribute to an increase of the IFT, which will increase the capillary forces in the cores. The wettability of the cores exposed to crude oil was investigated by the chromatographic wettability test and spontaneous imbibition test to be less water-wet. Table 9 summarize the experimental results from the tests.

Table 9 Experimental results of the oil production in %OOIP and wettability of the reference cores during SI and FI

Core	SKC1	SKC4
%R by SI [%OOIP]	51	6
%R by FI [%OOIP]	73	61
A_{wett}	0.205	0.174
WI	0.73	0.62
I_w	0.40	0.09
I_w^*	0.72	0.08
IFT [mN/m] of produced oil	32	30

7.5 Comparison water-wet and fractional-wet core

The two reference cores are constructed to be initially strongly water-wet while the two other cores are constructed to be initially fractional-wet by introducing crude oil to the cores. Figure 7.19 presents the results for one of the reference core (SKR2) and one of the less-water wet core (SKC4) during a spontaneous imbibition test followed by a forced imbibition test.

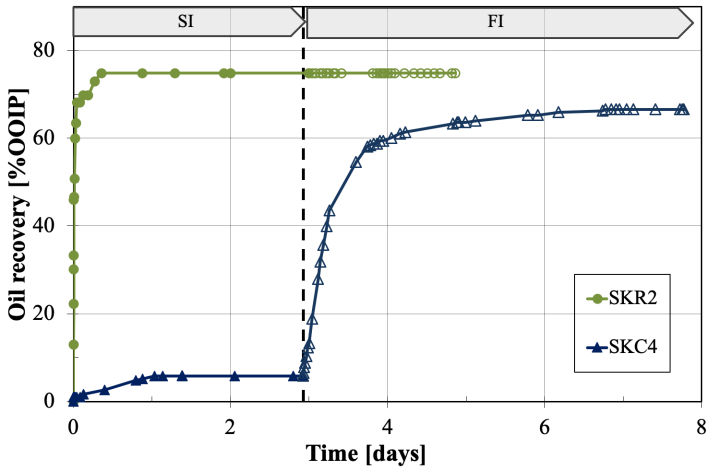

Figure 7.19 Oil recovery tests at 23°C with FW for a water-wet reference core (SKR2) at S_{wi}=20%, compared with a fractional-wet core exposed to crude oil at S_{wi}=20% with AN=0.67 mgKOH/g (SKC4).

Both cores produced more than over 60% OOIP, but for the water-wet core the oil is produced during SI, while for the less-water wet core the largest volume of oil is produced during the FI. When crude oil is introduced to the system, the capillary forces will decrease due to adsorption of polar components and less oil is produced during spontaneous imbibition. For the water-wet cores using an oil with high IFT, the imbibition process starts immediately, and the oil is produced due to positive capillary forces, both during SI and FI.

The spontaneous imbibition tests are performed on core scale (cm) where the oil have to be transported from the center of the core to the surface. The core is surrounded by the imbibing fluid (FW); hence the oil production takes place on all sides of the core. The oil production is rapid, and the recovery plateau is reached after 2-3 hours. The forced imbibition tests are performed at mm or µm scales, where the oil have to be transported from smaller to larger pores. The imbibing fluid is only injected at one end; hence FW will move into the largest pores and take the easiest way with lowest restrictions and with positive capillary forces. Then FW will imbibe into the narrow smaller pores. The oil production is controlled by the injection rate, and the recovery plateau is reached after more than 2 days compared to the spontaneous imbibition test.

7.6 Comparison and summary of all oil recovery tests

Table 10 summarize the experimental values from the oil recovery test for all the eight cores utilized in this experimental work together with Harestad (2019) and Radenkovic (2019). Two strongly water-wet reference cores (SKR1 and SKR2) and six cores exposed to different model crude oils (SKC1-SKC6).

Table 10 Summary of the experimental results during oil recovery tests

FI-test followed by SI-test					
Core	**SKR1**	**SKR2 (1)**	**SKC1**	**SKC2**	**SKC3**
Oil	mineral	mineral	C	B	A
AN	-	-	0.67	0.34	0.15
%R SI [%OOIP]	67	75	51	58	63
%R FI 1PV/day [%OOIP]	68	72	73	68	67
%R FI 4PV/day [%OOIP]	1	-	1	1	8
∑%R FI [%OOIP]	69	72	74	69	75

SI-test followed by FI-test				
Core	**SKR2 (2)**	**SKC4**	**SKC5**	**SKC6**
Oil	mineral	C	B	A
AN	-	0.67	0.34	0.15
%R SI [%OOIP]	75	6	37	58
%R FI 1PV/day [%OOIP]	-	61	18	2
%R FI 4PV/day [%OOIP]	-	2	11	2
∑%R [%OOIP]	75	69	66	62

As observed from table 10 the reference cores had approximately the same experimental results. There were observed favorable mobility during waterflooding, hence almost all of the oil was produced before water breakthrough. The mean oil production for the reference cores were 72 %OOIP.

In collaboration with Harestad (2019) and Radenkovic (2019), six cores were prepared to be less water-wet by introducing crude oils with different acid numbers. During the first oil recovery test performed on the cores, there were observed highest oil recoveries in the core exposed to the oil with AN=0.67 mgKOH/g. According to McDougall and Sorbie (1995) higher oil recoveries are achieved in weakly oil-wet systems. Core SKC1 with AN=0.67 mgKOH/g produced 73 %OOIP, core SKC2 with AN=0.34 mgKOH/g produced 68 %OOIP and core SKC3 with AN=0.15 mgKOH/g produced 67% OOIP during forced imbibition. Figure 7.20 presents the experimental results for the three cores. (Left) oil production profiles for the cores and (right) pressure-drop profiles for the three cores.

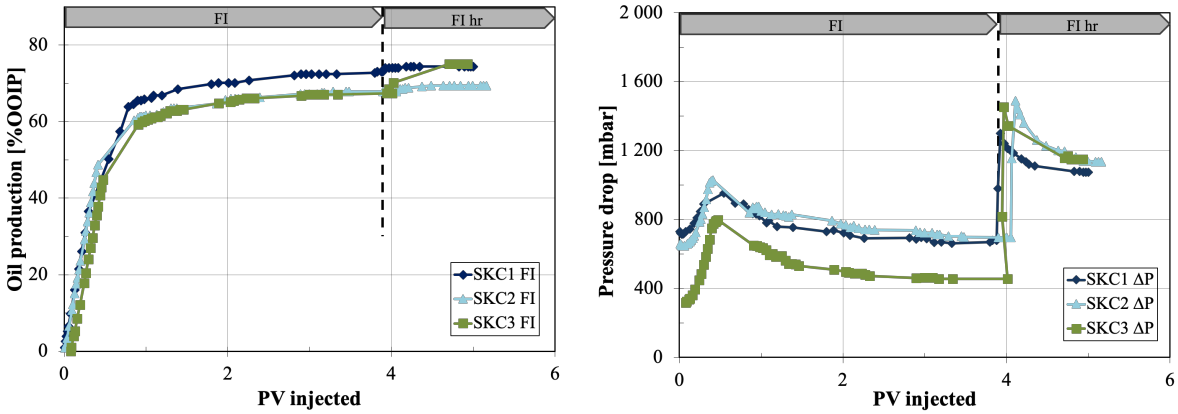

Figure 7.20 Forced imbibition at 23°C with FW for three cores exposed to crude oils with different AN. SKC1, AN=0.67mgKOH/g. SKC2, AN=0.34mgKOH/g. SKC3, AN=0.15mgKOH/g

As observed from figure 7.20, all cores have the same production profile. Core SKC3 with lowest AN produced 8 % more after the injection rate was increased four times, compared to the other two cores which only produce 1 % more. This core has lower viscous forces, due to lower pressure-drops. The increase in production after increased rate can be due to heterogeneity in the core. The pressure-drop profiles are also similar for core SKC1 and SKC2, but lower for the third core, SKC3. There are observed a delay in the pressure-build up after ½ PV injected and in the stabilization of ΔP at recovery plateau, which indicates active capillary forces during FI for all cores. Compared to the reference cores, ΔP stabilize 2 days earlier for the three cores.

The wettability of the cores was investigated by spontaneous imbibition, and it was observed that the core with AN=0.67 mgKOH/g were the less water-wet core compared to the other two.

Hence, the cores will be more neutral-wet when crude oil with a higher AN is introduced to the systems. This corresponds to Zhang and Austad (2005) which studied the wettability of carbonates dictated by the acid number of the crude oil. The oil production with SI was 51 %OOIP, 58 %OOIP and 63 %OOIP with decreasing AN, respectively. IFT will also decrease with higher AN, which will lead to a reduction in the positive capillary forces. Figure 7.21 presents the experimental results from the spontaneous imbibition for the three cores exposed to crude oils with different AN.

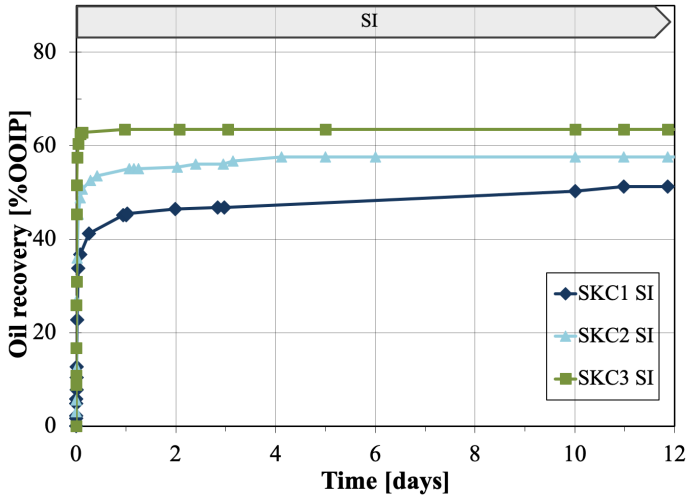

Figure 7.21 Spontaneous imbibition at 23°C with FW for three cores exposed to crude oils with different AN. SKC1, AN=0.67mgKOH/g. SKC2, AN=0.34mgKOH/g. SKC3, AN=0.15mgKOH/g.

During the second oil recovery tests, where the reversed procedure was conducted, the cores with increased AN had lower oil recovery during the spontaneous imbibition test. Core SKC4 with AN=0.67 mgKOH/g produced only 6 %OOIP, core SKC5 with AN=0.34 mgKOH/g produced 37 %OOIP, while core SKC6 with AN=0.15 mgKOH/g produced 58 %OOIP. During the forced imbibition test followed after the spontaneous imbibition test, the oil recovery was vice versa; core SKC4 with the highest AN produced 61 %OOIP more of the cumulative oil, core SKC5 produced 18 %OOIP, while core SKC6 with lowest AN produced only 2 %OOIP more. The total oil recovery for all six cores where overall approximately the same with a mean production of 69 %OOIP. Figure 7.22 presents the combined oil recovery test, SI+FI for core SKC4-SKC6.

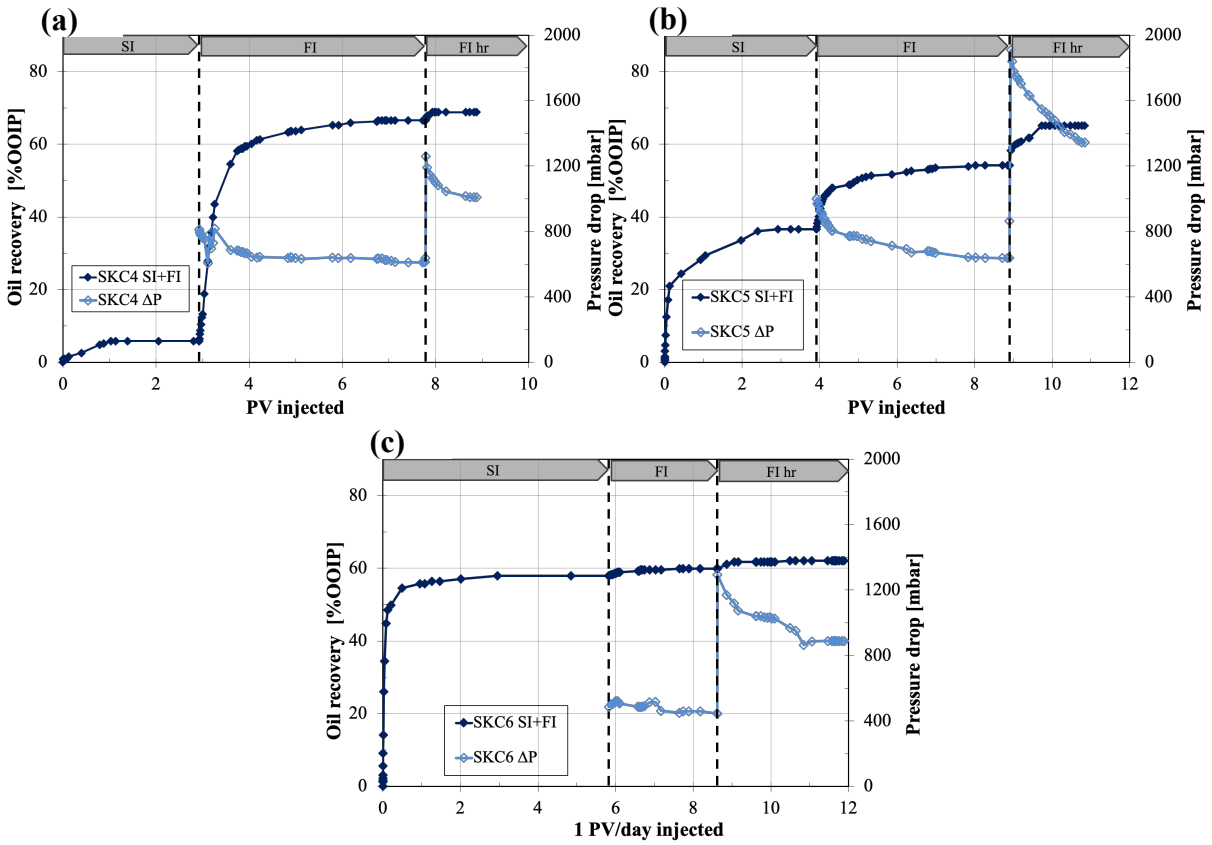

Figure 7.22 Oil recovery by spontaneous imbibition followed by forced imbibition with FW at 23°C for cores exposed to crude oil with S_{wi}=20%. (a) SKC4, AN=0.67 mgKOH/g. (b) SKC5, AN=0.34mgKOH/g. (c) SKC6, AN=0.15mgKOH/g.

Figure 7.22 presents the second oil recovery test for the three different systems. As explained, there are observed an increase in the oil recovery with SI with decreased AN of the crude oil. Core SKC4 produced less during SI, while core SKC6 produced almost all of the oil during SI. This is due to the capillary forces, which are stronger for the core with less contamination of polar organic components. The oil production for core SKC6 during SI were rapid and almost all of the oil was produced before 1 PV/day injected. The rapid imbibition rate and great volume of oil produced indicates that the system is more water-wet than core SKC4.

There are observed different ΔP in the three cores. SKC4 produced less during SI, however there was a delay in the pressure build up which indicates contribution of capillary forces in the oil production by FI. ΔP stabilized after 1 PV injected and the viscous forces were more dominant for the rest of the oil production. When the injection rate was increased, only 2 %OOIP was produced. SKC5 produced more oil during SI compared to SKC4, but fewer capillary forces were observed during FI and less than 60 %OOIP was produced. When the injection rate was increased, the ΔP increased and hence the oil production increased with 11%OOIP. The core had more cumulative oil left in the core to produce and the viscous forces

were more dominant than the capillary forces. SKC6 produced almost all of the oil during SI, and little or no capillary forces were observed during FI. When the injection rate was increased, only 2 %OOIP were produced by contribution of viscous forces.

The wettability of the cores was investigated during the oil recovery tests. Table 11 presents the calculated wetting indexes for the fractional-wet systems and the measured IFT of the produced oil.

Table 11 Wetting index for cores exposed to polar components, reference cores has Aw=0.282

Wetting index	**SKC1**	**SKC2**	**SKC3**	**SKC4**	**SKC5**	**SKC6**
Oil	C	B	A	C	B	A
A_w	0.205	0.207	0.281	0.174	0.248	0.306
WI	0.73	0.73	0.99	0.62	0.87	1.08
I_w	-	-	-	0.09	0.67	0.97
I_w^*	0.72	0.82	0.89	0.08	0.52	0.82
IFT [mN/m] of produced oil	32	27	27	30	28	-

The observed trend for oil production during the recovery tests are confirmed by the determined wetting indexes for the systems. The wetting indexes for the systems increases with decreasing AN. The cores saturated with oil C (AN=0.67 mgKOH/g) has the lowest wetting indexes. The cores saturated with oil B (AN=0.34 mgKOH/g) have higher values, but the cores saturated with oil A (AN=0.15 mgKOH/g) have the highest wetting indexes. There is less contamination of POC in the systems saturated with oil A, i.e. they are more water-wet compared to the other two systems. However, all systems utilized in this experimental work are on the water-wet side.

The measured IFT of the produced oil during FI also confirms that higher AN will contribute to more contamination of polar organic components in the m-oil.

7.7 Numerical core analyses

Relative permeability curves, as well as capillary pressure curves and fractional flow curves were modelled based on history matching (HM) of experimental data from the waterflooding experiments by the simulation software SENDRA. The curves were designed for the water-wet reference cores (SKR1 and SKR2) and for the first core exposed to crude oil (SKC1).

7.7.1 History matching procedure

There were performed two different procedures of the history matching of the experimental data. First, an automatic HM was performed, where SENDRA was allowed to find the best HM between the experimental and simulated data. Then a manual HM was performed to compare if a reasonably better match were obtained. As observed from the experimental work, most of the oil is produced at low injection rates. Hence, the experimental data from the higher injection rate is not used in this part. The experimental data for the HM are found in appendix B while the input parameters for the history match are found in appendix C.

During the experimental work, almost all of the oil in the cores were produced before water breakthrough during the displacement of water, and according to Chukwudeme et al. (2014) it is only possible to extract endpoint relative permeabilities from these unsteady-state displacement processes. The absolute permeabilities and effective permeabilities for the cores were calculated to determine the endpoint relative permeabilities (k_{rw} and k_{ro}) at initial water saturation (S_{wi}) and residual oil saturation (S_{or}). The calculation procedure of the permeability is described in section 7.1.4. The endpoint k_{rw} and k_{ro} were determined using equation (3.8) and (3.9) from section 3.3.1. Table 12 summarize the calculated permeabilities and endpoint saturations.

Table 12 Calculated absolute- and effective permeabilities to determine endpoint relative permeabilities.

	SKR1	**SKR2**	**SKC1**
K [mD]	4.02	4.09	4.12
$K_{eff,w}$ [mD]	0.36	0.29	0.35
$K_{eff,o}$ [mD]	3.22	3.37	4.12
S_{wi}	0.20	0.20	0.20
$1-S_{or}$	0.75	0.77	0.78
$k_{rw}(S_{or})$	0.09	0.07	0.09
$k_{ro}(S_{wi})$	0.80	0.82	0.62

The experimental endpoint relative permeabilities and S_{or} from table 12 where applied in SENDRA as input properties during the automatic HM, while the initial water saturation was constant at S_{wi}=20%. Then, $k_{rw}(S_{or})$, $k_{ro}(S_{wi})$ and S_{or} as well as the Corey exponents were estimated by the simulator, in order to obtain the best history match between experimental and simulated data. The simulated endpoint relative permeabilities and S_{or} are further used for construction of the relative permeability curves, capillary pressure curves and fractional flow curves where the values from the automatic HM are used. Table 13 shows the simulated output properties from SENDRA to create the curves based on automatic HM.

Table 13 Output values from SENDRA for automatic history matching of experimental data of strongly water-wet reference cores and fractional-wet core.

Saturation values	**SKR1**	**SKR2**	**SKC1**
S_{wi}	0.20	0.20	0.20
S_{or}	0.24	0.19	0.14
Corey			
N_w	2.72	1.00	1.00
N_o	2.24	2.69	2.16
$k_{rw}(S_{or})$	0.07	0.07	0.12
$k_{ro}(S_{wi})$	0.99	0.99	0.34
Skjæveland			
C_w	14916	14735	0
A_w	0.251	0.251	0.251
C_o	0	0.14	14828
A_o	0	2.0	0.251

First during the manual HM, the Skjæveland parameters were sat to 0, C_w=0 and C_o=0, respectively. Then the *Sor* was adjusted to a lower value than the calculated, approximately 0.05. The endpoint relative permeabilities were initially sat to 0.2 and were used to adjust the pressure at the start and end. At last, N_w and N_o were increased to around 3-5. The output values were changed until the best HM were achieved. The output values for the manual HM is given in table 14.

Table 14 Output values from SENDRA for manual history match of experimental data for strongly water-wet reference cores and fractional-wet core.

Saturation values	SKR1	SKR2	SKC1
S_{wi}	0.20	0.20	0.20
S_{or}	0.20	0.13	0.16
Corey			
N_w	4	3.5	4
N_o	3	2.8	2.5
$k_{rw}(S_{or})$	0.1	0.12	0.13
$k_{ro}(S_{wi})$	0.4	0.2	0.28
Skjæveland			
C_w	37938	49659	0
A_w	0.251	0.251	0.251
C_o	0	0	0
A_o	0.251	0.251	0.251

7.7.2 History matching

An automatic history match of experimental oil production and pressure-drop were performed on the reference cores. First, the estimated values from table 12 were implemented to the software, then new Corey and Skjæveland parameters were simulated to obtain the best match. The output values are listed in table 13. Figure 7.23 presents measured differential pressure (ΔP) and oil production (RF) from the forced imbibition displacements and the corresponding automatic history matched profiles reported by the SENDRA simulator for the strongly water-wet systems.

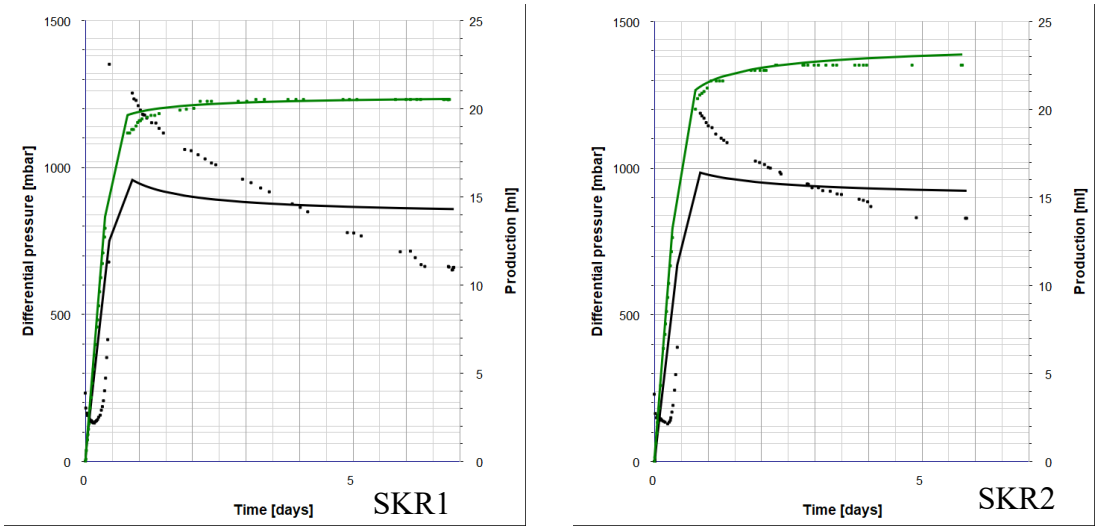

Figure 7.23 Automatic history match of differential pressure and oil production for the strongly water-wet systems. (left) reference core SKR1 and (right) reference core SKR2.

The experimental and simulated oil production were reasonably well matched, while the experimental and simulated differential pressure were not very reasonable matched. The characteristics of the oil recovery profile signalize a piston-like displacement, but the characteristics of ΔP does not signalize a high displacement efficiency. During a piston-like displacement, the trend of RF and ΔP should be significantly equal. ΔP peaks at water breakthrough, where the water saturation is lowest, and then ΔP gradually decreases and stabilize at a plateau, like the oil production stabilize at a recovery plateau. As observed from the experimental work, there were favorable mobility conditions for high displacement efficiency for the water-wet system according to the oil production. However, the time of the water breakthrough is not known, since it happened during the night and measurements were not possible to obtain. Also, the experimental ΔP are decreasing after the pressure build-up and stabilize later compared to the recovery plateau. Hence, the displacement is not piston-like for the water-wet systems. It seems that SENDRA assumes a piston-like displacement and tries to history match according to that. SENDRA is also not capable to identify the capillary forces, which is the essential for the cores in this experimental work. The differential pressure data implies capillary forces, but SENDRA is not capable to HM these data when it assumes piston-like displacement.

A more reasonable match of ΔP was tried to be achieved by a manual history match of the experimental data in SENDRA. The Corey exponents were increased to about 3-4 for both water and oil to match the peak in ΔP. The displacement is still favorable since most of the oil is produced before water breakthrough. The Sor was sat to a lower value than the calculated and the endpoint relative permeabilities were used to adjust the pressure at the start and end. The output values are listed in table 14 and Figure 7.24 presents the manual history match of the experimental data for the strongly water-wet reference cores.

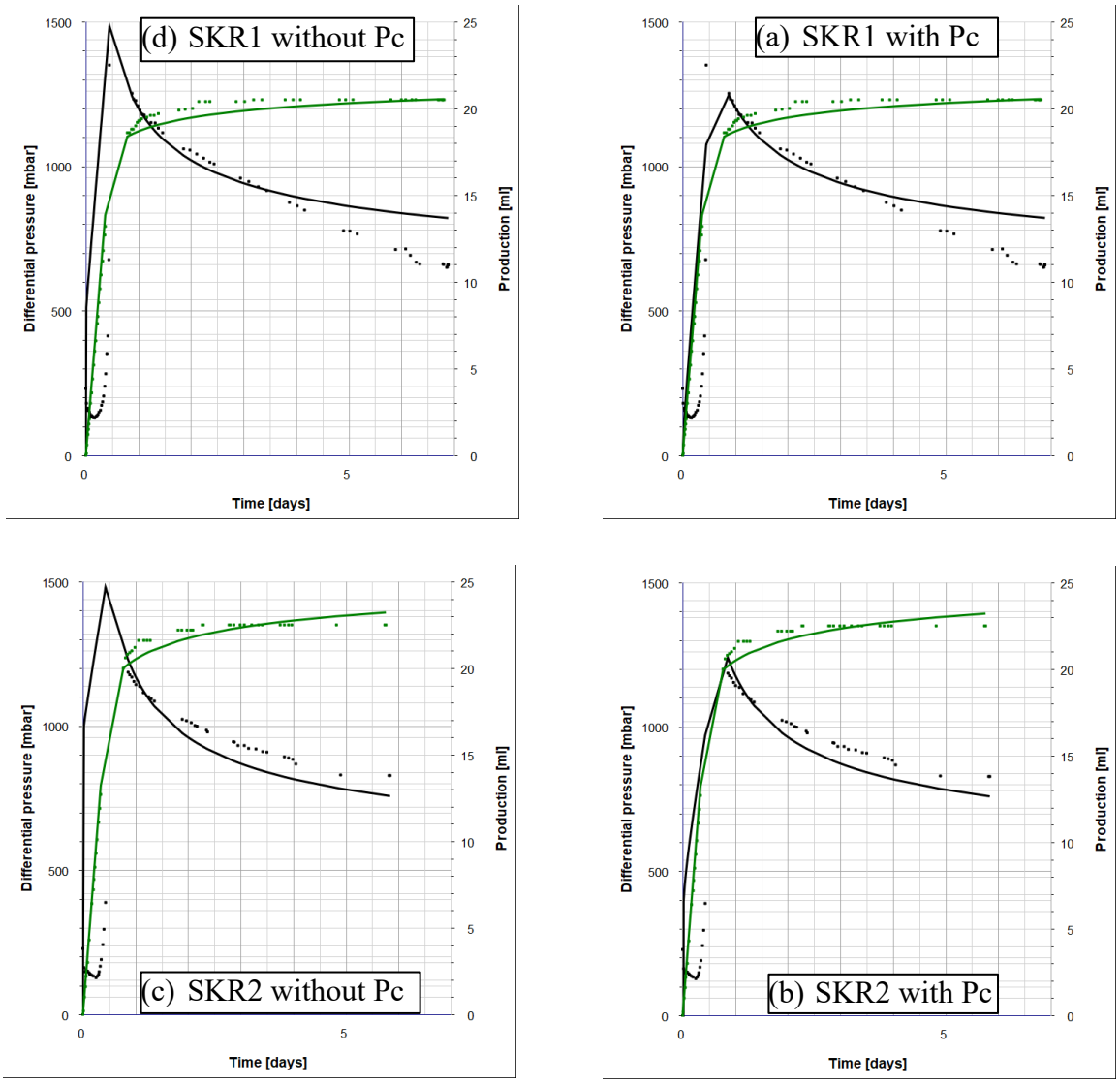

Figure 7.24 Manual history matching of experimental data for the strongly water-wet reference cores. (a) SKR1 without influence of Pc. (b) SKR1 with influence of Pc. (c) SKR2 without influence of Pc. (d) SKR2 with influence of Pc.

There are observed a reasonable better match of ΔP when it was performed manually. The trend of ΔP match better after the peak compared to the automatic history match. However, the values of the endpoint relative permeabilities of water are more equal for the automatic than the manual HM compared to the calculated values. The end of the automatic pressure curve is more stable compared to the manual, which extrapolates more negatively. There are observed a slightly improvement in the match of the peak for ΔP when the capillary forces are included. However, there are not observed significantly changes in the trend of ΔP. The oil production profile is extrapolating in positive direction when the capillary forces are included. It is already confirmed in the experimental work that the capillary forces affect the recovery for water-wet systems. The Corey exponents in table 14 are more equal for the reference cores compared to the Corey exponents from the automatic history match in table 13. The manual history match

output values are further used for construction of relative permeability curves, capillary pressure curves and the fractional flow curves for the strongly water-wet systems.

Figure 7.25 presents experimental differential pressure (ΔP) and oil production (RF) from the forced imbibition and the corresponding automatic history matched profiles reported by the SENDRA simulator for the core exposed to crude oil (SKC1)

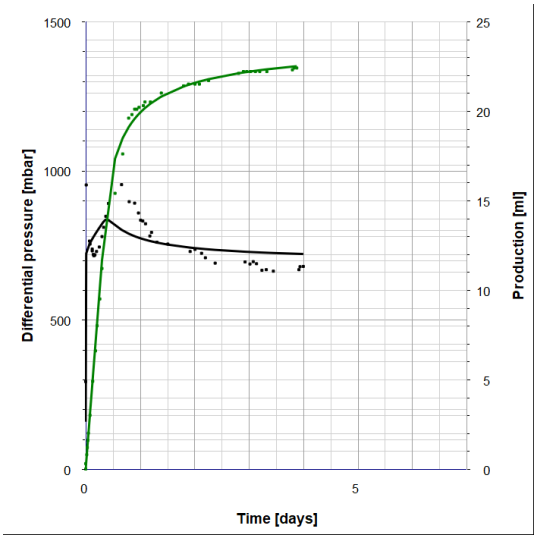

Figure 7.25 Automatic history match of differential pressure and oil production for a less water-wet system, SKC1 (AN = 0.67 mgKOH/g).

The experimental and simulated oil production were reasonably well matched. The automatic history match of the differential pressure was more reasonable compared to the water-wet reference cores, and the simulated values follows the trend of the endpoints of ΔP. However, SENDRA also assumes a piston-like displacement in this case and tries to history match according to that. Like the strongly water-wet system, the displacement is not piston-like but there are favorable mobility conditions. The output values are listed in table 13. A more reasonable HM of ΔP based on the experimental data were tried to be achieved with a manual history match. The output values are listed in table 14, and figure 7.26 presents the manual history match of the fractional-wet core.

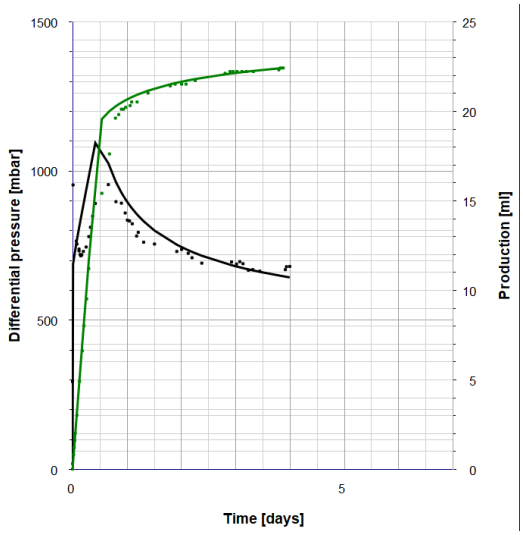

Figure 7.26 Manual history match of differential pressure and oil production for a less water-wet system, SKC1 (AN = 0.67 mgKOH/g).

The manual history match of SKC1 were reasonably better. However, compared to the automatic HM, the trend of ΔP for the simulated profile is extrapolating more negatively. There were not observed significantly changes in the oil production profile during the two different HM. Also, no changes were observed when the capillary pressure were included. The output values for the manual HM of experimental data for core SKC1 are listed in table 14. The automatic HM output values are further used for construction of relative permeability curves, capillary pressure curves and fractional flow curves for the fractional-wet system.

7.7.3 Relative permeability curves for strongly water-wet cores

Relative permeability curves were constructed by the Brooks and Corey (1964) correlations in section 5.2. The Corey parameters (N_w and N_o), the endpoint relative permeabilities and the S_{or} from the manual history match of ΔP and oil production in SENDRA were conducted in the correlation. The relative permeability curves for the strongly water-wet systems are presented in figure 7.27 (a) SKR1, (b) SKR2 and (c) comparison of the two reference cores.

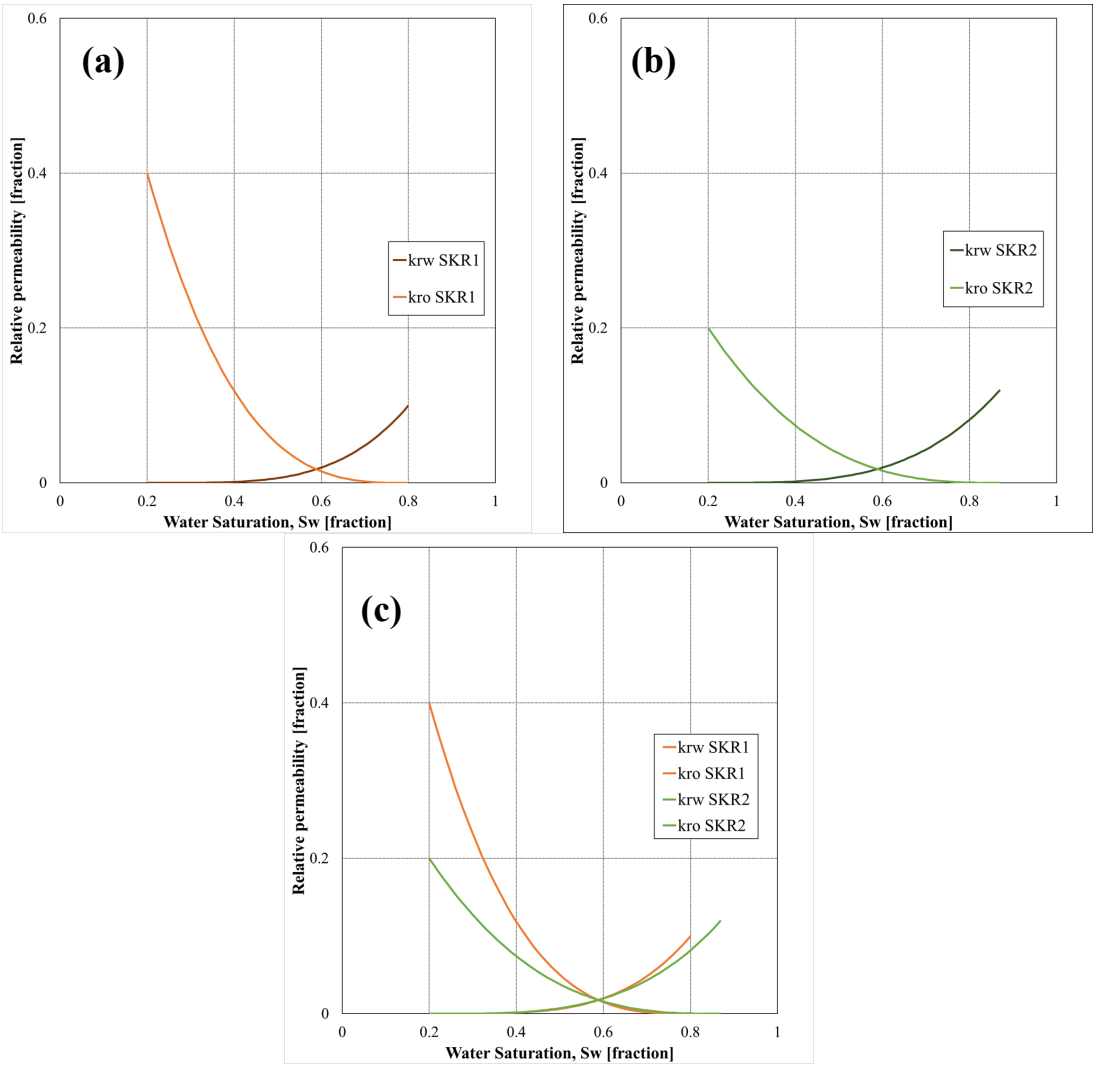

Figure 7.27 Relative permeability curves for strongly water-wet reference cores. (a) core SKR1, (b) core SKR2 (c) comparison of the relative permeability curves for the two reference cores.

The relative permeability curves designed for the strongly water-wet cores were designed based on the manual history match, and the output values are in table 14. The simulated endpoint relative permeability values are lower compared to the calculated values, and this also counts for S_{or} which is also lower. The relative permeability curves designed based on the history match of experimental data are strongly water-wet according to Craig (1971) three rules of thumb, which differentiate between strongly water-wet and oil-wet systems. The crossover saturation is greater than 50%, which indicates strongly water-wet cores. The observed difference in the shape of the relative permeability curves of water are probably due to the difference in the Corey exponents for water, observed in table 14. The simulated endpoint relative permeabilities of water and oil for SKR2 is lower compared to SKR1. The simulated

S_{or} is only 0.13 for SKR2 compared to 0.20 for SKR1. During the manual HM, the output values are taken from the best history match. From the experimental work, it is observed that core SKR2 produced 72 %OOIP while SKR1 produced 68 %OOIP during FI. Hence, the observed change in *Sor* can be due to this. However, the calculated Sor only change from 0.25 for SKR1 to 0.23 for SKR2.

7.7.4 Relative permeability curves for fractional-wet core

The relative permeability curves for core SKC1 which are exposed to crude oil, were constructed with the Brooks and Corey (1964) correlations in section 5.2. The Corey parameters (N_w and N_o), the endpoint relative permeabilities and the S_{or} from the automatic history match of ΔP and oil production in SENDRA were conducted in the correlation. Figure 7.28 presents the relative permeability curves for the less water-wet system compared to the strongly water-wet system.

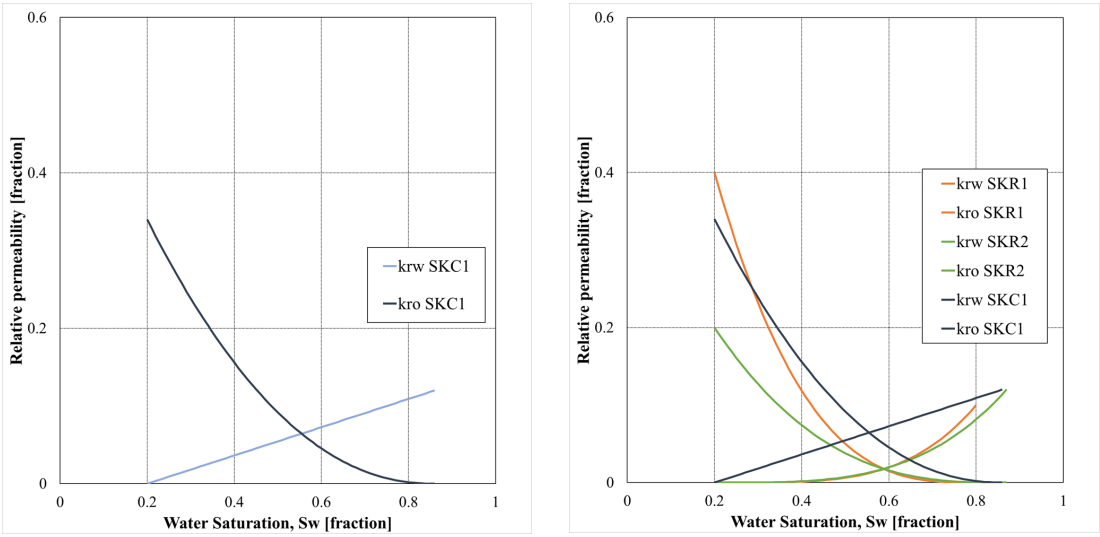

Figure 7.28 (left) Relative permeability curves for core SKC1 exposed to oil C (AN=0.67 mgKOH/g) compared to (right) the relative permeability curves for the strongly water-wet reference cores.

The relative permeability curves for the less water-wet system has also a crossover saturation greater than 50%. According to Craig (1971) the system is then strongly water-wet. There is observed a slightly reduction in the crossover saturation compared to the reference cores, but according to theory the crossover saturation should be even lower for the core exposed to POC. According to Anderson (1987a), the relative permeability of oil decreases while the relative permeability of water increases, when the core becomes more oil-wet. $k_{rw}(S_{or})$ for the less water-

wet core should be higher compared to the strongly water-wet cores, but in this case the value is approximately the same. However, the endpoint k_{rw} can also signal that a large volume of water is absorbed into the chalk material, and that only oil is produced before residual oil saturation. As observed from the experimental work, SKC1 produced 73 %OOIP during FI. S_{or} for SKC1 is closer to SKR2 than SKR1, and this can be due to the oil production. The shape of the relative permeability curve of oil is more straight compared to the others. The Corey exponents are lower compared to the strongly water-wet cores, and hence the shape become straighter.

The objective of this work was to verify if reliable relative permeability curves could be produced from oil recovery profiles and pressure-drop data to explain the wettability alteration by Smart Water injection. Based on the experimental work and results, it seems that SENDRA is not capable to produce reasonable relative permeability curves based on history matching of experimental data from this experimental study. SENDRA produce the relative permeability curves based on the oil production data, which has a favorable mobility ratio. The recovery profiles for the two systems are approximately identical, and hence the relative permeability curves are too. Only one set of reasonable relative permeability curves are produced by SENDRA, and this represents the strongly water-wet system after the wettability alteration by Smart Water.

The relative permeability curves based on the manual history matching was also strongly water-wet and had a crossover saturation greater than 50%. If another correlation or method was used, the curves may have looked different and the results could be more as expected with a decrease in the crossover saturation for the fractional-wet core. Further, if there had been relative permeabilities values in between, the shape of the curve could be changed, and the crossover saturation could have been reduced to a more reasonable value. In this case, the input data are not relevant to the entire saturation interval, and there is a large extrapolating of the curves.

7.7.5 Capillary pressure curves

Capillary pressure curves were constructed by the Skjæveland et al. (1998) correlation in section 5.3. The Skjæveland parameters (C_o and C_w) from the automatic history match of ΔP and oil production in SENDRA were conducted in the correlation. The curves for the two systems are presented in figure 7.29.

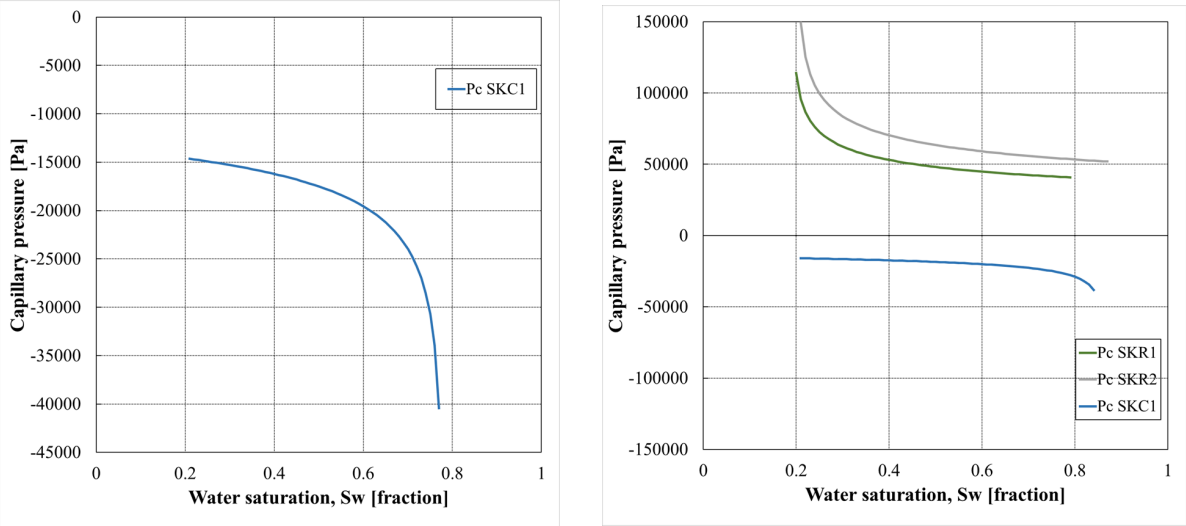

Figure 7.29 Capillary pressure curves for (left) fractional-wet system, core SKC1 and (right) compared with two water-wet reference cores

The capillary pressure curves are designed in the same way as the relative permeability curves, hence based on the manually history matching of experimental data for the strongly water-wet cores but based on the automatic history matching of experimental data for the fractional-wet core. The Skjæveland parameters for the strongly water-wet reference cores are in table 14 while the Skjæveland parameters for the fractional-wet cores are in table 13. The parameters are positive (C_w) for the strongly water-wet systems, which indicates that there are positive capillary forces in the cores. This is confirmed by SI in the experimental part, where almost all of the oil where produced rapidly. The positive capillary pressure curve is observed in figure 7.29 (right). At Pc=0, no more oil is produced during SI, the curve does not cross the saturation axis, which indicates that all the oil is produced at $S_{or.}$ The input parameters in SENDRA is limited, and it is not possible to choose where Pc should be zero.

For the fractional-wet core, the parameter is negative (C_o), and also the capillary pressure curve is negative. In the experimental work, core SKC1 produced 51 %OOIP during SI, which confirms that there are positive capillary forces in the core. It seems that SENDRA model the curve when there are high water saturations, which will result in a negative capillary pressure curve. Also, for mixed-wet systems, or systems exposed to crude oil, the capillary pressure curve should have crossed the S_w axis at 50% water saturation, as illustrated in figure 3.6 in section 3.3.2. However, it is difficult to say if the curves are reliable. They are based on pure extrapolation in an interval that is 10 times larger than where the information is achieved from.

The curves are most likely based on the section where there are high saturations, and then a lot of information before that is not counted for.

7.7.6 Fractional flow curves

Relative permeability curves can be used in the conventional fractional flow equation, which enabling construction of the fractional flow curves. According to McDougall and Sorbie (1995) Buckley-Leverett analysis can be carried out from the curves and utilized to predict the microscopic displacement efficiency that will be influenced by the systems wettability. The fractional flow curves for the two systems are presented in figure 7.30.

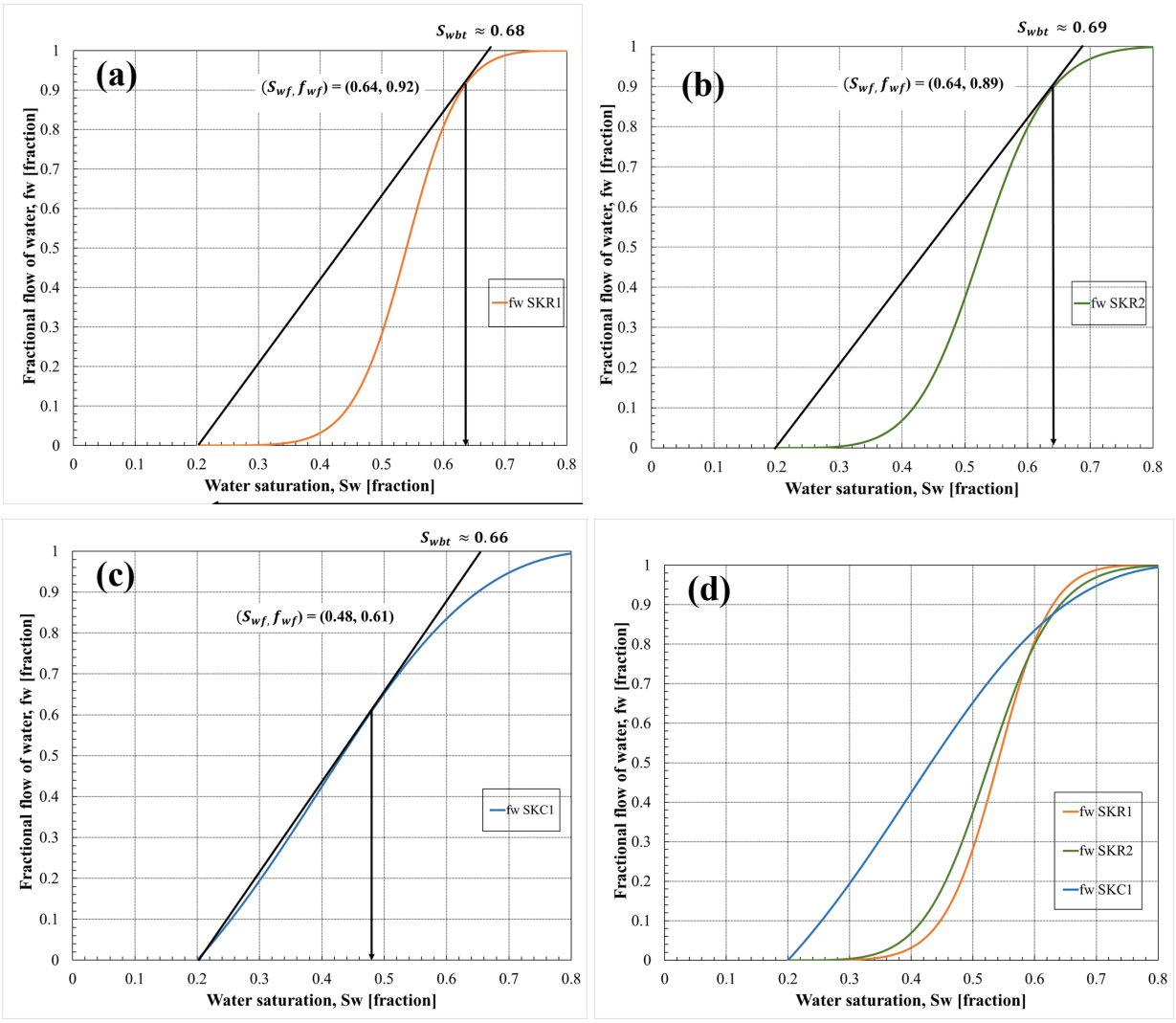

Figure 7.30 Fractional flow curves for two systems with different initial wettability. (a) Strongly water-wet reference core SKR1. (b) Strongly water-wet reference core SKR2. (c) Core SKC1 exposed to crude oil with AN=0.67 mgKOH/g, SKC1. (d) For both systems.

As seen from the conducted waterflooding experiments, the displacement in the strongly water-wet reference cores are most efficient at water breakthrough. The average water saturation at

breakthrough, S_{wbt} for the cores are SKR1=68%, SKR2=69% and SKC1=66%, and the front saturation S_{wf} for the cores are SKR1=64%, SKR2=64% and SKC1=48%, respectively. The slopes of the corresponding tangent increase as the system becomes more oil-wet, and there are observed a little increase from the strongly water-wet cores to the fractional-wet core. The fractional flow curves are based on the relative permeability curves, and the insufficient change in wettability corresponds to the slightly decrease in the crossover saturation observed in the relative permeability curves.

7.7.7 Summary and comparison of the numerical core analyses

The numerical core analyses were conducted together with Harestad (2019) and Radenkovic (2019). The produced relative permeability curves, capillary pressure curves and the fractional flow curves were compared to strengthen the results. The curves were constructed based on the automatic history match for the cores exposed to crude oil (SKC1-SKC3). Figure 7.31 presents the curves for the three cores exposed to crude oil (SKC1-SKC3) compared to the strongly water-wet reference cores.

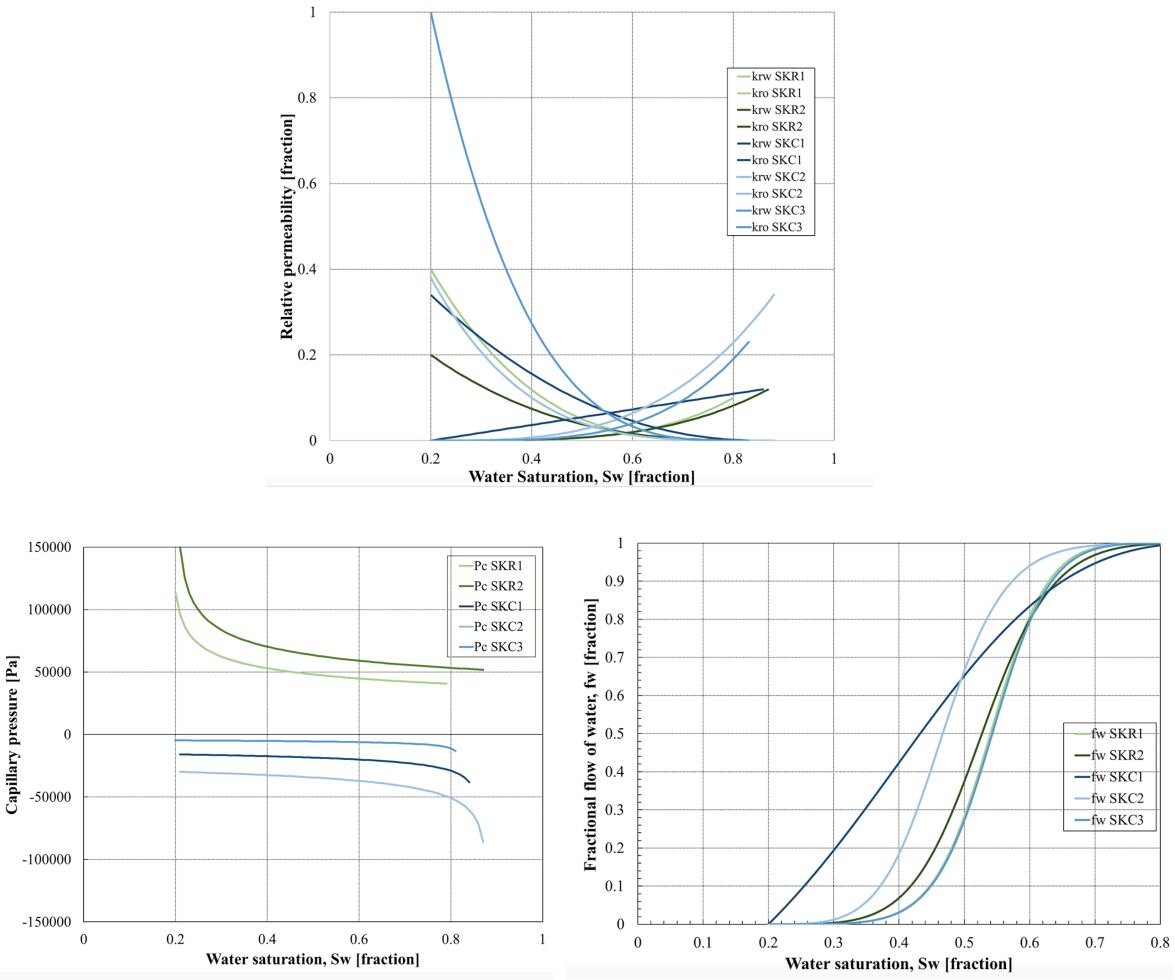

Figure 7.31 Comparison of: relative permeability curves based on the Corey correlation, capillary pressure curves based on Skjæveland correlation and fractional flow curves based on relative permeability for the strongly water-wet systems, with the three less water-wet systems exposed to different crude oils. (SKC1, oil C) (SKC2, oil B) (SKC3, oil A).

The crossover saturation is over 50% for all systems, and according to theory the systems are strongly water-wet. There is a small decrease in water saturation for the fractional-wet systems. The crossover saturation for the cores are, SKR1=60%, SKR2=59%, SKC1=56%, SKC2=52% and SKC3=60%, respectively. The crossover saturation should decrease with increasing AN, but core SKC2, which are saturated with oil B, and have the medium value of AN has the lowest crossover saturation. There is a small decrease in the crossover saturation for core SKC1 and SKC2 which are exposed to oil B and C, but the change is less than we would expect for cores exposed to crude oil. The crossover saturation should be even lower. Core SKC3 which are exposed to oil A are similar to the reference cores, and this is reasonable since the core is quite water-wet compared to the other two cores. The construction of the relative permeability curves is based on the experimental production profile for the cores, and as observed from table 10 in

section 7.6, all cores produced approximately the same amount of oil. Hence, only one set of relative permeability curves are constructed for the Smart Water EOR process.

The capillary pressure curves for the strongly water-wet systems indicates strong positive capillary forces, which are confirmed by SI-tests. The capillary pressure curves for the systems exposed to crude oil are negative. As mention earlier for core SKC1, it seems that SENDRA model the curves based on the high saturations, where the capillary forces probably are gone. From the experimental work, all cores exposed to crude oil produced oil during SI and positive capillary forces were confirmed in the cores. So, the curves are not so reliable for the cores exposed to oil.

The corresponding tangent to the fractional flow curves increases with increasing AN. Core SKC1 which are exposed to oil A with the highest AN has the lowest front saturation and largest tangent. The curve for core SKC3 which are exposed to oil A with lowest AN is equal to the reference cores, while the curve for SKC2 are in between the two cores. The curvature increases towards right when the AN of the system increases. However, all curves are on the water-wet side, and since the curves are based on relative permeability curves they will correlate to their results.

8 Conclusion and future work

The main objective of this thesis was to perform oil recovery tests on outcrop chalk material with different initial wettings to investigate the effect of wettability on waterflooding and relative permeability. The potential of modelling reliable relative permeability curves at different initial wettability based on experimental data with SENDRA was also investigated.
The main conclusions drawn from this study were:

8.1 Conclusion

- The purpose of the introduction of the mineral oil was to have the same conditions through the experiment, both for the strongly water-wet cores and the fractional-wet cores. It was observed that the interfacial tension was increased due to the mineral oil. Hence, IFT was a more dominant parameter in the capillary pressure equation than the contact angle, and higher oil recoveries than predicted were obtained throughout the experiment.
- The strongly water-wet reference cores prepared with mineral oil, had a mean production of 72 %OOIP during both spontaneous- and forced imbibition oil recovery tests. Recovery plateau was reached after 3 PV injected during the forced imbibition test. For the spontaneous imbibition test, the oil production was rapid, and recovery plateau was reached after only hours.
- The wettability of the cores was investigated by spontaneous imbibition and the chromatographic wettability test and was confirmed to be strongly water-wet.
- The fractional-wet cores prepared with adsorption of crude oil C with AN=0.67 mgKOH/g, had a mean production of 71.5 %OOIP during the forced oil recovery test. Recovery plateau was reached after 3.5 - 4 PV injected for both cores. For the spontaneous imbibition test, the oil production was slower, and the recovery plateau was reached after 12 PV injected for SKC1 and 3 PV injected for SKC4.
- The wettability of the cores was investigated by the chromatographic wettability test and was confirmed to be less water-wet, i.e. fractional-wet for both cores.
- The initial wettability of the cores was also investigated during spontaneous imbibition and was confirmed to be less water-wet. However, there was observed a slightly difference between the cores. A mild core cleaning procedure reduced the contamination of polar organic components in core SKC1 compared to core SKC4.

Hence, core SKC4 indicates the initial wetting of the fractional-wet system compared to core SKC1.

- Compared to the results from Harestad (2019) and Radenkovic (2019), the core with the highest AN had lowest imbibition rates and oil production, while the core with the lowest AN had highest imbibition rates and oil production during SI. The wetting indexes also decreased with increasing AN. However, the total oil production during FI for all cores were approximately the same, with a mean production of 71 %OOIP.
- During the history matching of the experimental data with the simulation software SENDRA, the characteristics of the oil recovery profile for all cores signalized a piston-like displacement. The ΔP data indicates strong capillary forces, but SENDRA was not capable to identify the capillary forces. Hence, SENDRA tried to HM according to a piston-like displacement which results in not a reasonable match of ΔP.
- Relative permeability curves for both systems were constructed based on the HM. SENDRA was not capable to produce reasonable relative permeability curves based on HM of the experimental data. The relative permeability curves were based on the oil production data, which had a favorable mobility ratio. The recovery profiles for the two systems were approximately the same, hence the relative permeability curves were too. Only one set of reasonable relative permeability curves were produced by SENDRA, which represents the strongly water-wet system after the wettability alteration by Smart Water.

8.2 Future work

The experimental work performed in this experimental study has given many interesting results which could be further investigated. Some suggestions are presented below:

- Further investigate the influence of pressure-drop on oil recovery by decreasing the injection rates for strongly water-wet cores. Then it could be possible to verify the influence of differential pressure on oil recovery.
- Produce a 100% oil-wet system to compare with the oil recovery tests and the relative permeability curves for the strongly water-wet and less water-wet, i.e. fractional-wet systems.
- For further work in investigation of the relative permeability curves based on the experimental data the JBN-method could be utilized to model the relative permeability curves.

- The simulation program SENDRA is only limited to forced imbibition experiments, and modelling of relative permeability and capillary pressure curves based on spontaneous imbibition was not possible. The simulation program ECLIPSE could be used for modelling relative permeability curves based on experimental data from SI.
- For measurements of relative permeability curves over the whole saturation interval and not only endpoints saturation, it could be convenient to use the steady-state method.

9 References

Alotaibi, M. B., Azmy, R., & Nasr-El-Din, H. A. (2010). *Wettability challenges in carbonate reservoirs.* Paper presented at the SPE Improved Oil Recovery Symposium.

Amott, E. (1959). Observations relating to the wettability of porous rock. *Society of Petroleum Engineers*, 156-162.

Anderson, W. G. (1986a). Wettability literature survey-part 1: rock/oil/brine interactions and the effects of core handling on wettability. *Journal of petroleum technology, 38*(10), 1125-1144.

Anderson, W. G. (1986b). Wettability literature survey-part 2: Wettability measurement. *Journal of petroleum technology, 38*(11), 1246-1262.

Anderson, W. G. (1987a). Wettability literature survey part 5: the effects of wettability on relative permeability. *Journal of petroleum technology, 39*(11), 1453-1468.

Anderson, W. G. (1987b). Wettability literature survey-part 4: Effects of wettability on capillary pressure. *Journal of petroleum technology, 39*(10), 1283-1300.

Anderson, W. G. (1987c). Wettability literature survey-part 6: the effects of wettability on waterflooding. *Journal of petroleum technology, 39*(12), 1605-1622.

Andreassen, E. (2019). *Production of Smart Water by Acid Flooding in Chalk: Temperature Limitation at Slightly Water-Wet Conditions.* (Master of Science), University of Stavanger, Stavanger.

Apostolos, K., Bryan, J., & Taheri, s. (2016). *Fundamentals of fluid flow in porous media*. Alberta: University of Calgary.

Austad, T. (2013). Water-based EOR in carbonates and sandstones: New chemical understanding of the EOR potential using "Smart Water". In *Enhanced Oil Recovery Field Case Studies* (pp. 301-335): Elsevier.

Austad, T., Shariatpanahi, S., Strand, S., Black, C., & Webb, K. (2011). Conditions for a low-salinity enhanced oil recovery (EOR) effect in carbonate oil reservoirs. *Energy&Fuels, 26*(1), 569-575.

Austad, T., Strand, S., Madland, M. V., Puntervold, T., & Korsnes, R. I. (2007). *Seawater in chalk: An EOR and compaction fluid.* Paper presented at the International petroleum technology conference.

Bjørlykke, K. (2015). *Petroleum geoscience : from sedimentary environments to rock physics* (2nd ed.). Heidelberg: Springer.

Brooks, R. H., & Corey, A. T. (1964). Hydraulic properties of porous media. *Hydrology Papers, Colorado State University, 24*, 37.

Buckley, J. S., & Fan, T. (2007). Crude oil/brine interfacial tensions1. *Petrophysics, 48*(03).

Chukwudeme, E. A., Fjelde, I., Abeysinghe, K. P., & Lohne, A. (2014). Effect of interfacial tension on water/oil relative permeability on the basis of history matching to coreflood data. *SPE Reservoir Evaluation Engineering, 17*(01), 37-48.

Craig, F. F. (1971). *The reservoir engineering aspects of waterflooding* (Vol. 3): HL Doherty Memorial Fund of AIME New York.

Cuiec, L. (1984). *Rock/crude-oil interactions and wettability: An attempt to understand their interrelation.* Paper presented at the SPE Annual Technical Conference and Exhibition.

Donaldson, E. C., & Alam, W. (2013). *Wettability*. Burlington: Elsevier Science.

du Noüy, P. L. (1925). An interfacial tensiometer for universal use. *The Journal of general physiology, 7*(5), 625.

Emitech. (1999). Technical Brief: Sputter Coating incorporating Emitech K500, K550, K575 and K675X. [https://crn2.3it.usherbrooke.ca/guide_sb/appareils/Emitech/SputterCoating.pdf].

Fan, T., & Buckley, J. S. (2007). Acid number measurements revisited. *SPE Journal, 12*(04), 496-500.
Fanchi, J. (2010). *Integrated Reservoir Asset Management: Principles and Best Practices*: Elsevier Science.
Fathi, S. J., Austad, T., & Strand, S. (2011). Water-based enhanced oil recovery (EOR) by "smart water": Optimal ionic composition for EOR in carbonates. *Energy&Fuels, 25*(11), 5173-5179.
Green, D. W., & Willhite, G. P. (1998). *Enhanced oil recovery* (Vol. vol. 6). Richardson, Tex: Henry L. Doherty Memorial Fund of AIME, Society of Petroleum Engineers.
Guan, H., Graham, G., & Juhasz, A. (2003). *Investigation of Wettability Alteration Following Scale Inhibitor Adsorption onto Carbonate and Clastic Reservoir Core Material-Static Tests and ESEM Studies.* Paper presented at the International Symposium on Oilfield Chemistry.
Harestad, A. (2019). *Effect of wettability on waterflooding and relative permeability at medium water-wet conditions.* (Master of Science), University of Stavanger, Stavanger.
Hopkins, P., Puntervold, T., & Strand, S. (2015). *Preserving initial core wettability during core restoration of carbonate cores.* Paper presented at the Proceedings of the International Symposium of the Society of Core Analysts.
Hopkins, P., Walrond, K., Strand, S., Puntervold, T., Austad, T., & Wakwaya, A. (2016). Adsorption of acidic crude oil components onto outcrop chalk at different wetting conditions during both dynamic adsorption and aging processes. *Energy&Fuels, 30*(9), 7229-7235.
Høgnesen, E. J., Strand, S., & Austad, T. (2005). *Waterflooding of preferential oil-wet carbonates: Oil recovery related to reservoir temperature and brine composition.* Paper presented at the SPE Europec/EAGE Annual Conference.
Instruments, N. Scanning Electron Microscopy. Retrieved from https://www.nanoscience.com/techniques/scanning-electron-microscopy/
Jadhunandan, P., & Morrow, N. R. (1995). Effect of wettability on waterflood recovery for crude-oil/brine/rock systems. *SPE Reservoir Engineering, 10*(01), 40-46.
Kleppe, J. (2017). *Derivation of the fractional flow equation for a one-dimensional oil-water system*. [Hand-out note 4: Buckley-Leverett Analysis]. TPG4150 Reservoir Recovery Techniques. Trondheim.
Korsnes, R., Wersland, E., Austad, T., & Madland, M. (2008). Anisotropy in chalk studied by rock mechanics. *Journal of Petroleum Science Engineering, 62*(1-2), 28-35.
Lake, L. W. (2010). *Enhanced oil recovery*. Richardson, Tex: Society of Petroleum Engineers.
Lake, L. W., Johns, R. T., Rossen, W. R., & Pope, G. A. (2014). *Fundamentals of enhanced oil recovery* (2 ed.). Richardson, Tex: Society of Petroleum Engineers.
Lindanger, M. (2019). *Production of Smart Water by Acid Flooding in Chalk cores: Oil Recovert at Intermediate Temperature.* (Master of Science), University of Stavanger, Stavanger.
Lucia, F. J. (2007). *Carbonate reservoir characterization: An integrated approach*. Texas, USA: Springer Science & Business Media.
Marickar, Y. F., Lekshmi, P., Varma, L., & Koshy, P. (2009). EDAX versus FTIR in mixed stones. *Urological research, 37*(5), 271-276.
Marshak, S. (2011). *Earth: Portrait of a Planet* (Fourth International Student ed.): WW Norton & Company.
McDougall, S. R., & Sorbie, K. S. (1995). The impact of wettability on waterflooding: pore-scale simulation. *SPE Reservoir Engineering, 10*(03), 208-213.

Milter, J. (1996). *Improved oil recovery in chalk : spontaneous imbibition affected by wettability, rock framework and interfacial tension.* (Philosophiae Doctor Doctoral), Department of Chemistry, University of Bergen, Bergen.
Mjøs, J. E. S., Strand, S., Puntervold, T., & Gaybaliyev, H. (2018). *Effect of Initial Wetting on Smart Water Potential in Carbonates.* Paper presented at the SPE EOR Conference at Oil and Gas West Asia.
Morrow, N. R. (1990). Wettability and its effect on oil recovery. *Journal of petroleum technology, 42*(12), 1476-1484.
Prores. Sendra software and core analysis services. Retrieved from https://www.prores.no/products-and-services/sendra-software-and-core-analysis-services/
Puntervold, T. (2008). *Waterflooding of carbonate reservoirs: EOR by wettability alteration.* (Philosophiae Doctor Doctoral), University of Stavanger,
Puntervold, T., Strand, S., & Austad, T. (2007a). New method to prepare outcrop chalk cores for wettability and oil recovery studies at low initial water saturation. *Energy&Fuels, 21*(6), 3425-3430.
Puntervold, T., Strand, S., & Austad, T. (2007b). Water flooding of carbonate reservoirs: Effects of a model base and natural crude oil bases on chalk wettability. *Energy&Fuels, 21*(3), 1606-1616.
Radenkovic, K. (2019). *Effect of wettability on waterflooding and relative permeability at quite water-wet conditions.* (MSc thesis), University of Stavanger, Stavanger.
Raza, S., Treiber, L., & Archer, D. (1968). Wettability of reservoir rocks and its evaluation. *Prod. Monthly, 32*(4), 2-7.
RezaeiDoust, A., Puntervold, T., Strand, S., & Austad, T. (2009). Smart water as wettability modifier in carbonate and sandstone: A discussion of similarities/differences in the chemical mechanisms. *Energy&Fuels, 23*(9), 4479-4485.
Salathiel, R. (1973). Oil recovery by surface film drainage in mixed-wettability rocks. *Journal of petroleum technology, 25*(10), 1216-1224.
Shariatpanahi, S., Hopkins, P., Aksulu, H., Strand, S., Puntervold, T., & Austad, T. (2016). Water based EOR by wettability alteration in dolomite. *Energy&Fuels, 30*(1), 180-187.
Skjæveland, S. M., Siqveland, L. M., Kjosavik, A., Hammervold, W. L., & Virnovsky, G. A. (1998). *Capillary pressure correlation for mixed-wet reservoirs.* Paper presented at the SPE India Oil and Gas Conference and Exhibition.
Springer, N., Korsbech, U. C., & Aage, H. K. (2003). *Resistivity Index Measurement without the Porous Plate.* Paper presented at the Proceedings International Symposium of the Society of Core Analysts.
Standing, M. (1975). *Notes on relative permeability relationships*. Lecture Notes. Trondheim, Norway.
Standnes, D. C., & Austad, T. (2000). Wettability alteration in chalk: 1. Preparation of core material and oil properties. *Journal of Petroleum Science Engineering, 28*(3), 111-121.
Strand, S., Høgnesen, E. J., & Austad, T. (2006a). Wettability alteration of carbonates—Effects of potential determining ions (Ca2+ and SO42−) and temperature. *Colloids and Surfaces A: Physicochemical Engineering Aspects, 275*(1-3), 1-10.
Strand, S., Puntervold, T., & Austad, T. (2008). Effect of temperature on enhanced oil recovery from mixed-wet chalk cores by spontaneous imbibition and forced displacement using seawater. *Energy&Fuels, 22*(5), 3222-3225.

Strand, S., Standnes, D. C., & Austad, T. (2006b). New wettability test for chalk based on chromatographic separation of SCN− and SO42−. *Journal of Petroleum Science Engineering, 52*(1-4), 187-197.
Taber, J. J., Martin, F., & Seright, R. (1997). EOR screening criteria revisited-Part 1: Introduction to screening criteria and enhanced recovery field projects. *SPE Reservoir Engineering, 12*(03), 189-198.
Thomas, S. (2008). Enhanced oil recovery-an overview. *Oil & Gas Science and Technology, 63*(1), 9-19.
Torrijos, I. D. P. (2017). *Enhanced oil recovery from Sandstones and Carbonates with "Smart Water".* (Philosophiae Doctor Doctoral), University of Stavanger, Stavanger.
Torrijos, I. P., Sæby, K. G., Strand, S., & Puntervold, T. (2019). *Impact of Temperature on Wettability Alteration by Smart Water in Chalk.* Paper presented at the IOR 2019–20th European Symposium on Improved Oil Recovery.
Webb, K. J., Black, C. J. J., & Tjetland, G. (2005). *A laboratory study investigating methods for improving oil recovery in carbonates.* Paper presented at the International petroleum technology conference.
Zhang, P., & Austad, T. (2005). *The relative effects of acid number and temperature on chalk wettability.* Paper presented at the SPE International Symposium on Oilfield Chemistry.
Zhang, P., & Austad, T. (2006). Wettability and oil recovery from carbonates: Effects of temperature and potential determining ions. *Elsevier, 279*(1-3), 179-187.
Zhang, P., Tweheyo, M. T., & Austad, T. (2007). Wettability alteration and improved oil recovery by spontaneous imbibition of seawater into chalk: Impact of the potential determining ions Ca2+, Mg2+, and SO42−. *Elsevier, 301*(1-3), 199-208.
Zolotukhin, A. B., & Ursin, J.-R. (2000). *Introduction to Petroleum Reservoir Engineering*. Kristiansand: Høyskoleforlaget.

Attended on the IOR NORWAY conference hosted by the national IOR Centre of Norway, 19-20th of March 2019. Presented a poster about the so far experimental work for the master thesis.

Effect of Wettability on Waterflooding and Relative permeability at Slightly Water-Wet Conditions

Agnes Kahlbom Wathne

Skule Strand, Tina Puntervold, Ivan D. Pinerez Torrijos

Department of Energy Resources, University of Stavanger, Norway

Introduction

Experimental data and field observations have confirmed that Smart Water EOR processes are wettability alterations towards more water-wet conditions increasing the oil recovery. No chemically induced wettability alteration are taking place during formation water (FW) injection. Seawater (SW) behaves as a Smart Water in chalk and significant increased recovery are observed as seen in figure 1.

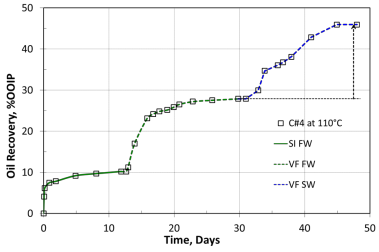

Figure 1 Oil recovery from chalk core, by spontaneous imbibition of FW, viscous flooding using FW and finally viscous flooding using SW. (Strand et al. 2008)

Objectives

Model relative permeability curves based on oil production profiles and pressure data from viscous flooding in different initial wetting states.

Methods

Hassler core holder (figure 2) is used for core cleaning, oil saturation, viscous flooding and chromatographic wettability tests.

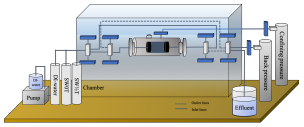

Figure 2 Illustration of the flooding set-up for core cleaning (only FW), viscous flooding (only FW) and chromatographic wettability test.

The chalk cores are initially cleaned and dried for initial water saturation (S_{wi}=20%). Then they are saturated with oil, and oil recovery tests are performed.

The pressure is measured during viscous flooding, and the data is used to model relative permeability curves for a water-wet and a fractional-wet system in Sendra.

The wettability of the cores is confirmed by spontaneous imbibition and chromatographic wettability tests.

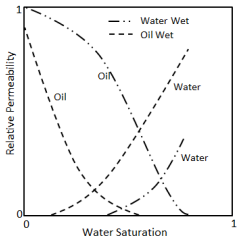

Figure 3 Illustration of relative permeability curves for a water-wet and an oil-wet system

Results

Oil recovery data for a very water-wet system.

The initial wetting was confirmed by a spontaneous imbibition test. The capillary forces were strong, and the oil recovery were approximately the same compared to the produced oil during viscous flooding.

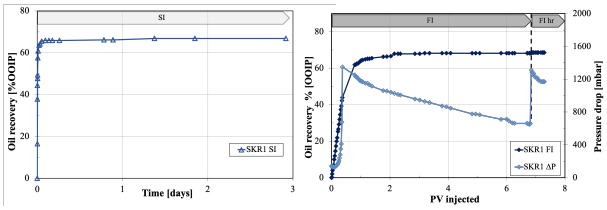

Figure 4 Oil production profile for a water-wet chalk core (Q1) during (left) spontaneous imbibition and (right) viscous flooding with formation water

Oil recovery data for a fractional-wet system.

The oil recovery profile in the fractional-wet system has the same trend compared to very water-wet system, but significantly differences in pressure drop are observed. This can be due to lower capillary forces in the fractional wet system.

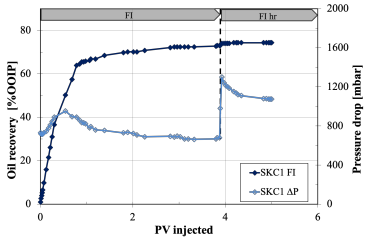

Figure 5 Oil production profile for a fractional-wet chalk core (C1) during viscous flooding with formation water

After an oil recovery plateau was reached, the flow rate was increased to 4PV/day. A slightly difference in the oil production from the water-wet core compared to the fractional-wet core is observed.

Further work

Initial wetting of the fractional wetted core will be verified by spontaneous imbibition tests and chromatographic wettability tests. Relative permeability curves will be modeled through production- and pressure drop data.

Investigate if the observed pressure data or end-points saturations could be used for modeling relative permeability curves, which describing the observed EOR effects, describe wettability differences, and the differences in oil production.

References

Strand, S., Puntervold, T., & Austad, T. (2008). Effect of temperature on enhanced oil recovery from mixed-wet chalk cores by spontaneous imbibition and forced displacement using seawater. *Energy&Fuels, 22*(5), 3222-3225.

Acknowledgement

The authors acknowledge the Research Council of Norway and the industry partners, ConocoPhillips Skandinavia AS, Aker BP ASA, Eni Norge AS, Equinor ASA, Neptune Energy Norge AS, Lundin Norway AS, Halliburton AS, Schlumberger Norge AS, Wintershall Norge AS, and DEA Norge AS, of The National IOR Centre of Norway for support.

Contact information

Agnes Kahlbom Wathne

Email: Ak.wathne@stud.uis.no

Phone: +47 48042420

IOR NORWAY 2019

Appendix A: Chemicals

Acid number solutions

Table 15 Chemicals for AN measurement

Solutions	Chemicals	Chemical formula	Description
Titrant	KOH (>85%) 2-propanol	KOH $CH_3CHOHCH_3$	2.8 g KOH (>85%) Dilute to 1000ml with 2-propanol ($CH_3CHOHCH_3$)
Spiking solution	Stearic Acid Acid titration solvent	$CH_3(CH_2)_{16}COOH$	0.5 g Stearic Acid - $CH_3(CH_2)_{16}COOH$ Dilute to 100 ml with Acid titration solvent
Standard solution	Potassium Hydrogen Phthalate (KHP) DI-water	$HOOCC_6H_4COOK$	0.2 g Potassium Hydrogen Phthalate, KHP Dilute to 500 ml with DI-water
Titration solvent	DI-water 2-propanol Toluene	$CH_3CHOHCH_3$ $C_6H_5CH_3$	6 ml DI-water Dilute with 494 ml 2-propanol and with 500 ml Toluene
Electrode/ electrolyte	Potassium chloride DI-water	KCl	Mettler DG-114 Electrode 3 M KCl in DI-water

Base number solutions

Table 16 Chemicals for BN measurement

Solutions	Chemicals	Chemical formula	Description
Titrant	Perchloric Acid (70%) Acetic Anhydride Acetic Acid	$HClO_4$ (70%) $(CH_3CO)_2O$ CH_3COOH	5 ml 70% Perchloric Acid $HClO_4$ 15 ml Acetic Anhydrite $(CH_3CO)_2O$ Dilute to 1000 ml with Acetic Acid CH_3COOH
Spiking solution	Quinoline Decane	C_9H_7N $CH_3(CH_2)_8CH_3$	0.5 g Quinoline C_9H_7N Dilute to 100 ml with Decane $C_{10}H_{22}$
Standard solution	Potassium Hydrogen Phthalate (KHP) Acetic Acid	$HOOCC_6H_4COOK$ CH_3COOH	0.2 g Potassium Hydrogen Phthalate, KHP Dilute to 250 ml with Acetic acid CH_3COOH
Titration solvent	Methyl Isobutyl Ketone MIBK	$(CH_3)_2CHCH_2COCH_3$	Methyl Isobutyl Ketone (MIBK), $(CH_3)_2CHCH_2COCH_3$
Electrode/ electrolyte	Sodium Perchlorate, (solid) 2-propanol	$NaClO_{4\ (s)}$ $CH_3CHOHCH_3$	Mettler DG-113Electrode Electrolyte: Saturated Sodium Perchlorate, $NaClO_{4\ (s)}$ in 2-propanol

Appendix B: Experimental data

Spontaneous and forced imbibition data

Table 17 SI data, reference core SKR1

Time [days]	Produced oil [ml]	Oil recovery [%OOIP]
0.0000	0.00	0.00
0.0007	5.00	16.47
0.0014	11.50	37.88
0.0021	13.50	44.47
0.0028	14.50	47.76
0.0035	15.00	49.41
0.0069	17.50	57.64
0.0104	18.50	60.94
0.0208	19.30	63.57
0.0313	19.50	64.23
0.0521	19.90	65.55
0.0938	20.00	65.88
0.1354	20.00	65.88
0.1771	20.00	65.88
0.2604	20.00	65.88
0.7813	20.10	66.21
0.8896	20.10	66.21
1.3757	20.30	66.86
1.8493	20.30	66.86
2.9167	20.30	66.86

Table 18 SI data, reference core SKR2

Time [days]	Produced oil [ml]	Oil recovery [%OOIP]
0.0000	0.00	0.00
0.0007	4.10	13.00
0.0014	7.00	22.19
0.0021	9.50	30.12
0.0028	10.50	33.29
0.0035	14.50	45.97
0.0069	14.70	46.60
0.0104	16.00	50.72
0.0208	18.90	59.92
0.0313	20.00	63.40
0.0417	21.50	68.16
0.0833	21.50	68.16
0.1250	22.00	69.74
0.1861	22.00	69.74
0.2694	23.00	72.91
0.3528	23.60	74.82
0.8736	23.60	74.82
1.2903	23.60	74.82
1.9167	23.60	74.82
2.9167	23.60	74.82

Table 19 SI data, SKC1

Time [days]	Produced oil [ml]	Oil recovery [%OOIP]
0.0000	0.00	0.00
0.0007	0.50	1.62
0.0014	0.70	2.27
0.0021	1.50	4.87
0.0028	1.80	5.84
0.0035	2.40	7.79
0.0069	3.20	10.39
0.0104	3.90	12.66
0.0208	7.00	22.72
0.0417	10.40	33.76
0.0833	11.30	36.68
0.2500	12.70	41.22
0.9410	13.90	45.12
1.0007	13.90	45.12
1.0278	14.00	45.44
1.9896	14.30	46.42
2.8403	14.40	46.74
2.9653	14.40	46.74
10.0069	15.50	50.31
10.9847	15.80	51.29
11.8597	15.80	51.29
12.8542	15.80	51.29

Table 20 SI data, SKC4

Time [days]	Produced oil [ml]	Oil recovery [%OOIP]
0.0000	0.00	0.00
0.0007	0.30	0.97
0.0014	030	0.97
0.0021	0.30	0.97
0.0028	0.30	0.97
0.0035	0.30	0.97
0.0069	0.30	0.97
0.0104	0.30	0.97
0.0208	0.30	0.97
0.0417	0.30	0.97
0.0833	0.30	0.97
0.1250	0.50	1.62
0.3931	0.80	2.60
0.7931	1.50	4.87
0.8764	1.60	5.19
1.0292	1.80	5.84
1.1333	1.80	5.84
1.3833	1.80	5.84
2.0500	1.80	5.84
2.8000	1.80	5.84
2.9250	1.80	5.84
10.0069	1.80	5.84
10.9847	1.80	5.84
11.8597	1.80	5.84
12.8542	1.80	5.84

Table 21 FI data, SKR1

Time [days]	Produced oil [ml]	Oil recovery [%OOIP]	ΔP [mBar]
0.00	0.00	0.0	142
0.01	0.10	0.3	135
0.02	0.60	2.0	138
0.04	1.20	4.0	133
0.05	1.50	5.0	134
0.06	1.80	6.0	131
0.07	2.10	7.0	130
0.09	3.00	10.0	129
0.11	3.60	12.0	134
0.13	4.40	14.7	137
0.15	5.20	17.3	141
0.17	6.00	20.0	149
0.19	6.60	22.0	156
0.22	7.60	25.3	173
0.23	8.00	26.6	185
0.25	8.80	29.3	205
0.27	9.60	32.0	239
0.29	10.40	34.6	282
0.32	11.20	37.3	352
0.33	11.80	39.3	413
0.36	12.70	42.3	677
0.37	13.20	44.0	1350
0.79	18.60	62.0	1252
0.83	18.60	62.0	1232
0.87	18.80	62.6	1227
0.90	18.80	62.6	1209
0.95	19.00	63.3	1194
0.98	19.20	63.9	1180
1.01	19.30	64.3	1178
1.03	19.30	64.3	1177
1.06	19.40	64.6	1167
1.16	19.50	64.9	1151
1.23	19.60	65.3	1150
1.30	19.60	65.3	1132
1.38	19.70	65.6	1116
1.77	19.90	66.3	1060
1.89	19.95	66.4	1056
2.03	20.00	66.6	1042
2.15	2040	67.9	1028
2.28	20.40	67.9	1014
2.36	20.40	67.9	1008
2.86	20.40	67.9	959
3.02	20.40	67.9	947
3.19	20.50	68.3	929
3.35	20.50	68.3	916
3.79	20.50	68.3	875
3.94	20.50	68.3	863
4.08	20.50	68.3	848
4.82	20.50	68.3	777
4.94	20.50	68.3	776
5.08	20.50	68.3	766
5.80	20.50	68.3	712
6.00	20.50	68.3	714
6.08	20.50	68.3	692
6.20	20.50	68.3	668
6.27	20.50	68.3	662
6.70	20.50	68.3	662
6.72	20.50	68.3	660
6.78	20.50	68.3	650
6.78	20.50	68.3	651
6.79	20.50	68.3	658
6.81	20.50	68.3	659
Increased injection rate: 4 PV/day injected			
6.84	20.55	68.4	1312
6.87	20.60	68.6	1288
6.89	20.60	68.6	1258
6.91	20.60	68.6	1257
6.93	20.60	68.6	1269
6.98	20.60	68.6	1223
7.03	20.60	68.6	1219
7.06	20.60	68.6	1208
7.09	20.60	68.6	1187
7.18	20.60	68.6	1172
7.22	20.60	68.6	1170
7.25	20.60	68.6	1171
7.29	20.60	68.6	1170

Table 22 FI-data, reference core SKR2

Time [days]	Produced oil [ml]	Oil recovery [%OOIP]	ΔP [mBar]
0.00	0.00	0.00	148
0.01	0.20	0.64	150
0.03	1.00	3.19	144
0.05	1.60	5.11	140
0.06	2.20	7.02	139
0.09	3.00	9.57	136
0.12	4.30	13.72	133
0.17	6.40	20.42	127
0.20	7.20	22.98	133
0.21	7.80	24.89	139
0.23	8.50	27.13	148
0.25	9.30	29.68	167
0.27	10.10	32.23	190
0.30	11.10	35.42	242
0.32	11.90	37.98	295
0.34	12.70	40.53	388
0.77	20.00	63.82	1186
0.81	20.60	65.74	1177
0.85	20.80	66.38	1169
0.89	20.90	66.70	1154
0.93	21.00	67.02	1143
0.99	21.20	67.65	1137
1.06	21.60	68.93	1115
1.16	21.60	68.93	1101
1.22	21.60	68.93	1094
1.28	21.60	68.93	1086
1.81	22.20	70.85	1023
1.88	22.20	70.85	1018
1.98	22.20	70.85	1011
2.05	22.20	70.85	1001
2.09	22.20	70.85	999
2.27	22.50	71.80	985
2.29	22.50	71.80	979
2.78	22.50	71.80	945
2.80	22.50	71.80	944
2.87	22.50	71.80	932
2.99	22.50	71.80	932
3.07	22.50	71.80	922
3.21	22.50	71.80	920
3.34	22.50	71.80	911
3.41	22.50	71.80	909
3.75	22.50	71.80	893
3.83	22.50	71.80	889
3.91	22.50	71.80	884
3.97	22.50	71.80	868
4.82	22.50	71.80	830
5.74	22.50	71.80	828
5.76	22.50	71.80	828
Increased injection rate: 4 PV/day injected			
5.79	22.50	71.80	1342
5.85	22.50	71.80	1297
5.97	22.50	71.80	1258
6.03	22.60	72.12	1256
6.05	22.60	72.12	1250
6.74	22.60	72.12	1202
6.80	22.60	72.12	1208
6.81	22.60	72.12	1202
6.92	22.60	72.12	1202
7.03	22.60	72.12	1195
7.11	22.60	72.12	1194
7.19	22.60	72.12	1195
7.29	22.60	72.12	1195
7.46	22.60	72.12	1194

Table 23 Combined oil recovery test (SI+FI). FI data, SKR2

Time [days]	Produced oil [ml]	Oil recovery [%OOIP]	ΔP [mBar]
3.00	23.60	74.82	302
3.04	23.60	74.82	152
3.08	23.60	74.82	155
3.14	23.60	74.82	161
3.17	23.60	74.82	164
3.21	23.60	74.82	166
3.26	23.60	74.82	164
3.31	23.60	74.82	165
3.33	23.60	74.82	169
3.41	23.60	74.82	168
3.81	23.60	74.82	170
3.86	23.60	74.82	189
3.90	23.60	74.82	185
Increased injection rate: 4 PV/day injected			
3.93	23.60	74.82	358
3.95	23.60	74.82	681
3.95	23.60	74.82	690
3.97	23.60	74.82	693
4.01	23.60	74.82	692
4.05	23.60	74.82	703
4.09	23.60	74.82	708
4.21	23.60	74.82	715
4.34	23.60	74.82	728
4.42	23.60	74.82	738
4.51	23.60	74.82	743
4.59	23.60	74.82	743
4.67	23.60	74.82	743
4.09	23.60	74.82	708
4.21	23.60	74.82	715
4.34	23.60	74.82	728

Table 24 FI-data, SKC1

Time [days]	Produced oil [ml]	Oil recovery [%OOIP]	ΔP [mBar]
0.00	0.00	0.0	737
0.00	0.30	1.0	731
0.02	0.80	2.6	719
0.03	1.20	3.9	715
0.04	1.60	5.2	716
0.05	2.00	6.5	718
0.08	3.00	9.8	729
0.13	4.90	16.0	744
0.18	6.60	21.5	779
0.21	8.00	26.1	810
0.26	9.50	31.0	847
0.30	11.20	36.5	890
0.54	15.40	50.2	953
0.68	17.60	57.4	896
0.79	19.60	63.9	891
0.85	19.80	64.6	858
0.90	20.10	65.5	834
0.94	20.10	65.5	831
0.98	20.20	65.9	822
1.06	20.30	66.2	781
1.09	20.50	66.8	793
1.19	20.50	66.8	760
1.39	21.00	68.5	754
1.80	21.40	69.8	729
1.89	21.50	70.1	736
2.01	21.50	70.1	723
2.09	21.50	70.1	708
2.26	2170	70.7	690
2.81	22.10	72.1	694
2.90	22.20	72.4	687
2.96	22.20	72.4	695
3.03	22.20	72.4	688
3.12	22.20	72.4	666
3.20	22.20	72.4	668
3.33	22.20	72.4	663
3.80	22.30	72.7	668
3.83	22.40	73.0	678
3.88	22.40	73.0	679

Time [days]	Produced oil [ml]	Oil recovery [%OOIP]	ΔP [mBar]
Increased injection rate: 4 PV/day injected			
3.89	22.40	73.0	981
3.93	22.70	74.0	1300
3.97	22.70	74.0	1241
4.01	22.70	74.0	1213
4.05	22.70	74.0	1200
4.08	22.70	74.0	1187
4.18	22.80	74.3	1153
4.24	22.80	74.3	1136
4.28	22.80	74.3	1120
4.34	22.80	74.3	1110
4.83	22.80	74.3	1080
4.89	22.80	74.3	1080
4.94	22.80	74.3	1074
4.97	22.80	74.3	1074
5.00	22.80	74.3	1074

Table 25 Combined oil recovery tests (SI+FI). FI data, SKC4

Time [days]	Produced oil [ml]	Oil recovery [%OOIP]	ΔP [mBar]	Time [days]	Produced oil [ml]	Oil recovery [%OOIP]	ΔP [mBar]
2.92	0.00	5.8	813	**Increased injection rate: 4 PV/day injected**			
2.93	0.20	6.5	809	7.79	20.50	66.5	638
2.94	0.60	7.8	796	7.79	20.60	66.9	1258
2.95	0.90	8.8	784	7.82	20.90	67.8	1190
2.97	1.40	10.4	775	7.88	21.00	68.2	1148
2.98	2.00	12.3	771	7.93	21.20	68.8	1125
3.00	2.30	13.3	760	7.98	21.20	68.8	1109
3.04	4.00	18.8	755	8.00	21.20	68.8	1096
3.11	6.80	27.9	607	8.06	21.20	68.8	1083
3.14	8.00	31.8	781	8.23	21.20	68.8	1045
3.18	9.20	35.7	695	8.65	21.20	68.8	1016
3.22	10.50	39.9	729	8.74	21.20	68.8	1008
3.26	11.60	43.5	817	8.82	21.20	68.8	1009
3.60	15.00	54.5	686	8.88	21.20	68.8	1008
3.74	16.10	58.1	685				
3.78	16.20	58.4	682				
3.82	16.30	58.8	675				
3.86	16.30	58.8	675				
3.90	16.50	59.4	668				
3.95	16.50	59.4	666				
4.05	16.70	60.0	646				
4.16	17.00	61.0	641				
4.23	17.10	61.3	645				
4.83	17.70	63.3	639				
4.89	17.80	63.6	644				
4.90	17.80	63.6	640				
4.99	17.80	63.6	639				
5.12	17.90	63.9	632				
5.79	18.30	65.2	641				
5.92	18.30	65.2	637				
6.18	18.50	65.9	638				
6.74	18.60	66.2	632				
6.77	18.70	66.5	636				
6.85	18.70	66.5	635				
6.91	18.70	66.5	625				
6.95	18.70	66.5	625				
7.05	18.70	66.5	622				
7.13	18.70	66.5	613				
7.41	18.70	66.5	612				
7.72	18.70	66.5	611				
7.76	18.70	66.5	613				
7.77	18.70	66.5	613				

Chromatographic data

Table 26 Chromatographic data reference core, SKR1

Thiocyanide			Sulfate		
PV	C/CO	Area under curve	PV	C/CO	Area under curve
0.63	0.000	0.000	0.71	0.000	0.000
0.71	0.378	0.015	0.79	0.022	0.001
0.79	0.598	0.039	0.87	0.113	0.005
0.87	0.784	0.056	0.95	0.339	0.018
0.95	0.892	0.067	1.04	0.433	0.031
1.04	0.927	0.074	1.12	0.625	0.042
1.12	0.977	0.076	1.20	0.720	0.054
1.20	0.986	0.079	1.28	0.804	0.061
1.28	0.988	0.080	1.36	0.929	0.070
1.36	0.994	0.080	1.44	0.873	0.072
1.44	0.996	0.080	1.52	0.925	0.072
1.52	0.992	0.080	1.60	0.982	0.077
1.60	0.983	0.080			

Total area thiocyanide	Total are sulfate	Area in between curves
0.807	**0.506**	**0.301**

Table 27 Chromatographic data reference core, SKR2

Thiocyanide			Sulfate		
PV	C/CO	Area under curve	PV	C/CO	Area under curve
0.60	0.000	0.000	0.76	0.000	0.000
0.68	0.159	0.006	0.83	0.043	0.002
0.76	0.434	0.023	0.91	0.153	0.007
0.83	0.695	0.044	0.99	0.346	0.019
0.91	0.855	0.060	1.06	0.546	0.035
0.99	0.911	0.068	1.14	0.749	0.050
1.06	0.934	0.072	1.22	0.791	0.060
1.14	0.964	0.073	1.30	0.890	0.065
1.22	0.977	0.075	1.37	0.998	0.073
1.30	0.989	0.076			
1.37	1.023	0.078			

Total area thiocyanide	Total are sulfate	Area in between curves
0.573	**0.310**	**0.263**

Table 28 Chromatographic data SKC1

Thiocyanide			Sulfate		
PV	C/CO	Area under curve	PV	C/CO	Area under curve
0.62	0.000	0.000	0.86	0.000	0.000
0.70	0.186	0.007	0.94	0.560	0.022
0.78	0.518	0.028	1.04	0.694	0.060
0.86	0.781	0.051	1.12	0.813	0.060
0.94	0.907	0.067	1.20	0.855	0.067
1.04	0.981	0.090	1.27	0.922	0.067
1.12	0.986	0.079	1.35	0.938	0.074
1.20	0.971	0.079	1.43	0.984	0.076
1.27	0.988	0.074	1.51	1.000	0.079
1.35	0.981	0.0780			
1.43	0.992	0.078			
1.51	1.004	0.079			

Total area thiocyanide	Total are sulfate	Area in between curves
0.711	**0.505**	**0.205**

Table 29 Chromatographic data SKC4

Thiocyanide			Sulfate		
PV	C/CO	Area under curve	PV	C/CO	Area under curve
0.53	0.000	0.000	0.68	0.000	0.000
0.61	0.026	0.001	0.76	0.012	0.001
0.68	0.179	0.008	0.84	0.229	0.009
0.76	0.529	0.028	0.92	0.517	0.029
0.84	0.854	0.054	1.00	0.790	0.052
0.92	0.972	0.072	1.08	0.894	0.067
1.00	0.999	0.078	1.24	1.012	0.149
1.08	1.020	0.080	1.31	0.949	0.077
1.24	0.998	0.158			
1.31	0.994	0.078			

Total area thiocyanide	Total are sulfate	Area in between curves
0.558	**0.384**	**0.174**

Appendix C: Input parameters for SENDRA

Table 30 Input paramters for history matching in SENDRA

Parameter	SKR1	SKR2	SKC1
Length [cm]	7.06	7.07	6.94
Diameter [cm]	3.78	3.79	3.79
Porosity [%]	47	49	49
Base permeability [mD]	4.02	4.09	4.12
Initial water saturation	0.20	0.20	0.20
Water viscosity [mPa.s]	0.85	0.85	0.85
Oil viscosity [mPa.s]	2.7	2.7	2.7
Water density [g/cm^3]	0.997	0.997	0.997
Oil density [g/cm^3]	0.783	0.783	0.783